JAERI 1329

JAERI 1329

Activation Cross Section Measurements at Neutron Energy from 13.3 to 14.9 MeV Using the FNS Facility

October 1993

日 本 原 子 力 研 究 所

Japan Atomic Energy Research Institute

JAERI レポートは，日本原子力研究所が研究成果編集委員会の審査を経て不定期に公刊している研究報告書です。

入手の問合わせは，日本原子力研究所技術情報部情報資料課（〒319－11 茨城県那珂郡東海村）あて，お申しこしください。なお，このほかに財団法人原子力弘済会資料センター（〒319－11 茨城県那珂郡東海村日本原子力研究所内）で複写による実費頒布をおこなっております。

JAERI reports are reviewed by the Board of Editors and issued irregularly.

Inquiries about availability of the reports should be addressed to Information Division, Department of Technical Information, Japan Atomic Energy Research Institute, Tokai-mura, Naka-gun, Ibaraki-ken 319－11, Japan.

編集兼発行　日本原子力研究所
印　　刷　いばらき印刷㈱

Activation Cross Section Measurements at Neutron Energy from 13.3 to 14.9 MeV Using the FNS Facility

Chikara KONNO, Yujiro IKEDA, Koji OISHI*, Kiyoshi KAWADE**, Hiroshi YAMAMOTO**, and Hiroshi MAEKAWA

Department of Reactor Engineering
Tokai Research Establishment,
Japan Atomic Energy Research Institute
Tokai-mura, Naka-gun, Ibaraki-ken 319-11

(Received March 15, 1993)

Abstract

Neutron activation cross sections are very basic nuclear data for fusion reactor nuclear design and neutron dosimetry. Systematic measurements of neutron activation cross sections in the neutron energy range from 13.3 to 14.9 MeV have been under way since 1984, using the intense D-T neutron source FNS. This paper compiles the activation cross sections of 89 reactions which encompass the (n, 2n), (n, n′), (n, p), (n, np) and (n, α) processes for 24 elements, as measured from 1988 to 1990. The cross sections for 8 of these reactions were measured for the first time. The present measurements provided data with a good accuracy, covering a wide energy range, for the fifteen reactions, which were reported previously at only one point. These measured data were compared with corresponding values in the literature and with the evaluated nuclear data from JENDL-3 and ENDF/B-V, -VI. Systematic trends for the (n, 2n), (n, p), (n, np) and (n, α) reaction cross sections at 14.9 MeV were examined, based on the data obtained at FNS.

Keywords: activation cross section, fusion reactor, neutron dosimetry, D-T neutron, FNS, (n, 2n), (n, n′), (n, p), (n, np), (n, α), JENDL-3, ENDF/B-V, ENDF/B-VI, systematics of reaction cross section

* Shimizu Corporation
** Faculty of Engineering, Nagoya University

FNSを用いた13.3から14.9 MeVの中性子に対する放射化断面積測定

日本原子力研究所東海研究所原子炉工学部

今野　力・池田裕二郎・大石　晃嗣*・河出　清**
山本　洋**・前川　洋

(1993年3月15日受理)

要　旨

中性子放射化断面積は，核融合炉の核設計や中性子ドシメトリーに対する基本的な核データである。1984年以来，FNSの強力なD-T中性子源を用い，13.3から14.9 MeVの中性子エネルギーに対する放射化断面積の系統的な測定が実施されている。本論文は，1988から1990年にかけて，24元素の(n, 2n)，(n, n′)，(n, p)，(n, np)及び(n, α)反応に関する合計89の反応について測定した放射化断面積のデータをまとめたものである。このうち，8反応の断面積は今回初めて測定されたものである。これまで1点の測定データしかない15の反応についても，広いエネルギー範囲で精度の良いデータを得た。今回測定した実験値を，文献値及びJENDL-3やENDF/B-V，-VIの評価値と比較検討した。また，FNSでこれまで得た測定値を基にして，14.9 MeVにおける(n, 2n)，(n, p)，(n, np)及び(n, α)反応のシステマティックスについて検討した。

＊　清水建設㈱
＊＊名古屋大学工学部

CONTENTS

目　　次

List of Tables

List of Figures

This is a blank page.

1. Introduction

Neutron activation cross sections around 14 MeV are very basic nuclear data needed to evaluate induced activity, gas production and radiation damage in fusion devices. They also provide the response functions required for neutron dosimetry of fusion environments. Finally, they are useful to confirm predictions of nuclear reaction theory. An abundance of activation cross section measurements have been performed, and various efforts have been devoted to making comprehensive nuclear data evaluations such as JENDL-3[1], ENDF/B-V[2], -VI[3], IRDF-90[4]. There are, however, large discrepancies for certain reactions among the experimental data by various experimentalists measured using different techniques, neutron sources and decay data, while few measured data exist for other reactions. Although nuclear data evaluators have attempted to provide the reasonable evaluations, it has been impractical to provide reliable cross section values when the data scatter widely or when there are few measured values. Therefore there are still strong needs for measured activation cross section data with uncertainties less then 10%.

Systematic measurements of neutron activation cross sections in the neutron energy range from 13.3 to 14.9 MeV have been under way since 1984 using an intense D-T neutron source at the FNS facility[5] and the unified experimental conditions. The first report[6] of this program was published in 1988. The report described the measuring techniques and data reduction method in detail, and emphasized the activation cross section for fusion reactor structural materials such as iron, nickel, chromium, titanium, molybdenum, zirconium, etc. The report dealt with cross section data measured for 110 reactions, which cover the (n, p), (n, np), (n, α) and (n, 2n) processes for 26 elements from ^{19}F to ^{204}Pb. As the second report, the present report compiles the activation cross section data for 89 reactions which encompass the (n, 2n), (n, n′), (n, p), (n, np) and (n, α) processes for 24 elements, which were measured from 1988 to 1990. The present objective is to accumulate cross section data not only for fusion structural materials but also for various nuclei of concern for basic nuclear physics. Emphasis is placed on cross sections for the medium and heavy mass region (A=60 to 238). The measured reactions are summarized in Table 1, along with the associated nuclear constants, which were taken from the Table of Isotopes[7]. The experimental procedure and data reduction method are almost the same as were used previously[6].

An investigation of systematic trends for (n, 2n), (n, p), (n, np) and (n, α) reactions was possible because of the extensive data obtained in the present experimental program. If all available data are taken into account without any screening, one concludes that there exist no clear correlations among the data. However, there should be a possibility to search for new systematic trends when the data to be considered are derived under consistent conditions and possess relatively small errors. This provided another objective for the present experimental program.

2. Experiment

2.1 Neutron Source

The experiment was performed at the Fusion Neutronics Source (FNS) facility[5] of the Japan Atomic Energy Research Institute. D–T neutrons were produced by bombarding a water–cooled, 3.7×10^{11} Bq tritiated–titanium target with a 350–keV deuteron beam (d^+). The target assembly was designed in order to reduce neutron scattering by the assembly itself as possible. The beam intensity was approximately 2 mA and the neutron yield was about 2×10^{11} n/s at the target.

2.2 Samples

Separated isotopes were used, whenever they were available, in order to distinguish reactions which produce the same nucleus. Natural materials were used in those instances where separated isotopes were not obtained. The samples, in powder form, were wrapped with a thin cartridge paper. The effective area of these samples was 10×10 mm^2. The chemical compositions, weights, thicknesses and abundances of samples are summarized in Table 2.

2.3 Irradiation

The samples were placed at a distance of 100 mm from the D–T neutron source. They were situated at various angles between 2.8° and 165° with respect to the d^+ beam. This corresponded to neutron energies from 13.3 to 14.9 MeV. The sample support was made of polystyrene foam. Figure 2.1 shows the schematic view of the typical irradiation setting. Irradiation times from 1 to 6 hours were selected, as appropriate to the particular half lives of the produced activities. Cross section measurements for reaction products with half lives above 20 minutes were considered.

2.4 Neutron flux monitor

The ^{93}Nb (n, 2n) ^{92m}Nb dosimetry reaction was adopted as the neutron flux monitor because the cross section is relatively large and flat around 14 MeV neutron energy, and the half–life of ^{92m}Nb is of convenient length (10.14 days). Samples were sandwiched between two niobium foils of $10\times10\times0.1$mm^3. The neutron flux was then determined using the reaction–rate and cross section of ^{93}Nb (n, 2n) ^{92m}Nb. The value 464 mb ($\pm4.2\%$)[6] was adopted as the standard cross section of ^{93}Nb (n, 2n) ^{92m}Nb for neutron energies from 13.3 to 14.9 MeV. This value was measured at FNS, based on the well–known cross section of ^{27}Al (n, α) ^{24}Na (ENDF/B–V[2]). However, according to the value in IRDF–90[4] and our recently measured data[8] for the corss section of ^{27}Al (n, α) ^{24}Na, the standard values for this reaction given in ENDF/B–V are high by 1~2%. Although the 464 mb value of the ^{93}Nb (n, 2n) ^{92m}Nb cross section may be somewhat high as a consequence, the difference is only 1~2%. Thererfore, the present experiment adopted 464 mb as the standard cross section of ^{93}Nb (n, 2n) ^{92m}Nb in order to maintain consistency with our previous results[6].

2.5 Gamma–ray measurement

After the irradiations, gamma–rays from the irradiated samples were measured using four germa-

nium detectors. Each niobium monitor foil was measured separately, and the photopeak count was utilized in the present experiment. One germanium detector was used as the standard detector and samples were set at a distance of 77 mm from this detector in order to reduce gamma-ray sum peak and the sample size effects. The absolute efficiency of the standard detector was determined to an accuracy of ±2% by fitting efficiency data measured using standard gamma-ray sources. The other detectors were used to measure relative gamma-ray yields. Samples were placed at the front surface of these detectors in order to achieve a higher detector efficiency. The efficiencies of the relative detectors were calibrated for each gamma-ray by measuring the same sample with both of the relative and standard detectors. The calibration sample was prepared by irradiating at a position close to the D-T neutron source in order to produce more intense activity.

2.6 Cross section determination

The reaction-rate, RR, was derived from the gamma-ray photopeak counts using the following equation,

$$RR=\frac{\lambda \cdot C \cdot A \cdot F}{W \cdot \varepsilon_f \cdot a \cdot b \cdot N_A \cdot (1-e^{-\lambda \cdot t_i}) \cdot e^{-\lambda \cdot t_c} \cdot (1-e^{-\lambda \cdot t_m})}\ , \qquad (1)$$

where,

λ : decay constant of radioactivity produced,
C : gamma-ray photopeak count,
A : target nuclide atomic weight,
F : correction factor,
W : sample weight,
ε_f : detector efficiency,
a : target nuclide isotopic abundance,
b : gamma-ray branching ratio,
N_A : Avogadro' s number (6.022045×10^{23}),
t_i : irradiation time,
t_c : cooling time,
t_m : measuring time.

All decay data except the gamma-ray branching ratio of ^{73}Ga were taken from the Table of Isotopes[7] in order to maintain consistency with our previous results[6]. The correction factor F includes self-absorption of γ-ray in the samples, counting losses due to the γ-ray sum peak, fluctuations of the neutron flux during irradiation and contributions from low energy neutrons. The details of these corrections are described in Ref. 6. As for monitor reaction ^{93}Nb (n, 2n) ^{92m}Nb, the average reaction-rate for the two niobium foils, in front and, in back of the sample, was adopted as the reaction-rate for the sample position. The difference between the reaction rates in front and back of the sample was 1~2%, which was mainly due to the difference of the distances from the neutron source to the niobium foils.

The cross section σ for the reaction under investigation was obtained from the following equation,

$$\sigma=\frac{RR}{RR_m}\cdot\sigma_m\ , \qquad (2)$$

where,

RR : reaction-rate of the reaction under investigation,
RR_m : averaged reaction-rate of the monitor reaction ^{93}Nb (n, 2n) ^{92m}Nb,
σ_m : cross section of the monitor reaction ^{93}Nb (n, 2n) ^{92m}Nb.

In cases where two different reactions produce the same activity in one sample, such as ^{61}Ni (n, p) ^{61}Co and ^{62}Ni (n, np) ^{61}Co in nickel, two samples with different isotopic abundances were irradiated and the contributions from these two reactions were resolved. Whenever a meta-stable state nucleus decayed to ground state nucleus by an isomeric transition during the gamma-ray measurement, the contribution of that meta-stable state was subtracted in deducing the reaction cross section corresponding to production of the ground state nuclei. The average reaction energy of the incident neutrons was determined using the measured cross section curve and the neutron spectrum calculated with the Monte Carlo code, MORSE-DD[9]. The details of these procedures are also described in Ref. 6.

2.7 Error estimation

The sources and typical values of the experimental errors are summarized in Table 3. The dominant error sources were γ-ray detector efficiency ($\pm$2%), photopeak counting statistics ($\pm$0.3 to $\pm$25%) and the standard cross section of ^{93}Nb (n, 2n) ^{92m}Nb for the neutron flux monitor ($\pm$4.2%). The typical experimental errors for the measured cross sections were $\pm$5 to $\pm$6%. For some reactions, such as ^{70}Ge (n, 2n) ^{69}Ge, ^{112}Cd (n, p) ^{112}Ag and ^{151}Eu (n, 2n) ^{150A}Eu, the experimental errors were relatively large ($\geq \pm$15%) since the errors of the gamma-ray branching ratios were larger than $\pm$10%, according to data from the Table of Isotopes[7]. In the some (n, np) reactions such as ^{84}Sr (n, np) ^{83}Sr, where the product of the (n, 2n) reaction decays to the product of the (n, np) reaction, the experimental errors were quite large ($\geq \pm$50%) since the cross sections were obtained from the difference of very similar values with large uncertainties. The procedures are given in detail in the respective discussions for each reaction.

3. Results and discussion

All of the measured cross sections are shown in Figs. 3.1 to 3.89, along with corresponding values from the literature and results from the comprehensive evaluations in JENDL–3[1] (released in December 1990) and ENDF/B–V[2], –VI[3]. The present data cover, in general, a wider energy region (from 13.3 to 14.9 MeV) compared with other data in the literature. Numerical values for the measured cross sections are given in table 4 along with the experimental errors. Discussions concerning each reaction are given below.

3.1 ^{60}Ni (n, p) $^{60m+g}$Co (Fig. 3.1)

Since this reaction is very important for the estimation of induced ^{60}Co activity in fusion reactor structural materials, and for dosimetry applications, accurate data are required. The experimental errors of the present results are about ±5%, which meet the requirement. The contribution from ^{61}Ni (n, np) ^{60}Co was negligibly small because the abundance of ^{61}Ni in the sample was less than 0.01%. The present results agree within experimental errors with those obtained by Greenwood[10], Bahal[11], Lees[12] and Levkovskij[13]. On the other hand, JENDL–3 and ENDF/B–V, which are based on the experimental data of Paulsen[14], are lower by 10% than the present values. Vonach[15] has pointed out that there are some problems with the data of Paulsen. A re–evaluation of JENDL–3 is strongly advised. ENDF/B–VI is in good agreement with the present results.

3.2 ^{61}Ni (n, p) ^{61}Co (Fig. 3.2) and ^{62}Ni (n, np) ^{61}Co (Fig. 3.3)

^{61}Co is produced by both the ^{61}Ni (n, p) ^{61}Co and ^{62}Ni (n, np) ^{61}Co reactions in irradiated Ni samples. The contributions of these respective reactions were determined by using enriched isotope samples of ^{61}Ni (88.84%) and ^{62}Ni (98.84%).

As for ^{61}Ni (n, p) ^{61}Co, the present data agree within experimental errors with recent experimental values measured by Ribannsky[16]. However, the data of Viennot[17] show a very different trend from the present results. It is very unreasonable from systematics for the excitation function of an (n, p) reaction in a medium nucleus like ^{61}Ni to rise rapidly around 13 MeV. Other experimental values are higher than the present results. The JENDL–3 and ENDF/B–VI also appear to overestimate the cross section by 15% and 30%, respectively.

As for ^{62}Ni (n, np) ^{61}Co, the errors of the present data are very small compared with those in the literature. The values in the literature are higher than the present data, while JENDL–3 values are considerably lower.

3.3 ^{63}Cu (n, α) $^{60m+g}$Co (Fig. 3.4)

This reaction is very important from the same reason as described for the ^{60}Ni (n, p) $^{60m+g}$Co reaction. The present results agree well with experimental data recently reported by Greenwood[10] and Garuska[18]. ENDF/B–V and –VI also show in good consistency with the present data. On the other hand, JENDL–3, which is based on the experimental data of Paulsen[14], appears to underestimate by 15%, in the same manner as observed for the ^{60}Ni (n, p) $^{60m+g}$Co reaction. Therefore, it is necessary to re–evaluate this reaction for JENDL–3.

3.4 ^{64}Zn (n, 2n) ^{63}Zn (Fig. 3.5)

There are a wealth of experimental data for this reaction and the present data are consistent with these values.

3.5 ^{64}Zn (n, p) ^{64}Cu (Fig. 3.6)

This reaction is often used as a dosimeter with a low threshold energy (1.5MeV). The present data agree with experimental data measured by Viennot[19], Casanova[20], Sigg[21] and Spangler[22], but other experimental values are generally higher than the present results. JENDL–3, which seems to be based on the experimental data of Santry[23], is higher by 15% than the present results. This would result in an overestimation of the calculated reaction rates using JENDL–3 by 15%. It is recommended that JENDL –3 be re–evaluated.

3.6 ^{66}Zn (n, 2n) ^{65}Zn (Fig. 3.7)

The present values agree well with experimental values measured by Paulsen[24]. Values from Bormann[25] are larger by 10% than the present ones, while those of Kayashima[26], Araminowitcz[27] and Qaim[28] are smaller by 10% than our values.

3.7 ^{67}Zn (n, p) ^{67}Cu (Fig. 3.8) and ^{68}Zn (n, np) ^{67} (Fig. 3.9)

^{67}Cu is produced by both the ^{67}Zn (n, p) ^{67}Cu and ^{68}Zn (n, np) ^{67}Cu reactions in zinc samples. Enriched isotopes of ^{67}Zn (94.60%) and ^{68}Zn (99.36%) were used in order to determine the contributions of each reaction.

The present data agree within experimental errors with data measured by Vinitskaja[29] for ^{67}Zn (n, p) ^{67}Cu. The experimental values of Viennot[19], Casanova[20] and Ranakumar[30] are much larger than the present results. It seems that their values are unreasonably large, based on the systematics of (n, p) reactions as described in section 4.

Experimental data for ^{68}Zn (n, np) ^{67}Cu are scarce since enriched isotope samples of ^{68}Zn are needed in order to measure the cross section. Only one value, measured by Qaim[31], is available. However, his result is four times smaller than the present values.

3.8 ^{68}Zn (n, α) ^{65}Ni (Fig. 3.10)

Experimental data from the literature references and the present results are in good mutual agreement, except for the result of Qaim[32], which is higher by 50% than the present values.

3.9 ^{70}Ge (n, 2n) ^{69}Ge (Fig. 3.11)

The uncertainties of the present results are rather large due to large uncertainty ($\pm$11%) in the gamma–ray branching ratio for the decay of ^{69}Ge. The present data agree with values recently measured by Hoang[33], Muyao[34] and Molla[35], while the experimental results of Casanova[20], Bormann[36] and Araminowicz[27] are much larger than ours.

3.10 ^{72}Ge (n, p) ^{72}Ga (Fig. 3.12) and ^{73}Ge (n, np) ^{72}Ga (Fig. 3.15)

^{72}Ga is produced by both the ^{72}Ge (n, p) ^{72}Ga and ^{73}Ge (n, np) ^{72}Ga reactions in germanium samples.

Enriched isotopes of ^{72}Ge (97.80%) and ^{73}Ge (74.30%) were used in order to separate each reaction contribution.

For ^{72}Ge (n, p) ^{72}Ga, the present results agree with data from Qaim[37] and Vinitskaja[38], while the values of Hoang[33], Rieppo[39] and Wood[40] are larger by 30% than ours.

As for ^{73}Ge (n, np) ^{72}Ga, the cross sections have been measured for the first time in the present experiment.

3.11 ^{72}Ge (n, α) ^{69m}Zn (Fig. 3.13)

The present data are consistent with result from the literature, except for the value reported by Rieppo[39], which is much higher than the present results.

3.12 ^{73}Ge (n, p) ^{73}Ga (Fig. 3.14) and ^{74}Ge (n, np) ^{73}Ga (Fig. 3.16)

^{73}Ga is produced by both the ^{73}Ge (n, p) ^{73}Ga and ^{74}Ge (n, np) ^{73}Ga reactions in germanium samples. The contribution of each reaction was distinguished by using enriched isotope samples of ^{73}Ge (74.30%) and ^{74}Ge (98.40%).

In ^{73}Ge (n, p) ^{73}Ga, the data of Hoang[33] and Vinitskaja[38] are in agreement, within experimental errors, with the present results, while values reported by Qaim[37], Casanova[20] and Wood[40] are larger by 30% than ours. The experimental result of Rieppo[39] is smaller than the present value. The reason is traceable to a difference in the branching ratio for the 297-keV gamma-ray. He adopted 87%, while 79.8% was used in the present measurement.

The cross section for ^{74}Ge (n, np) ^{73}Ga reaction was measured for the first time in the present experiment.

3.13 ^{74}Ge (n, α) ^{71m}Zn (Fig. 3.17)

The present data are in reasonable agreement with values from the literature references compared with the other reaction cross sections related to germanium (see above).

3.14 ^{75}As (n, 2n) ^{74}As (Fig. 3.18)

Values reported by Casanova[20] and Prasad[41] are larger by 20% than the present results. However, other experimental data are consistent with the present results. JENDL-3 is a little higher than the present data.

3.15 ^{75}As (n, p) ^{75}Ge (Fig. 3.19)

The present values agree with data reported by Rao[42], Bormann[43] and Bayhurst[44], while the results of Gupta[45] and Grochulski[46] are larger by a factor of 1.5 than ours. JENDL-3 data are higher by a factor of 1.5~2 than the present results.

3.16 ^{75}As (n, α) ^{72}Ga (Fig. 3.20)

The present data are in good consistency with many of the experimental data available except for those reported by Rao[42], Prasad[41] and Bormann[43], which are higher by 20% than the present results. The reason for this systematic discrepancy is that they adopted gamma-ray branching ratios different from 95.6% as given in the Table of Isotopes[7]. Rao and Prasad used 75% and 83.5%, respectively.

JENDL–3 is higher by 20% than the present values in the energy region below 14 MeV.

3.17 ^{85}Rb (n, 2n) ^{84m}Rb (Fig. 3.21)

The data reported in the literature scatter considerably. Those values measured by Pepelink[47], Regoug[48], Schwerer[49], Augustyniak[50] and Bormann[36] are smaller by 20% than the present results, although they are consistent each other. The results of Erlandsson[51], Sothras[52], Ghorai[53] and Husain[54] are in agreement with the present data. This observation indicates that there are some underlying systematic errors which influence the measurements.

3.18 ^{85}Rb (n, 2n) $^{84m+g}$Rb (Fig. 3.22)

The present results agree with data in the literature except those reported by Araminowicz[27] and Minetti[55], which are either much smaller or much higher than the present data, respectively. The value of Husain[54] is larger by 15% than the present ones. Our data support JENDL–3, rather than ENDF/B –VI, which is higher by 15% than the present results.

3.19 ^{85}Rb (n, p) ^{85m}Kr (Fig. 3.23)

The experimental errors of the present data are large due to poor gamma–ray counting statistics. The present data are consistent with experimental values in the literature except for the values reported by Erlandsson[51] and Husain[54], which are a little higher than the present results.

3.20 ^{85}Rb (n, α) ^{82}Br (Fig. 3.24)

Most values in the literature are in good agreement with the present data, although the results reported by Bormann[43),56] are higher by 30% than ours. JENDL–3 and ENDF/B–VI are consistent with the present data.

3.21 ^{87}Rb (n, 2n) $^{86m+g}$Rb (Fig. 3.25)

In this reaction the contribution of ^{85}Rb (n, γ) $^{86m+g}$Rb is not discriminated because a Rb sample with natural abundance was used in the experiment. The data of Bormann[56] are higher than the present results. The value of Araminowicz[27] is smaller than the present data, just as was observed in ^{85}Rb (n, 2n) $^{84m+g}$Rb. The other values from the literature are consistent with the present data. JENDL–3 and ENDF /B–VI are higher by 10% than the present results.

3.22 ^{87}Rb (n, p) ^{87}Kr (Fig. 3.26)

The present data agree with recent experimental results. Those values reported by Rao[42] and Husain[54] are smaller than ours. The reason for this discrepancy is because they used larger branching ratios (87% and 84%, respectively) for the 402.58 KeV gamma–ray rather than the value in the Table of Isotopes (50%)[7]. Both JENDL–3 and ENDF/B–VI are almost consistent with the present data, although the trend of ENDF/B–VI is different from that of JENDL–3.

3.23 ^{84}Sr (n, 2n) ^{83}Sr (Fig. 3.27)

Few investigations have been done for this reaction, mainly due to the small abundance of ^{84}Sr

(0.56%). The experimental errors of the present data are relatively large, mainly due to a large error (±10%) assigned for the gamma-ray branching ratio. The present data are in reasonable agreement with the values reported by Holub[57] and Rao[42], while the results reported by Husain[54] and Bormann[58] are smaller and much higher than ours, respectively.

3.24 ^{84}Sr (n, p) $^{84m+g}$Rb (Fig. 3.28)

There are very few experimental data in the literature for this reaction due to the very small abundance (0.56%) of ^{84}Sr. Only Qaim[37] has measured this reaction cross section previously, and the present values agree with his data very well.

3.25 ^{84}Sr (n, np) ^{83}Rb (Fig. 3.29)

In addition to the ^{84}Sr (n, np) ^{83}Rb reaction, ^{83}Rb is produced via decay of ^{83}Sr, which is the product of ^{84}Sr (n, 2n) ^{83}Sr. Since the half-life (86.2days) of ^{83}Rb is much longer than that (32.4hours) of ^{83}Sr, the gamma-rays emitted from ^{83}Rb was measured after ^{84}Sr decayed completely to ^{83}Rb. The reaction-rates for ^{84}Sr (n, 2n) ^{83}Sr + ^{84}Sr (n, np) ^{83}Rb were deduced from the ^{83}Rb activity. The reaction-rates for ^{84}Sr (n, np) ^{83}Rb were then obtained by subtracting the reaction rate for ^{84}Sr (n, 2n) ^{83}Sr, which was deduced separately. In this method. the final errors of the reaction-rates are quite large because of the subtraction of almost equal values. Moreover, the large error (±10%) of the branching ratio for the gamma-ray emitted from ^{83}Rb adds to the total error. Only Qaim[31] has previously measured this reaction cross section. Since he employed chemical separation of ^{83}Rb, the error in his value is small. The present data are consistent with his result even though the errors of present values are large.

3.26 ^{86}Sr (n, 2n) ^{85m}Sr (Fig. 3.30)

The present data agree with data reported by Fang[59], Dabek[60], Minetti[55] and Rieder[61], while values measured by Rao[62], Bormann[36], Eapen[63] and Husain[54] are much higher than the present data.

3.27 ^{86}Sr (n, 2n) $^{85m+g}$Sr (Fig. 3.31)

The present data agree with results reported by Molla[35], Holub[57], Bormann[36], Rieder[61] and Vonach[64]. Although the measured values of Araminowicz[27], Husain[54], Csikai[65] and Strohal[66] are mutually consistent, they are smaller by 30% than the present results. Those values reported by Fang[59] and Minetti[55] are a little higher than ours, while their data for ^{86}Sr (n, 2n) ^{85m}Sr agree with the present results. JENDL-3 is higher by 10% than the present data.

3.28 ^{88}Sr (n, 2n) ^{87m}Sr (Fig. 3.32)

The value recently measured by Muyao[34] is rather higher than the present ones. Those results reported by Husain[54] and Minetti[55] are also higher than ours. This difference seems due to the fact that they adopted a value of 100% for branching ratio of 388.4 keV, whereas we adopted the value of 82% taken from the Table of Isotopes[7]. The value reported by Rao[62] is lower than the present results.

3.29 ^{89}Y (n, 2n) ^{88}Y (Fig. 3.33)

^{88}Y is commonly used as a standard gamma-ray source. This reaction is very attractive for dosimetry applications because of the relatively long half-life (106.61days) and the small spread of the measured

cross section data. There are already many experimental data reported, which are mutually consistent as well as in agreement with our values. JENDL–3 and ENDF/B–VI are also in good agreement with the present data. This reaction is strongly recommended to be included in the list of dosimetry reactions.

3.30 ^{92}Mo (n, np) ^{91m}Nb (Fig. 3.34)

The cross section data for this reaction were obtained in the same method as was used for ^{84}Sr (n, np) ^{83}Rb. ^{91m}Mo, which is produced in the (n, 2n) reaction, decays to ^{91m}Nb. The cross section data for ^{92}Mo (n, 2n) ^{91m}Mo, which were measured previously[6] at FNS, were adopted to subtract the (n, 2n) reaction contribution. Since the cross sections for ^{92}Mo (n, 2n) ^{91m}Mo are not so large compared with those of ^{92}Mo (n, np) ^{91m}Nb, the errors of the derived cross sections of ^{92}Mo (n, np) ^{91m}Nb are not too large. Qaim[31] and Liskien[67] previously measured this reaction cross section. The present data are consistent with the results of Liskien, while it seems that the value of Qaim is too small.

3.31 ^{96}Ru (n, 2n) ^{95}Ru (Fig. 3.35)

The present data agree with values reported by Muyao[34], Alford[68] and Lu[69]. The results measured by Bormann[70] and Rieder[61] are much higher than ours. JENDL–3 is also higher than the present data because JENDL–3 is based on the data of Bormann. The result reported by Chaturverdi[71] is slightly higher than the present data.

3.32 ^{96}Ru (n, p) $^{96m+g}$Tc (Fig. 3.36)

Very few data have been previously reported. The present values are consistent with data in the literature, although the result reported by Gray[72] is a little bit higher. The discrepancy between the present data and JENDL–3 increases as the neutron energy increases, while JENDL–3 agrees with the present values below 14 MeV.

3.33 ^{96}Ru (n, np) ^{95m}Tc (Fig. 3.37) and ^{96}Ru (n, np) ^{95g}Tc (Fig. 3.38)

The cross section values for these reactions were obtained by the same method as described in ^{84}Sr (n, np) ^{83}Rb. It was assumed that ^{95}Ru decays to ^{95m}Tc and ^{95g}Tc with branching ratios of 2.6 and 97.4% [7], respectively. The isomeric transition of ^{95m}Tc to ^{95g}Tc was neglected because of the long half–life (61 days) and small isomeric transition ratio (3.9%) of ^{95m}Tc. Since the error of the gamma–ray branching ratio of ^{95}Ru is small (1.4%), the errors of the derived cross sections for ^{96}Ru (n, np) ^{95m}Tc and ^{96}Ru (n, np) ^{95g}Tc are not so large in comparison with those in ^{84}Sr (n, np) ^{83}Rb. Only Lu[73] has measured these reaction cross sections previously. The present data are consistent with his result for ^{96}Ru (n, np) ^{95m}Tc, while our values are much smaller than his for ^{96}Ru (n, np) ^{95g}Tc.

3.34 ^{99}Ru (n, p) ^{99m}Tc (Fig. 3.39)

Natural samples were used in this measurement. The present results include the contribution of ^{100}Ru (n, np) ^{99m}Tc. There are only two previously reported values and the contribution of ^{100}Ru (n, np) ^{99m}Tc is included in those cross sections, too. Our results agree with data in the literature.

3.35 ^{102}Pd (n, 2n) ^{101}Pd (Fig. 3.40)

The present data are in good agreement with values measured by Muyao[34], Augustyniak[74], White[75]

and Bormann[70]. Since Lu[69] adopted 30% (instead of 18% as given in the Table of Isotopes[7]) for the 296.29 keV gamma-ray branching ratio, his value is about half of the present ones. It seems that Chaturverdi[71], Araminowicz[27] and Temperley[76] also used almost the same branching ratio as that used by Lu, since their results show the same tendency as that of Lu. The JENDL-3 values are smaller by 15% than our results.

3.36 ^{102}Pd (n, np) ^{101m}Rh (Fig. 3.41)

The cross sections were measured for the first time in the present study. The present results were obtained by the same method as described in ^{84}Sr (n, np) ^{83}Rb. The rather large error of $\pm$5.5% for the gamma-ray branching ratio of ^{101m}Pd leads to substantial errors for the derived ^{102}Pd (n, np) ^{101m}Rh cross sections.

3.37 ^{105}Pd (n, p) $^{105m+g}$Rh (Fig. 3.42)

Natural samples were used in this measurement. The present data include a contribution from ^{106}Pd (n, np) $^{105m+g}$Rh. Only two experimental results have been reported previously. The present data agree with data reported by Lu[73], while the value of Prasad[77] is a little higher than ours. JENDL-3 results are lower by 15% than our present data, as similarly observed for ^{102}Pd (n, 2n) ^{101}Pd.

3.38 ^{106}Pd (n, p) ^{106m}Rh (Fig. 3.43)

Natural samples were used in this measurement. Data from the literature, except the value of Goncalves[78], are a little bit smaller than the present results.

3.39 ^{108}Pd (n, α) ^{105}Ru (Fig. 3.44)

The errors in the present data are large because of poor gamma-ray counting statistics. However, data from the literature are consistent with our results. They support JENDL-3.

3.40 ^{107}Ag (n, 2n) ^{106m}Ag (Fig. 3.45)

There are a wealth of experimental data in the literature, and the present results are in reasonable agreement with those values.

3.41 ^{106}Cd (n, 2n) ^{105}Cd (Fig. 3.46)

The present values are small compared with all other results in the literature. It seems that the data of Bormann[79] are too large, according to the systematics of the (n, 2n) reaction described in section 4. The value of Weigel[80] includes a contribution from the cross section of ^{106}Cd (n, np) ^{105}Ag. JENDL-3 values are also higher by 70% than the present results.

3.42 ^{106}Cd (n, p) ^{106m}Ag (Fig. 3.47)

Though the errors of the present data are large due to poor gamma-ray counting statistics, their values are consistent with those from the literature.

3.43 ^{106}Cd (n, np) ^{105}Ag (Fig. 3.48)

The cross section data for this reaction were obtained by the same method as that adopted for ^{84}Sr (n, np) ^{83}Rb. The large error of $\pm$9.9% for the gamma-ray branching ratio of ^{105}Cd dominates the errors of the derived cross sections of ^{106}Cd (n, np) ^{105}Ag. Only Lu[81] has measured this reaction previously. Since he adopted chemical separation of ^{105}Ag, the error in his value is small. The present data are consistent with his result.

3.44 ^{110}Cd (n, p) ^{110m}Ag (Fig. 3.49)

Natural samples were used in this measurement. The present results include a contribution from ^{111}Cd (n, np) ^{110m}Ag. The present data are noticeably small compared with the value of Kayashima[82].

3.45 ^{112}Cd (n, p) ^{112}Ag (Fig. 3.50)

Natural samples were used in this measurement. The present results include a contribution from ^{113}Cd (n, np) ^{112}Ag. Although values from the literature are somewhat scattered, the present data are consistent with them. The present results also support JENDL-3.

3.46 ^{113}Cd (n, p) ^{113}Ag (Fig. 3.51)

Natural samples were used in this measurement. The present results include a contribution from ^{114}Cd (n, np) ^{113}Ag. The present data are noticeably high compared with other values in the literature. JENDL-3 is smaller by a factor of 2 than the present values. Although the present data agree with ENDF /B-V at 13.3MeV, they become more discrepant as the neutron energy increases.

3.47 ^{113}In (n, 2n) ^{112m}In (Fig. 3.52)

The present data are in reasonable agreement with data in the literature.

3.48 ^{113}In (n, n′) ^{113m}In (Fig. 3.53)

This reaction is attractive for dosimetry applications because of the low threshold energy of 392keV. The present data are consistent with values reported by Demekhin[83], Reggoug[84] and Santry[85], while data from Ryves[86], Decowski[87] and Kozlowski[88] are considerably smaller than the present results. The reason for the discrepancy between the present data and the data of Decowski is that he obtained the cross section using a value of 100% for the gamma-ray branching ratio of 392.70keV, instead of 64%[7] which was employed in the present measurement.

3.49 ^{115}In (n, n′) ^{115m}In (Fig. 3.54)

This reaction is one of the most important standards in dosimetry applications. The present data support the values from JENDL-3 and ENDF/B-V. Although the data of Pepelink[47], Garlea[89] and Reggoug[84] are consistent each other, their values are larger by 20% than the present ones. Data recently measured by Csikai[90] and Guo[91] are smaller by 7% than ours. More experimental data are required to resolve this discrepancy.

3.50 ^{115}In (n, p) ^{115m}Cd (Fig. 3.55) and ^{115}In (n, p) ^{115g}Cd (Fig. 3.56)

For ^{115}In (n, p) ^{115m}Cd, the data reported by Leshchenko[92] and Levkovskij[13] are smaller than our results.

Since there is no transition from ^{115m}Cd to ^{115g}Cd, it is not necessary to consider the contribution from ^{115}In (n, p) ^{115m}Cd in the cross section determination for ^{115}In (n, p) ^{115g}Cd. The present values are consistent with the reported experimental data of ^{115}In (n, p) ^{115g}Cd.

3.51 ^{115}In (n, α) ^{112}Ag (Fig. 3.57)

The rather large uncertainties of the preset results are due to an error ($\pm$11.9%) in the gamma-ray branching ratio. Data from the literature are in agreement with the present results. JENDL-3 is also consistent with the present data.

3.52 ^{130}Ba (n, 2n) $^{129m+g}$Ba (Fig. 3.58)

Since the gamma-ray branching ratio for ^{129}Ba is unknown, gamma-rays emitted from daughter nuclei ^{129}Cs were measured. In this case, the reaction rate RR, was deduced using the following equations,

$$RR=\frac{A \cdot C \cdot (\lambda_2-\lambda_1)}{W \cdot a \cdot N_A \cdot \varepsilon_f \cdot b \cdot \lambda_1 \cdot \lambda_2 \cdot g}\ , \tag{3}$$

$$g=\frac{(1-e^{-\lambda_1 \cdot t_i}) \cdot e^{-\lambda_1 \cdot t_c} \cdot (1-e^{-\lambda_1 \cdot t_m})}{\lambda_1^2} - \frac{(1-e^{-\lambda_2 \cdot t_i}) \cdot e^{-\lambda_2 \cdot t_c} \cdot (1-e^{-\lambda_2 \cdot t_m})}{\lambda_2^2}\ , \tag{4}$$

where,

A : target nuclide atomic weight,
C : gamma-ray photopeak count,
λ_1 : decay constant of the mother nucleus,
λ_2 : decay constant of the daughter nucleus,
F : correction factor,
W : sample weight,
a : target nuclide isotopic abundance,
N_A : Avogadro's number (6.022045×10^{23}),
ε_f : detector efficiency,
b : gamma-ray branching ratio,
t_i : irradiation time,
t_c : cooling time,
t_m : measuring time.

Note that ^{129}Cs is also produced via the ^{130}Ba (n, np) reaction. The contribution of the (n, np) reaction was, however, neglected since the (n, np) reaction cross section was expected to be small, about several mb according to the systematics of (n, np) reaction cross sections as described in section 4. Only Lu[69] measured this reaction cross section previously. The present data agree with his data which also included the contribution from the (n, np) reaction. Although JENDL-3 is based on data of Lu, it is lower by 10% than the present data.

3.53 ^{132}Ba (n, 2n) $^{131m+g}$Ba (Fig. 3.59)

Only Lu[69] has measured this reaction cross secsion previously. The present data agree with his result as in the case for ^{130}Ba (n, 2n) $^{129m+g}$Ba. JENDL–3 is consistent with the present data.

3.54 ^{132}Ba (n, p) ^{132}Cs (Fig. 3.60)

The errors of the present data are large due to poor gamma–ray counting statistics. Since the natural abundance of ^{132}Ba is very small (0.101%), and this cross section is expected to be small, no experimental data have been reported. The present data are in agreement, within errors, with JENDL–3.

3.55 ^{134}Ba (n, 2n) ^{133m}Ba (Fig. 3.61)

Though we previously measured the cross section for this reaction using samples with natural abundance[6], we have measured this cross section again using enriched isotope samples with 63.90% abundance of ^{134}Ba. The present data are consistent with the previously measured results[6]. The present data agree well with values from the literature.

3.56 ^{134}Ba (n, 2n) $^{133m+g}$Ba (Fig. 3.62)

The cross sections of this reaction were measured for the first time in this study. There have been no experimental data produced due to difficulties in the activity measurements due to the small natural abundance (2.417%) of ^{134}Ba and the long half–life (10.66years) of ^{133}Ba. JENDL–3 is slightly lower than the present data.

3.57 ^{151}Eu (n, 2n) ^{150A}Eu (Fig. 3.63)

^{150A}Eu stands for the meta–stable state of ^{150}Eu whose half–life is 12.55 hours. The errors of the present data are rather large due to a large uncertainty ($\pm$17.9%) of gamma–ray branching ratio. The present data are in good agreement with corresponding results in the literature.

3.58 ^{151}Eu (n, 2n) ^{150B}Eu (Fig. 3.64)

^{150B}Eu stands for the meta–stable state of ^{150}Eu whose half–life is 35.8years. Qaim[93] and Nethaway[94] previously measured this reaction cross section. The present data are in good consistency with their results.

3.59 ^{151}Eu (n, α) ^{148m}Pm (Fig. 3.65)

The errors of the present data are rather large due to poor gamma–ray counting statistics. Only Qaim[95] has measured this reaction cross section previously. The present data agree with his result.

3.60 ^{153}Eu (n, 2n) ^{152m1}Eu (Fig. 3.66) and ^{153}Eu (n, 2n) ^{152m2}Eu (Fig. 3.67)

^{152m1}Eu stands for the meta–stable state of ^{152}Eu whose half–life is 9.30hours. ^{152m2}Eu stands for the meta–stable state of ^{152}Eu whose half–life is 96minutes. ^{152m2}Eu does not decay to ^{152m1}Eu. The present data are in agreement with the value reported by Bari[96], while the value from Qaim[93] is much larger than the present results for ^{153}Eu (n, 2n) ^{152m1}Eu. Contrary to the cross section for ^{153}Eu (n, 2n) ^{152m1}Eu, the

present results for ^{153}Eu (n, 2n) ^{152m2}Eu are in agreement with the data of Qaim[93], while the value of Bari[97] is much smaller than the present results. The value reported by Pruys[98] is much higher than the present data because he adopted 500mb for the cross section of the monitor reaction ^{153}Eu (n, 2n) ^{152m1}Eu, which is higher by 66% than the present measurement.

3.61 ^{153}Eu (n, 2n) $^{152m2+g}$Eu (Fig. 3.68)

^{152m2}Eu decays only to ^{152g}Eu. We obtained the sum of the cross section of ^{153}Eu (n, 2n) ^{152m2}Eu and ^{153}Eu (n, 2n) ^{152g}Eu since we measured the gamma-ray emitted from ^{152g}Eu after ^{152m2}Eu completely decayed to ^{152g}Eu. The present data are lower than the result of Qaim[93], which is the only one data point so far reported.

3.62 ^{153}Eu (n, p) ^{153}Sm (Fig. 3.69)

The present data agree with results reported by Bari[99] and Qaim[100], while the value reported by Pruys[98] is much higher than the present data. This is because of the large cross section for the monitor reaction, as pointed out in regard to the cross section of ^{153}Eu (n, 2n) ^{152m2}Eu. The result of Coleman[101] is also much higher than the present data. JENDL-3 is higher by 30% than the present data, while ENDF /B-V is much close to the present results.

3.63 ^{153}Eu (n, α) ^{150}Pm (Fig. 3.70)

The present data agree within the experimental errors with the value of Qaim[95], while the value of Pruys[98] is higher than the present ones. JENDL-3, which is based on the data of Qaim, is slightly higher than the present results. On the other hand, ENDF/B-V, which is based on data of Khurana[102], is higher by a factor of 5 than the present results.

3.64 ^{159}Tb (n, p) ^{159}Gd (Fig. 3.71)

The present data agree quite well with the value reported by Bari[99], while the results reported by Qaim[103] and Havlik[104] are a little bit smaller. The value of Bramlitt[105] is much smaller than our data. JENDL-3 gives values which are 20% smaller than the present data.

3.65 ^{169}Tm (n, 2n) ^{168}Tm (Fig. 3.72)

There are many previously reported experimental data and they are all reasonably consistent with the present results. This reaction is strongly recommended as a dosimetry reaction because the half-life of ^{168}Tm is conveniently long (93.1days) and the cross section is almost flat around 14MeV region.

3.66 ^{178}Hf (n, α) ^{175}Yb (Fig. 3.73)

The errors of the present data are rather large due to the large error ($\pm$16.7%) of the gamma-ray branching ratio. The values reported by Qaim[95] and Coleman[101] are slightly smaller than our results. JENDL-3 is significantly smaller by a factor of ten than the present data. A re-evaluation of this cross section is recommended.

3.67 ^{179}Hf (n, p) ^{179}Lu (Fig. 3.75)

This cross section was measured for the first time in the present study. The rather large errors of the present data are attributable to the large uncertainty (±21.6%) of the gamma-ray branching ratio. ENDF/B-VI is slightly lower than the present values, while JENDL-3 is about one third of the present results.

3.68 ^{179}Hf (n, n′) ^{179m2}Hf (Fig. 3.74) and ^{180}Hf (n, 2n) ^{179m2}Hf (Fig. 3.76)

These two reactions lead to the same radioactivity, ^{179m2}Hf. The contributions of ^{179}Hf (n, n′) ^{179m2}Hf and ^{180}Hf (n, 2n) ^{179m2}Hf were separated from each other using enriched isotope samples of ^{179}Hf (73.70%) and ^{180}Hf (96.20%). These reactions are both measured for the first time in the present study.

3.69 ^{180}Hf (n, n′) ^{180m}Hf (Fig. 3.77)

Only one experimental value, reported by Hillman[106], is available. The present data are in good agreement with his result.

3.70 ^{180}Hf (n, α) ^{177}Yb (Fig. 3.78)

The large errors of the present data are due to the large uncertainty (±19.6%) of the gamma-ray branching ratio as well as poor gamma-ray counting statistics. Only one experimental value reported by Hillman[106] is available. By comparison with the cross section for ^{180}Hf (n, n′) ^{180m}Hf, his result is much higher than ours. JENDL-3 is much smaller than the present results.

3.71 ^{185}Re (n, 2n) ^{184m}Re (Fig. 3.79) and ^{185}Re (n, 2n) ^{184g}Re (Fig. 3.80)

^{184m}Re decays to ^{184g}Re with the isomeric transition ratio of 74.7%. The cross sections of ^{185}Re (n, 2n) ^{184g}Re were obtained by subtracting the ^{185}Re (n, 2n) ^{184m}Re contribution. Only Druzhinin[107] has measured the cross sections of these reactions previously. His data are in consistent with ours for both reactions, although his errors are rather large for ^{185}Re (n, 2n) ^{184m}Re. Recently, rhenium has become important as a component of a tungsten alloy which has been proposed as a coating material for the divertor plate of a fusion reactor. The present data are important for the estimation of induced activities.

3.72 ^{187}Re (n, p) ^{187}W (Fig. 3.81)

The errors for the present data are rather large due to poor gamma-ray counting statistics. These results are slightly higher than those reported by Qaim[37] and Coleman[101].

3.73 ^{187}Re (n, α) ^{184}Ta (Fig. 3.82)

Only one experimental value has been reported by Coleman[101]. His result is much larger than our data, in contradiction to the situation for ^{187}Re (n, p) ^{187}W.

3.74 ^{188}Os (n, p) ^{188}Re (Fig. 3.83)

Natural samples were used in this measurement. The present data include a contribution from ^{189}Os (n, np) ^{188}Re. The errors of the present data are rather large mainly due to poor gamma-ray counting

statistics. Results reported by Qaim[37], Kovacs[108] and Csikai[109] are a little bit larger than ours.

3.75 ^{192}Os (n, 2n) $^{191m+g}$Os (Fig. 3.84)

The errors of present data are rather large mainly due to the uncertainty ($\pm$7.7%) of the gamma–ray branching ratio. The present data included a contribution from ^{190}Os (n, γ) $^{191m+g}$Os. These data are in reasonable agreement with values in the literature.

3.76 ^{191}Ir (n, 2n) ^{190m2}Ir (Fig. 3.85)

^{190m2}Ir stands for the meta–stable state of ^{190}Ir whose half–life is 3.25 hours. In the activity measurement for ^{190m2}Ir, gamma–rays emitted from the daughter nucleus ^{190m}Os following ^{190m2}Ir decay were measured. The reaction rates were deduced using the same equations as given in section 3.52 for ^{130}Ba (n, 2n) $^{129m+g}$Ba. Although the deduced cross section includes a component from the (n, np) reaction, this contribution is negligibly small since the (n, np) reaction cross section is only expected to be a few mb value, according to the systematics described in section 4. The present results agree with the value reported by Temperley[76], while the data reported by Qaim[28] and Bormann[70] are both higher by 30% than ours.

3.77 ^{191}Ir (n, 2n) $^{190m1+m2+g}$Ir (Fig. 3.86)

^{190m1}Ir stands for the meta–stable state of ^{190}Ir whose half–life is 1.2 hours. There is a 5% isomeric transition between ^{190m2}Ir and ^{190m1}Ir. ^{190m1}Ir decays to the ground state with a 100% isomeric transition. Since we measured the gamma–ray emitted from the decay of ^{190g}Ir after ^{190m2}Ir and ^{190m1}Ir decayed away completely, we therefore obtained the sum of the cross sections for ^{191}Ir (n, 2n) ^{190m2}Ir, ^{191}Ir (n, 2n) ^{190m1}Ir and ^{191}Ir (n, 2n) ^{190g}Ir. The present values agree with data reported by Bayhurst[110], Qaim[28] and Temperley[76].

3.78 ^{193}Ir (n, 2n) ^{192}Ir (Fig. 3.87)

The contribution from ^{191}Ir (n, γ) ^{192}Ir was included in the present result. Our values agree with data reported by Bayhurst[110], Qaim[28] and Temperley[76], while that of Druzhinin[111] is smaller by 15% than ours.

3.79 ^{232}Th (n, 2n) ^{231}Th (Fig. 3.88)

The major source of errors of the present data are due to an uncertainty of $\pm$7.8% for the gamma –ray branching ratio. Values from the literature, except for the result of Zysin[112], are consistent with the present data within the errors. Our results support ENDF/B–V, while JENDL–3 is smaller by 20% than the present values.

3.80 ^{238}U (n, 2n) ^{237}U (Fig. 3.89)

The present results are in good agreement within the errors with data from the literature. The present values support both JENDL–3 and ENDF/B–VI.

4. Systematics of the reaction cross sections

To date, we have measured neutron activation cross sections for one hundred ninety eight reactions, including the previously measured data[6]. Based on the results obtained in the present study, we have examined the systematic trends for (n, p), (n, np), (n, α) and (n, 2n) reaction cross sections.

4.1 (n, p) reaction

Cross sections at 14.9 MeV are plotted in Fig. 4.1 as a function of asymmetry parameter S= (N–Z) /A, where N, Z and A are neutron, proton and mass numbers of the target nuclei, respectively. It is evident that the cross section decreases as the asymmetry parameter increases. Using the present data, the systematic trend is expressed by a simple formula based on the statistical model, given as,

$$\sigma_{(n,p)}=31.42 \cdot (A^{\frac{1}{3}}+1)^2 \cdot exp\,(-29.07 \cdot S)\ , \qquad (5)$$

where,

$\sigma_{(n,p)}$: (n, p) cross section at 14.9 MeV,
S : asymmetry parameter; (N–Z)/A.

The solid line in Fig. 4.1 is a plot of eq. (5). It is noted that the present results lie in a narrow band near the curve derived from eq. (5).

4.2 (n, np) reaction

There are not so many experimental data for the (n, np) reaction. The present data at 14.9 MeV are plotted in Fig. 4.2 as a function of the asymmetry parameter. The cross section decreases, in general, as the asymmetry parameter increases in the same as the (n, p) reaction. Moreover, as has already been pointed out by Qaim[31], it seems that the systematic behavior of the (n, np) reaction has two trends, one for the lightest stable nuclei and the other for the neutron richer nuclei. Using the present data, the systematic trends are expressed by simple formulas based on the statistical model, given as,

$$\sigma_{(n,np)}=68.46 \cdot (A^{\frac{1}{3}}+1)^2 \cdot exp\,(-25.08 \cdot S) \quad \text{for Sn}>\text{Sp, for group A} \qquad (6)$$

$$\sigma_{(n,np)}=22.05 \cdot (A^{\frac{1}{3}}+1)^2 \cdot exp\,(-36.91 \cdot S) \quad \text{for Sn}<\text{Sp, for group B} \qquad (7)$$

where,

$\sigma_{(n,np)}$: (n, np) cross section at 14.9 MeV,
Sn : neutron separation energy,
Sp : proton separation energy.

The solid lines in Fig. 4.2 are plots of eqs. (6) and (7). There is a clear difference in the trends between group A and B, with respect to separation energies for protons and neutrons. The present study confirms the validity of a systematic scheme with two groups, as proposed by Qaim.

4.3 (n, α) reaction

The present data at 14.9 MeV are plotted in Fig. 4.3 as a function of the asymmetry parameter. The systematic behavior for the (n, α) reaction is very similar to that for the (n, p) reaction. Using the present data, the systematic trend is expressed by the following formula,

$$\sigma_{(n,\alpha)}=24.37 \cdot (A^{\frac{1}{3}}+1)^2 \cdot exp\,(-34.88 \cdot S)\ , \tag{8}$$

where,

$\sigma_{(n,\alpha)}$: (n, α) cross section at 14.9 MeV.

The solid line in Fig. 4.3 is a plot of eq. (8). This formula is expected to be valid for estimation of non-radioactive helium production reaction yields in the structural materials of a fusion reactor.

4.4 (n, 2n) reaction

The systematic behavior for the (n, 2n) reaction cross section is shown in Fig. 4.4, where the present data are plotted as a function of the asymmetry parameter. In contrast to the (n, p), (n, α) and (n, np) reactions, the (n, 2n) reaction exhibits a profile where the cross section for the lighter mass region ($Z<30$) increases rapidly with increase of the asymmetry parameter and then becomes almost constant for heavy-mass nuclei ($A>100$). Using the present data, the systematics can be expressed by the following formula,

$$\ln\,(\sigma_{(n,2n)})=7.434 \cdot (1-1.484 \cdot \exp\,(-27.37 \cdot S))\ , \tag{9}$$

where,

$\sigma_{(n,2n)}$: (n, 2n) cross section at 14.9 MeV.

The solid line in Fig. 4.4 is a plot of eq. (9).

5. Summary

Neutron activation cross sections have been measured in the range 13.3–14.9 MeV for 89 reactions on the (n, 2n), (n, n′), (n, p), (n, np) and (n, α) processes of 24 elements. This study has been systematically conducted with a nearly constant set of experimental conditions, using the FNS facility. All the cross sections were normalized based on the cross section (464 mb) of ^{93}Nb (n, 2n) ^{92m}Nb. For each reaction, the measured data were then compared with those found in the literature, as well with evaluated nuclear data files, e. g. JENDL–3, ENDF/B–V and–VI. Cross section values for the eight reactions ^{73}Ge (n, np) ^{72}Ga, ^{74}Ge (n, np) ^{73}Ga, ^{102}Pd (n, np) ^{101m}Rh, ^{132}Ba (n, p) ^{132}Cs, ^{134}Ba (n, 2n) $^{133m+g}$Ba, ^{179}Hf (n, n′) ^{179m2}Hf, ^{179}Hf (n, p) ^{179}Lu and ^{180}Hf (n, 2n) ^{179m2}Hf were measured for the first time. For the fifteen reactions ^{68}Zn (n, np) ^{67}Cu, ^{84}Sr (n, p) $^{84m+g}$Rb, ^{84}Sr (n, np) ^{83}Rb, ^{96}Ru (n, np) ^{95m}Tc, ^{96}Ru (n, np) ^{95g}Tc, ^{106}Cd (n, np) ^{105}Ag, ^{110}Cd (n, p) ^{110m}Ag, ^{130}Ba (n, 2n) $^{129m+g}$Ba, ^{132}Ba (n, 2n) $^{131m+g}$Ba, ^{151}Eu (n, α) ^{148m}Pm, ^{180}Hf (n, n′) ^{180m}Hf, ^{180}Hf (n, α) ^{177}Yb, ^{185}Re (n, 2n) ^{184m}Re, ^{185}Re (n, 2n) ^{184g}Re and ^{187}Re (n, α) ^{184}Ta, where only one point data had been reported previously, the present experiment provides data with reasonable accuracy covering a relatively wide energy range. These results provide new input for consideration in the next versions of the evaluated nuclear data files, and for updating the cross section data libraries.

It is proposed that the reactions of ^{89}Y (n, 2n) ^{88}Y and ^{169}Tm (n, 2n) ^{168}Tm are to be included as new dosimetry reactions for D–T neutron flux determination. The cross sections for the low threshold reactions ^{64}Zn (n, p) ^{64}Cu, ^{113}In (n, n′) ^{113m}In and ^{115}In (n, n′) ^{115m}In were measured with adequate accuracy. It is suggested that the cross section of ^{64}Zn (n, p) ^{64}Cu around the 14 MeV energy region is to be re–evaluated because there appears to be a considerable overestimation in the current evaluations.

Better definition of the systematic trends of (n, p), (n, np), (n, α) and (n, 2n) reaction cross sections near 14 MeV could be established by the availability of a large body of consistent data provided by the present study. In particular, by focusing on the systematics for the (n, np) cross section at 14 MeV region, it was confirmed that there are two distinct trends corresponding to a difference of separation energy for protons and neutrons. The systematics for the (n, α) exhibits a general trend with respect to the asymmetry parameter [(N–Z)/A] even though there are relatively few data points. This formula is expected to be adequate for the estimation of helium production from non–radioactive reactions associated with structural materials of a fusion reactor. These results encouraged us to pursue a more refined formalization of the systematics of 14–MeV reactions in order to provide a more accurate estimation capability.

Acknowledgments

The authors gratefully acknowledge Mr. T. Nakamura, the ex-head of Fusion Neutronics Laboratory, for his great support throughout the experiment. They appreciate the contributions by students of Nagoya University in a part of measurements. They are indebted to Messrs. J. Kusano, C. Kutsukake, S. Tanaka and Y. Abe of Division of Reactor Physics Facilities for operation of the FNS accelerator. They also thank Dr. D. L. Smith, Argonne National Laboratory, for his critical review of this paper.

This work was done in part under the Cooperative Research Program between Japan Atomic Energy Research Institute and Nagoya University.

References

1) Shibata K., et al.: "Japanese Evaluated Nuclear Data Library, version-3", JAERI 1319 (1990).
2) "Evaluated Neutron Data File, ENDF/B-V, " ENDF/B Summary Documentation, Compiled by R. Kinsey, ENDF-201, 3rd Edition, Brookhaven National Laboratory (1979).
3) ENDF/B-VI Summary Documentation, Compiled by P. F. Rose, ENDF-201, 4th Edition, Brookhaven National Laboratory (1991).
4) Kocherov N. P., et al.: Proc. 7th ASTM EURATOM Symp. on Reactor Dosimetry, Strasbourg, France, Aug. 27-31, 1990, p. 357.
5) Nakamura T., et al.: Proc. 4th Symp. on Accelerator Sci. Tecnol., RIKEN, Saitama, Nov. 24-26, 1982, pp 155-156.
6) Ikeda Y., et al.: "Activation Cross Section Measurements for Fusion Reactor Structural Materials at Neutron Energy from 13.3 to 15.0 MeV Using FNS Facility," JAERI 1312 (1988).
7) Lederer C. M., Shiely V. S.(edited): "Table of Isotopes," 7th Edition, John Wiley and Sons, Inc. New York (1978).
8) Ikeda Y., et al.: J. Nucl Sci. Technol., to be published.
9) Nakagawa M., et al.: "MORSE-DD, A General Monte Carlo Code Using Multigroup Double Differential Form Cross-Sections," JAERI-M 84-126 (1984).
10) Greenwood L. R., et al.: Proc. 13th Int. Symposium (Part II) on Influence of Radiation on Material Properties, Philadelphia, ASTM STP 956 (1987), p. 743.
11) Bahal B. M., et al.: GKSS-84-E (1984).
12) Lees E. W., et al.: AERE-R-9390 (1979).
13) Levkovskij V. N., et al.: Jadernaya Fizika, **10** (1), 44 (1969).
14) Paulsen A., et al.: Nucleonik, **10**, 91 (1967).
15) Vonach H., et al.: Proc. a Specialists' Meeting on Neutron Activation Cross Sections for Fission and Fusion Energy Applications, ANL, USA, Sep. 13-15, 1989, p. 165.
16) Ribannski I., et al.: EXFOR 30811.004 (1985).
17) Viennot M., et al.: Proc. Int. Conf. on Nuclear Data for Science and Technology, Antwerp, Sep. 6 -10, 1982, p. 406.
18) Garuska U., et al.: INR-1871/I/PL/AU (1980).
19) Viennot M., et al.: EXFOR 30644.018 (1982).
20) Casanova J. L., et al.: Anales de Fisica y Quimica, **72**, (3), 186 (1976).
21) Sigg R.A.: Dissertation Abstracts sec. B, **37**, 2237, 7611 (1976).
22) Spangler R., et al.: Trans. Amer. Nucl. Soc., **22**, 818 (1975).
23) Santry D. C., et al.: Can. J. Phys., **50**, 2536 (1972).
24) Paulsen A., et al.: Kerntechnik, **26**, 34 (1975).
25) Bormann M., et al.: Nucl. Phys., **A 130**, 195 (1969).
26) Kayashima K., et al.: NEANDC (J) -61 U, 94 (1979).
27) Araminowicz J., et al.: INR-1464, 14 (1973).
28) Qaim S. M.: Nucl. Phys., **A 185**, 614 (1972).
29) Vinitskaja G. P., et al.: Jadernaya Fizika, **5**, (6), 1175 (1967).
30) Ranakumar N., et al.: Bull. Am. Phys. Soc., **13**, 602 (DE 7) (1968).
31) Qaim S. M.: Nucl. Phys., **A 382**, 255 (1982).
32) Qaim S. M.: Proc. Conf. on Chemical Nuclear Data, Measurements and Applicat., Univ. of Kent, Canterbury, Sep. 20-22, 1971, p. 121.

33) Hoang H. M., et al.: Z. Phys., **A 342**, 283 (1992).
34) Muyao Z., et al.: Chinese J. of Nucl. Phys., **9**, 34 (1987).
35) Molla N. T., et al.: INDC (BAN)–002, 1 (1983).
36) Bormann M., et al.: Z. Phys., **A 277**, 203 (1976).
37) Qaim S. M.: Nucl. Phys., **A 283**, 269 (1977).
38) Vinitskaya G. P.: EXFOR 40009.013 (1968).
39) Rieppo R., et al.: J. Inorg. Nucl. Chem., **38**, 1927 (1976).
40) Wood R. E.: Phys. Rev., **154**, 1108 (1967).
41) Prasad P. R., et al.: Nucl. Phys., **A 138**, 85 (1969).
42) Rao P. V., et al.: Phys. Rev., **C 3**, 629 (1971).
43) Bormann M.: Proc. First IAEA Conf. on Nuclear Data for Reactors, Paris, Oct. 17–21, 1966, part 1, p. 225.
44) Bayhurst B. P., et al.: J. Inorg. Nucl. Chem., **23**, 173 (1961).
45) Gupta J. P., et al.: Pramana, **24**, 637 (1985).
46) Grochulski W, et al.: Acta Physica Polonica sec. B, **6**, 139 (1975).
47) Pepelink R., et al.: NEANDC (E)–262 U (5), 32 (1985).
48) Reggoug A., et al.: Univ. Mohammed V, Rabat, annual reports–5, 14 (1982).
49) Schwere O., et al.: Oesterr. Akad. Wiss., **113**, 153 (1976).
50) Augustiniak W., et al.: Acta Physica Polonica sec. **B**, **7**, 347 (1976).
51) Erlandsson B., et al.: Physica Scripta, **19**, 3, 251 (1979).
52) Sothras S.: EXFOR 10835.006 (1977).
53) Ghorai S. K., et al.: Nucl. Phys., **A 223**, 118 (1974).
54) Husain H., et al.: Phys. Rev., **C 1**, 1233 (1970).
55) Minetti B., et al.: Nucl. Phys., **A 118**, 449 (1968).
56) Bormann M., et al.: EANDC (E)–150, 30 (1972).
57) Holub E., et al.: J. of Phys. pt. G, **2**, 405 (1976).
58) Bormann M., et al.: EANDC (E)–66, 42 (1966).
59) Fang M. H., et al.: High Energy Physics and Nuclear Physics, **7**, (5), 639 (1983).
60) Dabek M. H., et al.: J. of Radioanal. Chem., **46**, 357 (1978).
61) Rieder R., et al.: EANDC (OR)–38, 1 (1965).
62) Rao C. V. S., et al.: Proc. Nuclear Physics and Solid State Physics Sympos., Bombay, Dec. 28–31, 1978, part 2, p. 113.
63) Eapen P. K., et al.: J. Inorg. Nucl. Chem., **37**, 1121 (1975).
64) Vonach H., et al.: Oesterr. Akad. Wiss., **96**, 120 (1959).
65) Csikai J., et al.: Acta Physica Hungaria, **23**, 87 (1967).
66) Strohal F., et al.: Nucl. Phys., **30**, 49 (1962).
67) Liskien H., et al.: EXFOR 22125.004 (1989).
68) Alford W. L., et al.: Bull. Am. Phys. Soc., **19**, 1123 (FB 4) (1974).
69) Lu W. D., et al.: Phys. Rev., **C 1**, 350 (1970).
70) Bormann M., et al.: Nucl. Phys., **A 157**, 481 (1970).
71) Chaturverdi L., et al.: INDC (SEC)–61, 123 (1977).
72) Gray P. R., et al.: Nucl. Phys., **75**, 215 (1966).
73) Lu W. D., et al.: Phys. Rev., **C 1**, 358 (1970).
74) Augustyniak W., et al.: EXFOR 30444.002 (1971).
75) White R. L., et al.: Bull. Am. Phys. Soc., **17**, 687 (FD 10) (1972).
76) Temperley R. L., et al.: BRL–1491 (1970).
77) Prasad R., et al.: Nuovo Cimento sec. A, **3**, (3), 467 (1971).
78) Goncalves I. F., et al.: Intern. J. of Rad. Appl. and Inst., part A, **38**, (11), 989 (1987).

79) Bormann M., et al.: Nucl. Phys., **A 115**, 309 (1968).
80) Weigel H., et al.: Radiochimica Acta, **22**, 11 (1975).
81) Lu W. D., et al.: Radiochimica Acta, **12**, 61 (1969).
82) Kayashima K., et al.: NEANDC (J)–61 U, 94 (1974).
83) Demekhin V. L., et al.: Proc. 6th All Union Conference on Neutron Physics, Kiev, Oct. 2–6, 1983, part 3, p. 195.
84) Reggoug A., et al.: EXFOR 30643.017 (1982).
85) Santry D. C., et al.: Can. J. Phys., **54**, 757 (1976).
86) Ryves T. B., et al.: J. of Phys. pt. G, **9**, 1549 (1983).
87) Decowski P., et al.: Nucl. Phys., **A 204**, 121 (1973).
88) Kozlowski T., et al.: Acta Physica Polonica, **33**, 409 (1968).
89) Garlea I., et al.: INDC (ROM)–15 (1983).
90) Csikai J., et al.: Z. Phys., **A 337**, 39 (1990).
91) Guo F. P., et al.: INDC (CPR)–16 (1989).
92) Leschenko B. E., et al.: Proc. 1st Intern. Conf. on Neutron Physics, Kiev, Sep. 14–16, 1987, part 3, p. 327.
93) Qaim S. M.: Nucl. Phys., **A 224**, 319 (1974).
94) Nethaway D. R.: Nucl. Phys., **A 190**, 635 (1972).
95) Qaim S. M.: Radiochimica Acta, **35**, 9 (1984).
96) Bari A.: EXFOR 10431.004 (1971).
97) Bari A.: EXFOR 10431.005 (1971).
98) Pruys H. S., et al.: J. Inorg. Nucl. Chem., **37**, 1587 (1975).
99) Bari A., et al.: J. of Radioanal. Chem., **75**, 189 (1982).
100) Qaim S. M.: EXFOR 20933.008 (1974).
101) Coleman R. F., et al.: Proc. Phys. Soc. (London), **73**, 215 (1959).
102) Khurana C. S., et al.: Nucl. Phys., **69**, 153 (1965).
103) Qaim S. M.: Radiochem. and Radioanal. Letters, **25**, 335 (1976).
104) Havlik E.: Acta Physica Austriaca, **34**, 209 (1971).
105) Bramlitt E. T., et al.: Phys. Rev., **131**, 2649 (1975).
106) Hillman M., et al.: J. Inorg. Nucl. Chem., **31**, 909 (1969).
107) Druzhinin A. A., et al.: Jadernaya Fizika, **5** (1), 18 (1967).
108) Kovacs P., et al.: EXFOR 30290.010 (1975).
109) Csikai J., et al.: Nucl. Phys., **A 91**, 222 (1967).
110) Bayhurst B. P., et al.: Phys. Rev., **C 12**, 451 (1975).
111) Druzhinin A. A., et al.: Jadernaya Fizika, **14** (1), 682 (1971).
112) Zysin Y. A., et al.: Atomnaja Energija, **8**, 360 (1960).
113) Browne E. and Firestone R. B.: "Tables of Radioactive Isotopes", John Wiley and Sons, Inc. New York (1986).

Table1 List of measured reactions and associated decay data

Target Nucleus	Abundance [%]	Reaction**	Product	Half-life		Gamma-ray Energy [keV]	Branching Ratio [%]	Q-value*** [MeV]
^{60}Ni*	99.81	(n, p)	$^{60m+g}$Co	5.272±0.001	y	1332.47	100	−2.041
^{61}Ni*	88.84	(n, p)	^{61}Co	1.650±0.005	h	67.42	86±3	0.531
^{62}Ni*	98.83	(n, np)	^{61}Co	1.650±0.005	h	67.42	86±3	−11.137
^{63}Cu	69.10	(n, α)	$^{60m+g}$Co	5.272±0.011	y	1332.47	100	1.714
^{64}Zn*	99.85	(n, 2n)	^{63}Zn	38.0±0.1	m	669.42	8.4±0.4	−11.862
^{64}Zn*	99.85	(n, p)	^{64}Cu	12.699±0.008	h	511.00	38.6±1.4	0.208
^{66}Zn*	98.41	(n, 2n)	^{65}Zn	244.0±0.2	d	1115.52	50.75±0.10	−11.060
^{67}Zn*	94.60	(n, p)	^{67}Cu	62.01±0.14	h	184.53	47.0±3.3	0.208
^{68}Zn*	99.36	(n, np)	^{67}Cu	62.01±0.14	h	184.53	47.0±3.3	−9.900
^{68}Zn*	99.36	(n, α)	^{65}Ni	2.520±0.002	h	1481.84	23.5±0.8	0.765
^{70}Ge*	97.10	(n, 2n)	^{69}Ge	39.05±0.10	h	1106.40	27±3	−11.637
^{72}Ge*	97.80	(n, p)	^{72}Ga	14.12±0.02	h	833.95	95.6±0.2	−3.209
^{72}Ge*	97.80	(n, α)	^{69m}Zn	13.76±0.03	h	438.70	94.8±0.3	1.042
^{73}Ge*	74.30	(n, p)	^{73}Ga	4.86±0.03	h	297.32	79.8±2.3#	−0.781
^{73}Ge*	74.30	(n, np)	^{72}Ga	14.12±0.02	h	833.95	95.6±0.2	−9.992
^{74}Ge*	98.41	(n, np)	^{73}Ga	4.86±0.03	h	297.32	79.8±2.3#	−10.981
^{74}Ge*	98.41	(n, α)	^{71m}Zn	3.92±0.05	h	386.28	92±5	−0.609
^{75}As	100.00	(n, 2n)	^{74}As	17.79±0.05	d	595.90	60±2	−10.246
^{75}As	100.00	(n, p)	^{75}Ge	82.78±0.04	m	264.61	11.1±1.1	−0.395
^{75}As	100.00	(n, α)	^{72}Ga	14.12±0.02	h	833.95	95.6±0.2	1.204
^{85}Rb	72.17	(n, 2n)	^{84m}Rb	20.5±0.2	m	247.00	64.5±0.2	−10.942
^{85}Rb	72.17	(n, 2n)	$^{84m+g}$Rb	32.77±0.14	d	881.60	74±1	−10.478
^{85}Rb	72.17	(n, p)	^{85m}Kr	4.480±0.008	h	304.87	14.0±0.4	0.095
^{85}Rb	72.17	(n, α)	^{82}Br	35.344±0.013	h	776.49	83.4±0.9	0.986
^{87}Rb	27.83	(n, 2n)	$^{86m+g}$Rb	18.82±0.02	d	1077.20	8.79±0.09	−9.929
^{87}Rb	27.83	(n, p)	^{87}Kr	76.31±0.62	m	402.58	50±3	−3.106
^{84}Sr	0.56	(n, 2n)	^{83}Sr	32.4±0.20	h	762.70	30±3	−12.048
^{84}Sr	0.56	(n, p)	$^{84m+g}$Rb	32.77±0.14	d	881.59	74±1	−0.107
^{84}Sr	0.56	(n, np)	^{83}Rb	86.2±0.10	d	529.64	30±1.5	−9.016
^{86}Sr	9.80	(n, 2n)	^{85m}Sr	68.0±0.2	m	231.68	84.5±1.0	−11.489
^{86}Sr	9.80	(n, 2n)	$^{85m+g}$Sr	64.85±0.03	d	514.00	99.27±0.04	−11.728
^{88}Sr	82.60	(n, 2n)	^{87m}Sr	2.805±0.003	h	388.40	82±1	−11.502
^{89}Y	100.00	(n, 2n)	^{88}Y	106.61±0.02	d	898.02	91.3±0.7	−11.469
^{92}Mo*	97.37	(n, np)	^{91m}Nb	62	d	104.50	0.56	−7.564
^{96}Ru	5.50	(n, 2n)	^{95}Ru	1.65±0.02	h	336.40	71±1	−10.694
^{96}Ru	5.50	(n, p)	$^{96m+g}$Tc	4.35±0.4	d	778.22	99.1±0.1	0.528
^{96}Ru	5.50	(n, np)	^{95m}Tc	61±2	d	204.12	66.2±2.5	−7.351
^{96}Ru	5.50	(n, np)	^{95g}Tc	20.00±0.1	h	765.76	93±1	−7.390
^{99}Ru	12.70	(n, p)	^{99m}Tc	6.007±0.002	h	140.51	89.0±0.2	0.346
^{102}Pd	1.00	(n, 2n)	^{101}Pd	8.47±0.06	h	296.29	18±1	−10.568
^{102}Pd	1.00	(n, np)	^{101m}Rh	4.34±0.01	d	306.77	87±1	−7.961

*Separated isotope was used.

**(n, np) means (n, np)+(n, pn)+(n, d).

***Q-value for (n, np) was calculated for (n, np), not for (n, d).

Data were taken from Ref. 113.

Table1 (continued–1)

Target Nucleus	Abundance [%]	Reaction**	Product	Half–life		Gamma–ray Energy [keV]	Branching Ratio [%]	Q–value*** [MeV]
^{105}Pd	22.20	(n, p)	^{105}Rh	35.47±0.08	h	318.90	19±1	0.215
^{106}Pd	27.30	(n, p)	^{106m}Rh	130±2	m	450.80	24.4±0.4	−2.896
^{108}Pd	26.70	(n, α)	^{105}Ru	4.44±0.02	h	469.37	17.8±0.6	2.061
^{107}Ag	51.83	(n, 2n)	^{105m}Ag	8.5±0.1	d	450.98	28.47±0.70	−9.634
^{106}Cd	1.25	(n, 2n)	^{105}Cd	56.0±0.5	m	961.84	4.7±0.3	−10.866
^{106}Cd	1.25	(n, p)	^{106m}Ag	8.5±0.1	d	450.97	28.4±1.2	0.492
^{106}Cd	1.25	(n, np)	^{105}Ag	41.29±0.07	d	443.00	17.1±1.7	−7.345
^{110}Cd	12.50	(n, p)	^{110m}Ag	252.2±0.3	d	657.75	94.4±0.6	−2.229
^{112}Cd	24.10	(n, p)	^{112}Ag	3.14±0.02	h	617.40	42±5	−3.176
^{113}Cd	12.20	(n, p)	^{113}Ag	5.37±0.05	h	298.40	9.0	−1.228
^{113}In	4.30	(n, 2n)	^{112m}In	20.9±0.2	m	155.00	13±1	−9.443
^{113}In	4.30	(n, n′)	^{113m}In	99.47±0.07	m	392.70	64±1	−0.392
^{115}In	95.70	(n, n′)	^{115m}In	4.486±0.004	h	336.00	45.9±0.1	−0.336
^{115}In	95.70	(n, p)	^{115m}Cd	44.8±0.3	d	933.60	1.7	−0.503
^{115}In	95.70	(n, p)	^{115g}Cd	53.38±0.04	h	527.90	28.1±0.1	−0.330
^{115}In	95.70	(n, α)	^{112}Ag	3.14±0.02	h	617.40	42±5	3.061
^{130}Ba*	32.90	(n, 2n)	$^{129m+g}$Ba	2.20±0.05	h			−10.328
			^{129}Cs##	32.35±0.10	h	371.92	32±2	
^{132}Ba*	8.20	(n, 2n)	$^{131m+g}$Ba	12.0±0.1	d	123.73	28±1	−9.798
^{132}Ba*	8.20	(n, p)	^{132}Cs	6.474±0.014	d	667.50	97.5±0.2	−0.496
^{134}Ba*	63.90	(n, 2n)	^{133m}Ba	38.9±0.1	h	275.60	17.5±0.8	−9.758
^{134}Ba*	63.90	(n, 2n)	$^{133m+g}$Ba	10.66±0.12	y	356.01	62±1	−10.328
^{151}Eu*	97.70	(n, 2n)	^{150A}Eu	12.55±0.05	h	333.90	3.9±0.7	−7.965
^{151}Eu*	97.70	(n, 2n)	^{150B}Eu	35.8±1.0	y	333.90	94±3	−7.965
^{151}Eu*	97.70	(n, α)	^{148m}Pm	41.29±0.11	d	629.90	89.2±1.7	7.730
^{153}Eu*	99.20	(n, 2n)	^{152m1}Eu	9.30±0.05	h	344.31	2.14±0.10	−8.598
^{153}Eu*	99.20	(n, 2n)	^{152m2}Eu	96±1	m	89.85	72±1	−8.698
^{153}Eu*	99.20	(n, 2n)	$^{152m2+g}$Eu	13.2±0.3	y	344.31	27.2±0.4	−8.550
^{153}Eu*	99.20	(n, p)	^{153}Sm	46.8±0.1	h	103.18	28.3±1.2	−0.024
^{153}Eu*	99.20	(n, α)	^{150}Pm	2.68±0.02	h	333.92	73± 4	5.834
^{159}Tb	100.00	(n, p)	^{159}Gd	18.56±0.08	h	363.30	10	−0.192
^{169}Tm	100.00	(n, 2n)	^{168}Tm	93.1±0.1	d	198.25	50±3	−8.034
^{178}Hf*	92.40	(n, α)	^{175}Yb	4.19±0.01	d	396.32	6±1	7.903
^{179}Hf*	73.70	(n, n′)	^{179m2}Hf	24.8±0.3	d	453.49	65±4	−1.106
^{179}Hf*	73.70	(n, p)	^{179}Lu	4.59±0.06	h	214.33	11.6±2.5	−0.570
^{180}Hf*	96.20	(n, 2n)	^{179m2}Hf	24.8±0.3	d	453.49	65±4	−8.494
^{180}Hf*	96.20	(n, n′)	^{180m}Hf	5.5±0.1	h	332.07	94.4±0.2	−1.142
^{180}Hf*	96.20	(n, α)	^{177}Yb	1.88±0.1	h	150.60	19.9±3.6	6.853
^{185}Re	37.40	(n, 2n)	^{184m}Re	169±8	d	104.73	13.73±0.64	−7.870
^{185}Re	37.40	(n, 2n)	^{184g}Re	38.0±0.5	d	112.07	17.21±0.85	−7.682
^{187}Re	62.60	(n, p)	^{187}W	23.85±0.08	h	479.53	21	−0.530

*Separated isotope was used.

**(n, np) means (n, np)+(n, pn)+(n, d).

***Q–value for (n, np) was calculated for (n, np), not for (n, d).

daughter nucleus ^{129}Cs of $^{129m+g}$Ba was measured.

Table1 (continued-2)

Target Nucleus	Abundance [%]	Reaction**	Product	Half-life		Gamma-ray Energy [keV]	Branching Ratio [%]	Q-value*** [MeV]
^{187}Re	62.60	(n, α)	^{184}Ta	8.7±0.1	h	414.01	74±1	7.262
^{188}Os	13.30	(n, p)	^{183}Re	16.98±0.02	h	155.04	15.2±0.5	−1.337
^{192}Os	41.00	(n, 2n)	$^{191m+g}$OS	15.4±0.1	d	129.52	26±2	−7.558
^{191}Ir	38.50	(n, 2n)	^{190m2}Ir	3.25±0.20	h			−8.069
			^{190m}Os###	9.9±0.1	m	616.50	98.6±1.0	
^{191}Ir	38.50	(n, 2n)	$^{190m1+m2+g}$Ir	11.78±0.10	d	371.24	22.7±2.2	−8.249
^{193}Ir	61.50	(n, 2n)	^{192}Ir	74.17±0.07	d	316.50	82.9±0.1	−7.764
^{232}Th	100.00	(n, 2n)	^{231}Th	25.52±0.01	h	84.21	7.8±0.6	−6.436
^{238}U*	99.27	(n, 2n)	^{237}U	6.752±0.002	d	208.01	23	−6.153

*Separated isotope was used.

**(n, np) means (n, np)+(n, pn)+(n, d).

***Q-value for (n, np) was calculated for (n, np), not for (n, d).

daughter nucleus ^{190m}Os of ^{190m2}Ir was measured.

Table2 List of chemical properties, weights, thicknesses and abundances of samples

Target Nucleus	Chemical Form	Weight [mg]	Thickness** [mm]	Abundance [%]
^{60}Ni*	Ni: powder	90	1.9	^{58}Ni: 0.19, ^{60}Ni: 99.81
^{61}Ni*	Ni: powder	30	1.0	^{58}Ni: 3.45, ^{60}Ni: 6.12, ^{61}Ni: 88.84, ^{62}Ni: 1.40, ^{63}Ni: 0.20
^{62}Ni*	Ni: powder	30	1.0	^{58}Ni: 0.32, ^{60}Ni: 0.63, ^{61}Ni: 0.13, ^{62}Ni: 98.83, ^{63}Ni: 0.09
^{63}Cu	Cu: metal	700	1.0	natural(^{63}Cu: 69.10, ^{65}Cu: 30.90)
^{64}Zn*	ZnO: powder	40	1.0	^{64}Zn: 99.85, ^{66}Zn: 0.15
^{66}Zn*	ZnO: powder	40	1.0	^{64}Zn: 0.86, ^{66}Zn: 98.41, ^{67}Zn: 0.20, ^{68}Zn: 0.53
^{67}Zn*	ZnO: powder	30	1.0	^{64}Zn: 1.11, ^{66}Zn: 1.95, ^{67}Zn: 94.60, ^{68}Zn: 2.28, ^{70}Zn: 0.05
^{68}Zn*	ZnO: powder	40	1.0	^{64}Zn: 0.32, ^{66}Zn: 0.21, ^{67}Zn: 0.10, ^{68}Zn: 99.36, ^{70}Zn: 0.01
^{70}Ge*	GeO_2: powder	35	1.0	^{70}Ge: 97.10, ^{72}Ge: 1.18, ^{73}Ge: 0.27, ^{74}Ge: 1.20, ^{76}Ge: 0.25
^{72}Ge*	GeO_2: powder	35	1.0	^{70}Ge: 0.57, ^{72}Ge: 97.80, ^{73}Ge: 0.47, ^{74}Ge: 0.97, ^{76}Ge: 0.19
^{73}Ge*	GeO_2: powder	35	0.9	^{70}Ge: 3.10, ^{72}Ge: 6.00, ^{73}Ge: 74.30, ^{74}Ge: 14.60, ^{76}Ge: 2.00
^{74}Ge*	GeO_2: powder	40	0.9	^{70}Ge: 1.47, ^{72}Ge: 2.13, ^{73}Ge: 0.54, ^{74}Ge: 95.20, ^{76}Ge: 0.66
^{75}As	As_2O_3: powder	80	1.0	natural(^{75}As: 100)
^{85}Rb	RbCl: powder	80	1.5	natural(^{85}Rb: 72.17, ^{87}Rb: 27.83)
^{87}Rb	RbCl: powder	80	1.5	natural(^{85}Rb: 72.17, ^{87}Rb: 27.83)
^{84}Sr	SrF_2: powder	80	1.2	natural(^{84}Sr: 0.56, ^{86}Sr: 9.80, ^{87}Sr: 7.00, ^{88}Sr: 82.60)
^{86}Sr	SrF_2: powder	80	1.2	natural(^{84}Sr: 0.56, ^{86}Sr: 9.80, ^{87}Sr: 7.00, ^{88}Sr: 82.60)
^{88}Sr	SrF_2: powder	80	1.2	natural(^{84}Sr: 0.56, ^{86}Sr: 9.80, ^{87}Sr: 7.00, ^{88}Sr: 82.60)
^{89}Y	Y_2O_2: powder	50	1.2	natural(^{89}Y: 100)
^{92}Mo*	Mo: powder	60	1.2	^{92}Mo: 97.37, ^{94}Mo: 0.68, ^{95}Mo: 0.52, ^{96}Mo: 0.37, ^{97}Mo: 0.18, ^{98}Mo: 0.40, ^{100}Mo: 0.50
^{96}Ru	$RuCl_3$: powder	55	1.1	natural(^{96}Ru: 5.50, ^{98}Ru: 1.86, ^{99}Ru: 12.70, ^{100}Ru: 12.60, ^{101}Ru: 17.00, ^{102}Ru: 31.60, ^{104}Ru: 18.70)
^{99}Ru	$RuCl_3$: powder	55	1.1	natural(^{96}Ru: 5.50, ^{98}Ru: 1.86, ^{99}Ru: 12.70, ^{100}Ru: 12.60, ^{101}Ru: 17.00, ^{102}Ru: 31.60, ^{104}Ru: 18.70)
^{102}Pd	Pd: metal	130	0.1	natural(^{102}Pd: 1.00, ^{104}Pd: 11.00, ^{105}Pd: 22.20, ^{106}Pd: 27.30, ^{108}Pd: 26.70, ^{110}Pd: 11.80)

*Separated isotope was used.

**Included thickness of cartridge paper if powder.

Table2 (continued-1)

Target Nucleus	Chemical Form	Weight [mg]	Thickness** [mm]	Abundance [%]
^{105}Pd	Pd: metal	130	0.1	natural(^{102}Pd: 1.00, ^{104}Pd: 11.00, ^{105}Pd: 22.20, ^{106}Pd: 27.30, ^{108}Pd: 26.70, ^{110}Pd: 11.80)
^{106}Pd	Pd: metal	130	0.1	natural(^{102}Pd: 1.00, ^{104}Pd: 11.00, ^{105}Pd: 22.20, ^{106}Pd: 27.30, ^{108}Pd: 26.70, ^{110}Pd: 11.80)
^{108}Pd	Pd: metal	130	0.1	natural(^{102}Pd: 1.00, ^{104}Pd: 11.00, ^{105}Pd: 22.20, ^{106}Pd: 27.30, ^{108}Pd: 26.70, ^{110}Pd: 11.80)
^{107}Ag	Ag: metal	500	0.5	natural(^{107}Ag: 51.83, ^{109}Ag: 48.17)
^{106}Cd	Cd: metal	85	0.5	natural(^{106}Cd: 1.25, ^{108}Cd: 0.89, ^{110}Cd: 12.50, ^{111}Cd: 12.80, ^{112}Cd: 24.10, ^{113}Cd: 12.20, ^{114}Cd: 28.70, ^{116}Cd: 7.50)
^{110}Cd	Cd: metal	85	0.5	natural(^{106}Cd: 1.25, ^{108}Cd: 0.89, ^{110}Cd: 12.50, ^{111}Cd: 12.80, ^{112}Cd: 24.10, ^{113}Cd: 12.20, ^{114}Cd: 28.70, ^{116}Cd: 7.50)
^{112}Cd	Cd: metal	85	0.5	natural(^{106}Cd: 1.25, ^{108}Cd: 0.89, ^{110}Cd: 12.50, ^{111}Cd: 12.80, ^{112}Cd: 24.10, ^{113}Cd: 12.20, ^{114}Cd: 28.70, ^{116}Cd: 7.50)
^{113}Cd	Cd: metal	85	0.5	natural(^{106}Cd: 1.25, ^{108}Cd: 0.89, ^{110}Cd: 12.50, ^{111}Cd: 12.80, ^{112}Cd: 24.10, ^{113}Cd: 12.20, ^{114}Cd: 28.70, ^{116}Cd: 7.50)
^{113}In	In: metal	370	0.5	natural(^{113}In: 4.23, ^{115}In: 95.77)
^{115}In	In: metal	370	0.5	natural(^{113}In: 4.23, ^{115}In: 95.77)
^{130}Ba*	$BaCO_3$: powder	21	1.0	^{130}Ba: 32.90, ^{132}Ba: 0.40, ^{134}Ba: 4.63, ^{135}Ba: 6.23, ^{136}Ba: 6.21, ^{137}Ba: 7.18, ^{138}Ba: 42.45
^{132}Ba*	$BaCO_3$: powder	25	0.8	^{130}Ba: 0.10, ^{132}Ba: 8.20, ^{134}Ba: 10.80, ^{135}Ba: 11.00, ^{136}Ba: 8.60, ^{137}Ba: 9.60, ^{138}Ba: 51.70
^{134}Ba*	$BaCO_3$: powder	33	1.0	^{132}Ba: 0.40, ^{134}Ba: 63.90, ^{135}Ba: 14.30, ^{136}Ba: 5.00, ^{137}Ba: 3.70, ^{138}Ba: 12.70
^{151}Eu*	Eu_2O_3: powder	40	0.4	^{151}Eu: 97.70, ^{153}Eu: 2.30
^{153}Eu*	Eu_2O_3: powder	40	0.4	^{151}Eu: 0.80, ^{153}Eu: 99.20
^{159}Tb*	TbO_3: powder	60	0.5	natural(^{159}Tb: 100)
^{169}Tm	Tm: powder	70	0.6	natural(^{169}Tm: 100)
^{178}Hf*	HfO_2: powder	60	0.6	^{174}Hf: 0.05, ^{176}Hf: 0.80, ^{177}Hf: 1.90, ^{178}Hf: 92.40, ^{179}Hf: 3.30, ^{180}Hf: 1.60
^{179}Hf*	HfO_2: powder	60	0.7	^{174}Hf: 0.05, ^{176}Hf: 0.20, ^{177}Hf: 1.50, ^{178}Hf: 4.60, ^{179}Hf: 73.70, ^{180}Hf: 20.00
^{180}Hf*	HfO_2: powder	50	0.7	^{174}Hf: 0.05, ^{176}Hf: 0.20, ^{177}Hf: 0.50, ^{178}Hf: 2.00, ^{179}Hf: 1.10, ^{180}Hf: 96.20
^{185}Re	Re: powder	60	0.4	natural(^{185}Re: 37.40, ^{187}Re: 62.60)

* Separated isotope was used.

** Included thickness of cartridge paper if powder.

Table2 (continued-2)

Target Nucleus	Chemical Form	Weight [mg]	Thickness** [mm]	Abundance [%]
^{187}Re	Re: powder	60	0.4	natural(^{185}Re: 37.40, ^{187}Re: 62.60)
^{188}Os	Os: powder	60	0.6	natural(^{184}Os: 0.02, ^{186}Os: 1.59, ^{187}Os: 1.64, ^{188}Os: 13.30, ^{189}Os: 16.10, ^{190}Os: 26.40, ^{192}Os: 41.00)
^{192}Os	Os: powder	60	0.6	natural(^{184}Os: 0.02, ^{186}Os: 1.59, ^{187}Os: 1.64, ^{188}Os: 13.30, ^{189}Os: 16.10, ^{190}Os: 26.40, ^{192}Os: 41.00)
^{191}Ir	Ir: powder	105	1.0	natural(^{191}Ir: 38.50, ^{193}Ir: 61.50)
^{193}Ir	Ir: powder	105	1.0	natural(^{191}Ir: 38.50, ^{193}Ir: 61.50)
^{232}Th	Th: metal	190	0.5	natural(^{232}Th: 100)
^{238}U*	U: metal	70	0.3	^{234}U: 0.01, ^{235}U: 0.72, ^{238}U: 99.27

*Separated isotope was used.

**Included thickness of cartridge paper if powder.

Table 3 Parameters needed to deduce the reaction rate, the cross section and their estimated errors

Items	Estimated error (%)
1. Statistics of gamma-ray count	±0.3~25
2. Detector efficiency	±2.0
3. Sample weight	<±0.1
4. Irradiation, cooling and measuring time	<±0.1
5. Self-absorption of gamma-ray in a sample	<±0.5
6. Half-life (decay constant)	<±0.1~3
7. Gamma-ray branching ratio	±0.1~20
8. Correction factor for mean source position	<±0.1
9. Correction factor due to fluctuation of neutron flux during irradiation	<±0.1
10. Correction factor due to sum-peak of gamma-ray	<±0.1
11. Standard reaction cross section	±4.2

Table 4 Numerical values for the measured cross sections

Table Format

Reaction Type		
Neutron Energy [MeV]	Cross Section [mb]	Error [mb]
14.91	1.303E+02*	6.9E+00
•	•	•
•	•	•
•	•	•
•	•	•
•	•	•
•	•	•

*: Reads as 1.303×10^2.

^{60}Ni (n, p) $^{60m+g}$Co

Neutron Energy [MeV]	Cross Section [mb]	Error [mb]
14.91	1.303E+02	6.9E+00
14.65	1.326E+02	6.9E+00
14.42	1.432E+02	7.5E+00
13.98	1.483E+02	7.7E+00
13.74	1.548E+02	8.6E+00
13.56	1.589E+02	8.3E+00
13.32	1.582E+02	8.3E+00

^{61}Ni (n, p) ^{61}Co

Neutron Energy [MeV]	Cross Section [mb]	Error [mb]
14.92	5.93E+01	3.6E+00
14.22	6.47E+01	4.0E+00
13.56	6.65E+01	4.1E+00

^{62}Ni (n, np) ^{61}Co

Neutron Energy [MeV]	Cross Section [mb]	Error [mb]
14.99	6.32E+00	4.1E-01
14.19	2.44E+00	1.6E-01
13.50	1.273E+00	9.0E-02

^{63}Cu (n, α) $^{60m+g}$Co

Neutron Energy [MeV]	Cross Section [mb]	Error [mb]
14.91	3.98E+01	2.2E+00
14.66	4.11E+01	2.2E+00
14.42	4.18E+01	2.3E+00
14.22	4.33E+01	2.4E+00
13.98	4.51E+01	2.4E+00
13.75	4.58E+01	2.5E+00
13.56	4.56E+01	2.5E+00
13.33	4.60E+01	2.5E+00

^{64}Zn (n, 2n) ^{63}Zn

Neutron Energy [MeV]	Cross Section [mb]	Error [mb]
14.97	1.93E+02	1.4E+01
14.69	1.70E+02	1.3E+01
14.24	1.287E+02	9.7E+00
13.77	8.79E+01	6.8E+00
13.40	4.85E+01	4.0E+00

^{64}Zn (n, p) ^{64}Cu

Neutron Energy [MeV]	Cross Section [mb]	Error [mb]
14.90	1.274E+02	8.3E+00
14.64	1.353E+02	8.7E+00
14.21	1.438E+02	9.3E+00
13.97	1.496E+02	9.7E+00
13.74	1.56E+02	1.0E+01
13.56	1.75E+02	1.1E+01
13.32	1.92E+02	1.2E+01

^{66}Zn (n, 2n) ^{65}Zn

Neutron Energy [MeV]	Cross Section [mb]	Error [mb]
14.95	7.64E+02	3.8E+01
14.68	7.20E+02	3.2E+01
14.23	6.47E+02	3.0E+01
13.76	5.45E+02	2.5E+01
13.35	4.42E+02	2.1E+01

^{67}Zn (n, p) ^{67}Cu

Neutron Energy [MeV]	Cross Section [mb]	Error [mb]
14.93	3.53E+01	3.1E+00
14.66	3.79E+01	3.3E+00
14.22	3.65E+01	3.2E+00
13.98	3.43E+01	3.0E+00
13.57	3.80E+01	3.3E+00
13.33	3.42E+01	3.0E+00

^{68}Zn (n, np) ^{67}Cu

Neutron Energy [MeV]	Cross Section [mb]	Error [mb]
14.97	9.03E+00	8.5E-01
14.70	7.67E+00	7.0E-01
14.24	5.28E+00	5.2E-01
13.99	4.09E+00	3.8E-01
13.60	2.76E+00	2.5E-01
13.42	2.18E+00	2.1E-01

^{68}Zn (n, α) ^{65}Ni

Neutron Energy [MeV]	Cross Section [mb]	Error [mb]
14.93	9.45E+00	6.5E-01
14.67	9.56E+00	6.5E-01
14.22	9.04E+00	6.3E-01
13.98	9.09E+00	6.4E-01
13.57	8.65E+00	5.9E-01
13.33	8.56E+00	6.0E-01

^{70}Ge (n, 2n) ^{69}Ge

Neutron Energy [MeV]	Cross Section [mb]	Error [mb]
14.96	5.87E+02	7.1E+01
14.45	4.99E+02	6.0E+01
13.99	4.07E+02	4.9E+01
13.36	2.66E+02	3.2E+01

^{72}Ge (n, p) ^{72}Ga

Neutron Energy [MeV]	Cross Section [mb]	Error [mb]
14.93	3.36E+01	1.6E-01
14.43	3.34E+01	1.6E-01
13.98	3.18E+01	1.5E-01
13.34	2.94E+01	1.3E-01

^{72}Ge (n, α) ^{69m}Zn

Neutron Energy [MeV]	Cross Section [mb]	Error [mb]
14.94	6.86E+00	4.3E-01
14.43	6.44E+00	4.1E-01
13.98	6.17E+00	3.8E-01
13.34	5.47E+00	3.3E-01

^{73}Ge (n, p) ^{73}Ga

Neutron Energy [MeV]	Cross Section [mb]	Error [mb]
14.93	2.10E+01	1.3E+00
14.43	2.06E+01	1.2E+00
13.98	1.97E+01	1.2E+00
13.34	1.80E+01	1.1E+00

^{73}Ge (n, np) ^{72}Ga

Neutron Energy [MeV]	Cross Section [mb]	Error [mb]
14.98	6.94E+00	4.4E-01
14.46	4.59E+00	3.1E-01
13.99	2.92E+00	2.4E-01
13.50	1.27E+00	1.8E-01

^{74}Ge (n, np) ^{73}Ga

Neutron Energy [MeV]	Cross Section [mb]	Error [mb]
14.98	4.20E+00	2.9E-01
14.46	2.63E+00	1.9E-01
13.99	1.60E+00	1.2E-01
13.51	7.91E-01	8.0E-02

^{74}Ge (n, α) ^{71m}Zn

Neutron Energy [MeV]	Cross Section [mb]	Error [mb]
14.95	3.29E+00	2.8E-01
14.68	3.28E+00	2.8E-01
14.44	2.94E+00	2.5E-01
14.23	2.81E+00	2.4E-01
13.99	2.82E+00	2.4E-01
13.57	2.50E+00	2.1E-01
13.34	2.31E+00	2.0E-01

^{75}As (n, 2n) ^{74}As

Neutron Energy [MeV]	Cross Section [mb]	Error [mb]
14.93	9.91E+02	6.2E+01
14.67	1.007E+03	6.3E+01
14.44	9.66E+02	6.0E+01
14.23	9.31E+02	5.8E+01
13.99	9.58E+02	6.0E+01
13.76	9.19E+02	5.7E+01
13.57	8.72E+02	5.5E+01
13.34	8.04E+02	5.1E+01

^{75}As (n, p) ^{75}Ge

Neutron Energy [MeV]	Cross Section [mb]	Error [mb]
14.92	1.72E+01	1.9E+00
14.66	1.77E+01	2.0E+00
14.42	1.82E+01	2.1E+00
14.22	1.89E+01	2.2E+00
13.98	1.86E+01	2.2E+00
13.75	1.87E+01	2.1E+00
13.56	1.96E+01	2.2E+00
13.33	1.98E+01	2.3E+00

^{75}As (n, α) ^{72}Ga

Neutron Energy [MeV]	Cross Section [mb]	Error [mb]
14.93	1.055E+01	5.1E-01
14.67	1.024E+01	5.0E-01
14.43	1.037E+01	4.9E-01
14.23	1.051E+01	4.9E-01
13.98	1.007E+01	4.9E-01
13.75	9.73E+00	4.6E-01
13.57	9.58E+00	4.9E-01
13.34	9.36E+00	4.8E-01

^{85}Rb (n, 2n) ^{84m}Rb

Neutron Energy [MeV]	Cross Section [mb]	Error [mb]
14.94	6.83E+02	3.5E+01
14.68	6.63E+02	3.6E+01
14.44	6.30E+02	3.7E+01
14.23	6.13E+02	4.0E+01
13.99	5.73E+02	3.8E+01
13.76	5.51E+02	3.3E+01
13.57	5.22E+02	2.9E+01
13.34	4.74E+02	2.5E+01

^{85}Rb (n, 2n) $^{84m+g}Rb$

Neutron Energy [MeV]	Cross Section [mb]	Error [mb]
14.94	1.056E+03	4.8E+01
14.67	1.042E+03	4.8E+01
14.44	9.97E+02	4.6E+01
14.23	9.62E+02	4.4E+01
13.99	9.17E+02	4.2E+01
13.76	8.73E+02	4.0E+01
13.57	8.38E+02	3.9E+01
13.34	7.91E+02	3.6E+01

^{85}Rb (n, p) ^{85m}Kr

Neutron Energy [MeV]	Cross Section [mb]	Error [mb]
14.92	4.07E+00	6.7E-01
14.66	3.55E+00	5.7E-01
14.42	3.91E+00	4.6E-01
14.22	3.86E+00	4.4E-01
13.98	3.96E+00	3.8E-01
13.75	4.03E+00	6.6E-01
13.56	3.97E+00	5.5E-01
13.33	3.91E+00	6.7E-01

^{85}Rb (n, α) ^{82}Br

Neutron Energy [MeV]	Cross Section [mb]	Error [mb]
14.95	6.53E+00	3.9E-01
14.68	6.43E+00	4.6E-01
14.44	5.33E+00	4.4E-01
14.23	5.11E+00	4.4E-01
13.99	5.01E+00	4.2E-01
13.76	4.72E+00	3.6E-01
13.57	4.62E+00	3.5E-01
13.34	4.24E+00	2.5E-01

^{87}Rb (n, 2n) $^{86m+g}$Rb

Neutron Energy [MeV]	Cross Section [mb]	Error [mb]
14.94	1.192E+03	5.7E+01
14.67	1.211E+03	6.1E+01
14.43	1.179E+03	6.1E+01
14.22	1.109E+03	5.6E+01
13.98	1.102E+03	5.2E+01
13.75	1.050E+03	5.6E+01
13.57	1.025E+03	5.3E+01
13.33	1.063E+03	5.6E+01

^{87}Rb (n, p) ^{87}Kr

Neutron Energy [MeV]	Cross Section [mb]	Error [mb]
14.94	1.109E+01	1.0E+00
14.67	1.016E+01	9.1E-01
14.43	9.62E+00	8.5E-01
14.22	9.88E+00	9.3E-01
13.98	1.020E+01	9.2E-01
13.75	9.03E+00	8.3E-01
13.57	8.84E+00	8.3E-01
13.33	8.91E+00	8.5E-01

^{84}Sr (n, 2n) ^{83}Sr

Neutron Energy [MeV]	Cross Section [mb]	Error [mb]
14.96	7.17E+02	8.0E+01
14.69	6.07E+02	6.9E+01
14.24	5.02E+02	5.7E+01
13.99	4.58E+02	5.5E+01
13.59	3.08E+02	3.5E+01
13.38	2.34E+02	2.8E+01

^{84}Sr (n, p) $^{84m+g}$Rb

Neutron Energy [MeV]	Cross Section [mb]	Error [mb]
14.92	8.80E+01	8.0E+00
13.98	9.68E+01	8.4E+00
13.33	9.87E+01	8.7E+00

^{84}Sr (n, np) ^{83}Rb

Neutron Energy [MeV]	Cross Section [mb]	Error [mb]
14.95	1.3E+02	1.0E+02
13.99	1.04E+02	7.1E+01
13.34	8.7E+01	4.1E+01

^{86}Sr (n, 2n) ^{85m}Sr

Neutron Energy [MeV]	Cross Section [mb]	Error [mb]
14.95	2.34E+02	1.3E+01
14.68	2.22E+02	1.3E+01
14.45	2.03E+02	1.2E+01
14.24	1.88E+02	1.1E+01
13.99	1.646E+02	9.5E+00
13.76	1.371E+02	8.0E+00
13.59	1.239E+02	7.3E+00
13.37	1.004E+02	5.9E+00

^{86}Sr (n, 2n) $^{85m+g}Sr$

Neutron Energy [MeV]	Cross Section [mb]	Error [mb]
14.95	9.73E+02	5.2E+01
14.68	9.04E+02	5.0E+01
14.44	8.52E+02	4.7E+01
14.23	8.15E+02	4.5E+01
13.99	7.36E+02	4.0E+01
13.76	6.79E+02	3.9E+01
13.58	6.11E+02	3.5E+01
13.36	5.29E+02	3.0E+01

^{88}Sr (n, 2n) ^{87m}Sr

Neutron Energy [MeV]	Cross Section [mb]	Error [mb]
14.94	2.64E+02	1.4E+01
14.68	2.63E+02	1.4E+01
14.44	2.49E+02	1.4E+01
14.23	2.35E+02	1.3E+01
13.99	2.21E+02	1.2E+01
13.76	2.02E+02	1.1E+01
13.58	1.88E+02	1.0E+01
13.36	1.623E+02	8.9E+00

^{89}Y (n, 2n) ^{88}Y

Neutron Energy [MeV]	Cross Section [mb]	Error [mb]
14.95	1.071E+03	4.7E+01
14.68	1.011E+03	4.4E+01
14.44	9.68E+02	4.2E+01
14.23	9.34E+02	4.1E+01
13.99	8.31E+02	3.6E+01
13.76	7.72E+02	3.4E+01
13.58	6.81E+02	3.0E+01
13.36	6.17E+02	2.7E+01

^{92}Mo (n, np) ^{91m}Nb

Neutron Energy [MeV]	Cross Section [mb]	Error [mb]
14.94	1.78E+02	1.4E+01
14.67	1.76E+02	1.3E+01
14.43	1.66E+02	1.2E+01
14.22	1.69E+02	1.3E+01

^{96}Ru (n, 2n) ^{95}Ru

Neutron Energy [MeV]	Cross Section [mb]	Error [mb]
14.95	6.24E+02	3.5E+01
14.68	5.91E+02	3.5E+01
14.44	5.59E+02	3.1E+01
14.23	5.22E+02	2.9E+01
13.99	4.81E+02	2.7E+01
13.76	4.39E+02	2.5E+01
13.57	4.19E+02	2.4E+01
13.34	4.09E+02	2.4E+01

^{96}Ru (n, p) $^{96m+g}$Tc

Neutron Energy [MeV]	Cross Section [mb]	Error [mb]
14.90	1.205E+02	8.9E+00
14.65	1.251E+02	7.7E+00
14.42	1.355E+02	8.7E+00
14.21	1.431E+02	9.6E+00
13.98	1.479E+02	9.1E+00
13.74	1.519E+02	9.1E+00
13.56	1.573E+02	8.6E+00
13.32	1.646E+02	9.4E+00

^{96}Ru (n, np) ^{95m}Tc

Neutron Energy [MeV]	Cross Section [mb]	Error [mb]
14.94	6.15E+01	6.0E+00
14.68	6.02E+01	5.8E+00
14.44	5.39E+01	5.7E+00
14.23	5.27E+01	5.8E+00
13.99	4.63E+01	5.8E+00
13.57	4.18E+01	5.9E+00
13.34	3.79E+01	8.4E+00

^{96}Ru (n, np) ^{95g}Tc

Neutron Energy [MeV]	Cross Section [mb]	Error [mb]
14.94	3.60E+02	5.8E+01
14.68	3.46E+02	5.5E+01
14.44	3.18E+02	5.2E+01
14.23	3.10E+02	4.9E+01
13.99	3.09E+02	4.6E+01
13.76	2.87E+02	4.2E+01
13.58	2.30E+02	4.0E+01
13.36	1.95E+02	3.9E+01

^{99}Ru (n, p) ^{99m}Tc

Neutron Energy [MeV]	Cross Section [mb]	Error [mb]
14.94	1.33E+01	1.5E+00
14.67	1.32E+01	1.4E+00
14.43	1.33E+01	1.5E+00
14.22	1.14E+01	1.2E+00
13.98	1.18E+01	1.3E+00
13.75	1.16E+01	1.2E+00
13.57	1.15E+01	1.2E+00
13.33	1.13E+01	1.2E+00

^{102}Pd (n, 2n) ^{101}Pd

Neutron Energy [MeV]	Cross Section [mb]	Error [mb]
14.94	1.179E+03	9.1E+01
14.67	1.127E+03	8.7E+01
14.44	1.094E+03	8.4E+01
14.23	1.081E+03	8.4E+01
13.99	1.012E+03	7.9E+01
13.76	9.60E+02	7.4E+01
13.57	8.99E+02	6.9E+01
13.35	8.32E+02	6.5E+01

^{102}Pd (n, np) ^{101m}Rh

Neutron Energy [MeV]	Cross Section [mb]	Error [mb]
14.95	2.7E+02	1.2E+02
14.68	2.8E+02	1.1E+02
14.44	2.4E+02	1.1E+02
14.23	1.9E+02	1.1E+02
13.99	2.2E+02	1.0E+02
13.76	1.96E+02	9.6E+01
13.57	1.90E+02	9.0E+01
13.34	1.74E+02	8.3E+01

^{105}Pd (n, p) ^{105}Rh

Neutron Energy [MeV]	Cross Section [mb]	Error [mb]
14.95	4.27E+01	3.3E+00
14.68	3.90E+01	3.0E+00
14.44	3.80E+01	2.9E+00
14.23	3.59E+01	2.8E+00
13.99	3.39E+01	2.6E+00
13.76	3.16E+01	2.5E+00
13.57	3.17E+01	2.5E+00
13.34	2.82E+01	2.2E+00

^{106}Pd (n, p) ^{106m}Rh

Neutron Energy [MeV]	Cross Section [mb]	Error [mb]
14.94	9.97E+00	8.1E-01
14.68	9.61E+00	7.9E-01
14.44	8.94E+00	8.3E-01
14.23	9.32E+00	9.3E-01
13.99	8.32E+00	8.5E-01
13.76	7.32E+00	7.6E-01
13.57	7.84E+00	8.1E-01
13.34	6.72E+00	8.3E-01

^{108}Pd (n, α) ^{105}Ru

Neutron Energy [MeV]	Cross Section [mb]	Error [mb]
14.96	3.33E+00	4.9E-01
14.68	2.52E+00	3.8E-01
14.44	2.67E+00	4.1E-01
14.23	2.18E+00	3.7E-01
13.99	2.27E+00	4.1E-01
13.76	1.91E+00	3.4E-01
13.58	1.84E+00	3.2E-01
13.35	1.56E+00	3.1E-01

^{107}Ag (n, 2n) ^{106m}Ag

Neutron Energy [MeV]	Cross Section [mb]	Error [mb]
14.94	5.57E+02	3.3E+01
14.67	5.38E+02	3.2E+01
14.43	5.27E+02	3.2E+01
14.22	5.25E+02	3.2E+01
13.98	4.69E+02	2.8E+01
13.75	4.88E+02	2.9E+01
13.57	4.67E+02	2.8E+01
13.34	4.47E+02	2.7E+01

^{106}Cd (n, 2n) ^{105}Cd

Neutron Energy [MeV]	Cross Section [mb]	Error [mb]
14.94	5.60E+02	5.7E+01
14.67	5.89E+02	6.8E+01
14.44	5.66E+02	7.4E+01
14.23	4.70E+02	7.7E+01
13.99	5.27E+02	8.4E+01
13.76	4.86E+02	9.1E+01
13.58	4.10E+02	9.7E+01
13.35	3.89E+02	9.8E+01

^{106}Cd (n, p) ^{106m}Ag

Neutron Energy [MeV]	Cross Section [mb]	Error [mb]
14.90	4.96E+01	6.2E+00
14.66	5.41E+01	6.1E+00
14.43	6.02E+01	8.0E+00
14.22	5.78E+01	6.4E+00
13.75	5.65E+01	5.9E+00
13.57	6.81E+01	7.5E+00
13.34	5.69E+01	6.7E+00

^{106}Cd (n, np) ^{105}Ag

Neutron Energy [MeV]	Cross Section [mb]	Error [mb]
14.95	1.7E+02	1.0E+02
14.68	1.4E+02	1.1E+02
14.44	1.2E+02	1.1E+02
14.23	1.5E+02	1.1E+02
13.57	1.2E+02	1.1E+02

^{110}Cd (n, p) ^{110m}Ag

Neutron Energy [MeV]	Cross Section [mb]	Error [mb]
14.95	9.82E+00	7.8E-01
14.68	8.65E+00	5.5E-01
14.44	8.57E+00	6.5E-01
14.23	7.39E+00	6.2E-01
13.99	6.56E+00	4.8E-01
13.76	7.60E+00	9.8E-01
13.58	7.43E+00	8.4E-01
13.35	5.46E+00	4.9E-01

^{112}Cd (n, p) ^{112}Ag

Neutron Energy [MeV]	Cross Section [mb]	Error [mb]
14.95	1.81E+01	2.4E+00
14.68	1.76E+01	2.3E+00
14.44	1.63E+01	2.1E+00
14.23	1.47E+01	1.9E+00
13.99	1.38E+01	1.8E+00
13.76	1.29E+01	1.7E+00
13.58	1.19E+01	1.6E+00
13.35	1.06E+01	1.4E+00

^{113}Cd (n, p) ^{113}Ag

Neutron Energy [MeV]	Cross Section [mb]	Error [mb]
14.96	2.75E+01	2.8E+00
14.69	2.59E+01	2.5E+00
14.45	2.14E+01	2.6E+00
14.24	1.82E+01	2.6E+00
13.99	1.47E+01	2.1E+00
13.76	1.65E+01	2.3E+00
13.59	1.32E+01	2.0E+00
13.37	1.02E+01	1.8E+00

^{113}In (n, 2n) ^{112m}In

Neutron Energy [MeV]	Cross Section [mb]	Error [mb]
14.93	1.17E+03	1.1E+02
14.67	1.19E+03	1.1E+02
14.23	1.16E+03	1.1E+02
13.57	1.07E+03	1.0E+02
13.34	1.017E+03	9.7E+01

^{113}In (n, n′) ^{113m}In

Neutron Energy [MeV]	Cross Section [mb]	Error [mb]
14.64	6.08E+01	4.6E+00
14.41	6.76E+01	5.1E+00
14.21	7.37E+01	5.4E+00
13.97	7.36E+01	5.7E+00
13.74	8.14E+01	6.1E+00
13.56	8.71E+02	7.1E+00
13.32	9.35E+02	8.1E+00

^{115}In (n, n′) ^{115m}In

Neutron Energy [MeV]	Cross Section [mb]	Error [mb]
14.90	6.01E+01	3.1E+00
14.64	6.02E+01	3.1E+00
14.41	6.17E+01	3.2E+00
14.21	6.43E+01	3.3E+00
13.97	6.76E+01	3.5E+00
13.74	7.11E+01	3.7E+00
13.56	7.59E+01	3.9E+00
13.32	8.75E+01	4.5E+00

^{115}In (n, p) ^{115m}Cd

Neutron Energy [MeV]	Cross Section [mb]	Error [mb]
14.96	1.13E+01	1.3E+00
14.69	1.04E+01	1.2E+00
14.45	8.0E+00	1.0E+00
14.23	9.0E+00	1.2E+00
13.99	7.51E+00	9.8E-01
13.76	6.73E+00	8.7E-01
13.58	5.13E+00	7.3E-01
13.36	5.49E+00	8.2E-01

^{115}In (n, p) ^{115g}Cd

Neutron Energy [MeV]	Cross Section [mb]	Error [mb]
14.94	4.89E+00	2.9E-01
14.68	4.72E+00	2.8E-01
14.23	4.35E+00	2.6E-01
13.57	3.59E+00	2.2E-01
13.34	3.41E+00	2.1E-01

^{115}In (n, α) ^{112}Ag

Neutron Energy [MeV]	Cross Section [mb]	Error [mb]
14.96	2.66E+00	3.5E-01
14.69	2.42E+00	3.2E-01
14.23	1.90E+00	2.5E-01
13.58	1.41E+00	1.9E-01
13.36	1.29E+00	1.7E-01

^{130}Ba (n, 2n) $^{129m+g}Ba$

Neutron Energy [MeV]	Cross Section [mb]	Error [mb]
14.94	1.61E+03	1.0E+02
14.67	1.61E+03	1.0E+02
14.43	1.499E+03	9.5E+01
13.98	1.491E+03	9.6E+01
13.57	1.370E+03	8.8E+01
13.34	1.324E+03	8.7E+01

^{132}Ba (n, 2n) $^{131m+g}Ba$

Neutron Energy [MeV]	Cross Section [mb]	Error [mb]
14.92	1.65E+03	1.1E+02
14.67	1.72E+03	1.2E+02
13.99	1.67E+03	1.1E+02
13.57	1.67E+03	1.3E+02
13.35	1.420E+03	9.5E+01

^{132}Ba (n, p) ^{132}Cs

Neutron Energy [MeV]	Cross Section [mb]	Error [mb]
14.95	2.01E+01	4.6E+00
14.68	1.78E+01	4.1E+00
13.99	1.49E+01	3.5E+00
13.34	1.27E+01	2.9E+00

^{134}Ba (n, 2n) ^{133m}Ba

Neutron Energy [MeV]	Cross Section [mb]	Error [mb]
14.94	8.59E+02	5.8E+01
14.67	8.49E+02	5.8E+01
14.43	8.34E+02	5.7E+01
14.22	7.75E+02	5.3E+01
13.98	7.91E+02	5.4E+01
13.75	7.83E+02	5.3E+01
13.57	7.19E+02	4.9E+01
13.33	7.61E+02	5.2E+01

^{134}Ba (n, 2n) $^{133m+g}$Ba

Neutron Energy [MeV]	Cross Section [mb]	Error [mb]
14.93	1.79E+03	1.7E+02
14.67	1.83E+03	1.8E+02
14.43	1.75E+03	1.7E+02
14.22	1.73E+03	1.6E+02
13.98	1.68E+03	1.7E+02
13.75	1.68E+03	1.6E+02
13.57	1.59E+03	1.5E+02
13.33	1.69E+03	1.6E+02

^{151}Eu (n, 2n) ^{150A}Eu

Neutron Energy [MeV]	Cross Section [mb]	Error [mb]
14.92	4.76E+02	8.9E+01
14.66	4.97E+02	9.3E+01
14.22	5.00E+02	9.4E+01
13.98	5.07E+02	9.5E+01
13.56	5.05E+02	9.5E+01
13.33	5.4E+02	1.0E+02

^{151}Eu (n, 2n) ^{150B}Eu

Neutron Energy [MeV]	Cross Section [mb]	Error [mb]
14.93	1.13E+03	1.1E+02
14.66	1.08E+03	1.0E+02
14.22	1.034E+03	1.0E+02
13.98	1.07E+03	1.0E+02
13.56	1.045E+03	9.6E+01
13.33	1.06E+03	1.0E+02

^{151}Eu (n, α) ^{148m}Pm

Neutron Energy [MeV]	Cross Section [mb]	Error [mb]
14.94	2.50E+00	5.3E-01
14.67	2.33E+00	5.1E-01
14.23	1.81E+00	4.4E-01
13.98	2.12E+00	4.8E-01
13.57	1.75E+00	3.5E-01
13.34	2.02E+00	5.4E-01

^{153}Eu (n, 2n) ^{152m1}Eu

Neutron Energy [MeV]	Cross Section [mb]	Error [mb]
14.92	3.00E+02	2.3E+01
14.66	3.01E+02	2.3E+01
14.22	3.12E+02	2.4E+01
13.98	3.09E+02	2.4E+01
13.56	3.10E+02	2.4E+01
13.33	3.28E+02	2.6E+01

^{153}Eu (n, 2n) ^{152m2}Eu

Neutron Energy [MeV]	Cross Section [mb]	Error [mb]
14.93	7.58E+01	4.1E+00
14.67	7.57E+01	4.2E+00
14.22	7.47E+01	4.2E+00
13.98	7.07E+01	4.0E+00
13.57	6.90E+01	4.0E+00
13.33	6.79E+01	4.2E+00

^{153}Eu (n, 2n) $^{152m2+g}$Eu

Neutron Energy [MeV]	Cross Section [mb]	Error [mb]
14.93	1.41E+03	1.4E+02
14.66	1.30E+03	1.3E+02
14.22	1.28E+03	1.2E+02
13.98	1.29E+03	1.2E+02
13.56	1.32E+03	1.2E+02

^{153}Eu (n, p) ^{153}Sm

Neutron Energy [MeV]	Cross Section [mb]	Error [mb]
14.95	5.44E+00	5.7E-01
14.68	5.07E+00	5.3E-01
14.23	4.28E+00	5.5E-01
13.99	3.97E+00	4.7E-01
13.57	3.97E+00	4.7E-01
13.34	3.45E+00	4.3E-01

^{153}Eu (n, α) ^{150}Pm

Neutron Energy [MeV]	Cross Section [mb]	Error [mb]
14.94	1.75E+00	2.0E-01
14.67	1.66E+00	1.9E-01
14.23	1.55E+00	1.8E-01
13.99	1.50E+00	1.8E-01
13.57	1.32E+00	1.6E-01
13.34	1.26E+00	1.6E-01

^{159}Tb (n, p) ^{159}Gd

Neutron Energy [MeV]	Cross Section [mb]	Error [mb]
14.95	6.98E+00	5.8E-01
14.68	6.04E+00	5.1E-01
14.44	6.07E+00	5.1E-01
14.23	5.51E+00	4.3E-01
13.99	5.09E+00	4.3E-01
13.76	4.78E+00	4.0E-01
13.58	4.30E+00	3.9E-01
13.35	3.93E+00	3.3E-01

^{169}Tm (n, 2n) ^{168}Tm

Neutron Energy [MeV]	Cross Section [mb]	Error [mb]
14.93	2.10E+03	1.7E+02
14.66	2.06E+03	1.6E+02
14.43	2.09E+03	1.7E+02
14.22	2.07E+03	1.6E+02
13.75	2.05E+03	1.6E+02
13.56	2.06E+03	1.6E+02
13.33	2.07E+03	1.6E+02

^{178}Hf (n, α) ^{175}Yb

Neutron Energy [MeV]	Cross Section [mb]	Error [mb]
14.96	3.57E+00	8.8E-01
14.69	3.04E+00	7.5E-01
13.99	2.34E+00	6.1E-01
13.36	1.68E+00	4.2E-01

^{179}Hf (n, n′) ^{179m2}Hf

Neutron Energy [MeV]	Cross Section [mb]	Error [mb]
14.91	7.2E+00	1.2E+00
14.65	7.4E+00	1.1E+00
13.98	8.6E+00	1.1E+00
13.32	9.3E+00	1.1E+00

^{179}Hf (n, p) ^{179}Lu

Neutron Energy [MeV]	Cross Section [mb]	Error [mb]
14.97	8.6E+00	3.2E+00
14.69	6.8E+00	2.6E+00
13.99	4.1E+00	1.7E+00
13.38	2.9E+00	1.3E+00

^{180}Hf (n, 2n) ^{179m2}Hf

Neutron Energy [MeV]	Cross Section [mb]	Error [mb]
14.95	2.42E+01	2.1E+00
14.68	2.28E+01	2.0E+00
13.99	1.76E+01	1.5E+00
13.35	1.35E+01	1.2E+00

^{180}Hf (n, n′) ^{180m}Hf

Neutron Energy [MeV]	Cross Section [mb]	Error [mb]
14.92	1.165E+01	6.5E-01
14.66	1.172E+01	6.5E-01
14.42	1.197E+01	6.6E-01
13.98	1.210E+01	6.7E-01
13.56	1.303E+01	7.2E-01
13.32	1.327E+01	7.4E-01

^{180}Hf (n, α) ^{177}Yb

Neutron Energy [MeV]	Cross Section [mb]	Error [mb]
14.94	9.5E-01	5.5E-01
14.67	9.0E-01	5.3E-01
14.43	9.0E-01	5.4E-01

^{185}Re (n, 2n) ^{184m}Re

Neutron Energy [MeV]	Cross Section [mb]	Error [mb]
14.93	3.47E+02	2.9E+01
14.67	3.59E+02	3.0E+01
14.43	3.35E+02	2.8E+01
14.22	3.41E+02	2.8E+01
13.98	3.21E+02	2.6E+01
13.75	3.32E+02	2.7E+01
13.57	3.25E+02	2.6E+01
13.33	3.12E+02	2.6E+01

^{185}Re (n, 2n) ^{184g}Re

Neutron Energy [MeV]	Cross Section [mb]	Error [mb]
14.93	1.420E+03	7.4E+01
14.66	1.385E+03	7.2E+01
14.43	1.370E+03	7.2E+01
14.22	1.414E+03	7.3E+01
13.98	1.389E+03	7.2E+01
13.75	1.416E+03	7.4E+01
13.56	1.436E+03	7.5E+01
13.33	1.399E+03	7.3E+01

^{187}Re (n, p) ^{187}W

Neutron Energy [MeV]	Cross Section [mb]	Error [mb]
14.95	6.60E+00	7.5E-01
14.68	5.96E+00	6.5E-01
14.44	5.33E+00	4.1E-01
14.23	4.88E+00	7.9E-01
13.99	5.10E+00	7.1E-01
13.76	4.40E+00	7.6E-01
13.57	4.00E+00	7.1E-01
13.34	4.51E+00	5.1E-01

^{187}Re (n, α) ^{184}Ta

Neutron Energy [MeV]	Cross Section [mb]	Error [mb]
14.96	6.3E-01	1.1E-01
14.70	5.58E-01	9.7E-02
14.47	4.45E-01	6.4E-02

^{188}Os (n, p) ^{188}Re

Neutron Energy [MeV]	Cross Section [mb]	Error [mb]
14.96	5.4E+00	1.4E+00
14.69	4.66E+00	9.1E-01
14.45	4.01E+00	7.9E-01
14.23	3.61E+00	8.4E-01
13.99	4.05E+00	9.2E-01
13.76	2.74E+00	7.7E-01
13.58	2.40E+00	7.8E-01
13.36	2.36E+00	4.4E-01

^{192}Os (n, 2n) $^{191m+g}$Os

Neutron Energy [MeV]	Cross Section [mb]	Error [mb]
14.92	1.92E+03	1.8E+02
14.66	2.05E+03	1.9E+02
14.42	2.04E+03	1.9E+02
14.22	2.06E+03	1.9E+02
13.98	2.12E+03	2.0E+02
13.75	2.13E+03	2.0E+02
13.56	2.09E+03	2.0E+02
13.33	2.16E+03	2.0E+02

^{191}Ir (n, 2n) ^{190m2}Ir

Neutron Energy [MeV]	Cross Section [mb]	Error [mb]
14.94	1.374E+02	8.7E+00
14.67	1.377E+02	9.3E+00
14.43	1.311E+02	7.7E+00
14.23	1.266E+02	7.5E+00
13.98	1.238E+02	7.8E+00
13.57	1.165E+02	7.5E+00
13.34	1.105E+02	7.5E+00

^{191}Ir (n, 2n) $^{190m1+m2+g}Ir$

Neutron Energy [MeV]	Cross Section [mb]	Error [mb]
14.93	1.81E+03	2.0E+02
14.66	1.76E+03	2.0E+02
14.43	1.73E+03	1.9E+02
14.22	1.75E+03	2.0E+02
13.98	1.79E+03	2.0E+02
13.56	1.76E+03	2.0E+02
13.33	1.79E+03	2.0E+02

^{193}Ir (n, 2n) ^{192}Ir

Neutron Energy [MeV]	Cross Section [mb]	Error [mb]
14.92	1.95E+03	1.0E+02
14.66	1.97E+03	1.0E+02
14.43	2.04E+03	1.0E+02
14.22	2.04E+03	1.0E+02
13.98	2.02E+03	1.0E+02
13.56	2.03E+03	1.0E+02
13.33	2.05E+03	1.0E+02

^{232}Th (n, 2n) ^{231}Th

Neutron Energy [MeV]	Cross Section [mb]	Error [mb]
14.88	1.10E+03	1.0E+02
14.63	1.18E+03	1.1E+02
13.97	1.42E+03	1.3E+02
13.32	1.83E+03	1.7E+02

^{238}U (n, 2n) ^{237}U

Neutron Energy [MeV]	Cross Section [mb]	Error [mb]
14.86	6.30E+02	3.2E+01
14.62	6.96E+02	3.6E+01
14.40	7.79E+02	4.0E+01
14.20	8.62E+02	4.4E+01
13.74	1.029E+03	5.3E+01
13.31	1.230E+03	6.3E+01

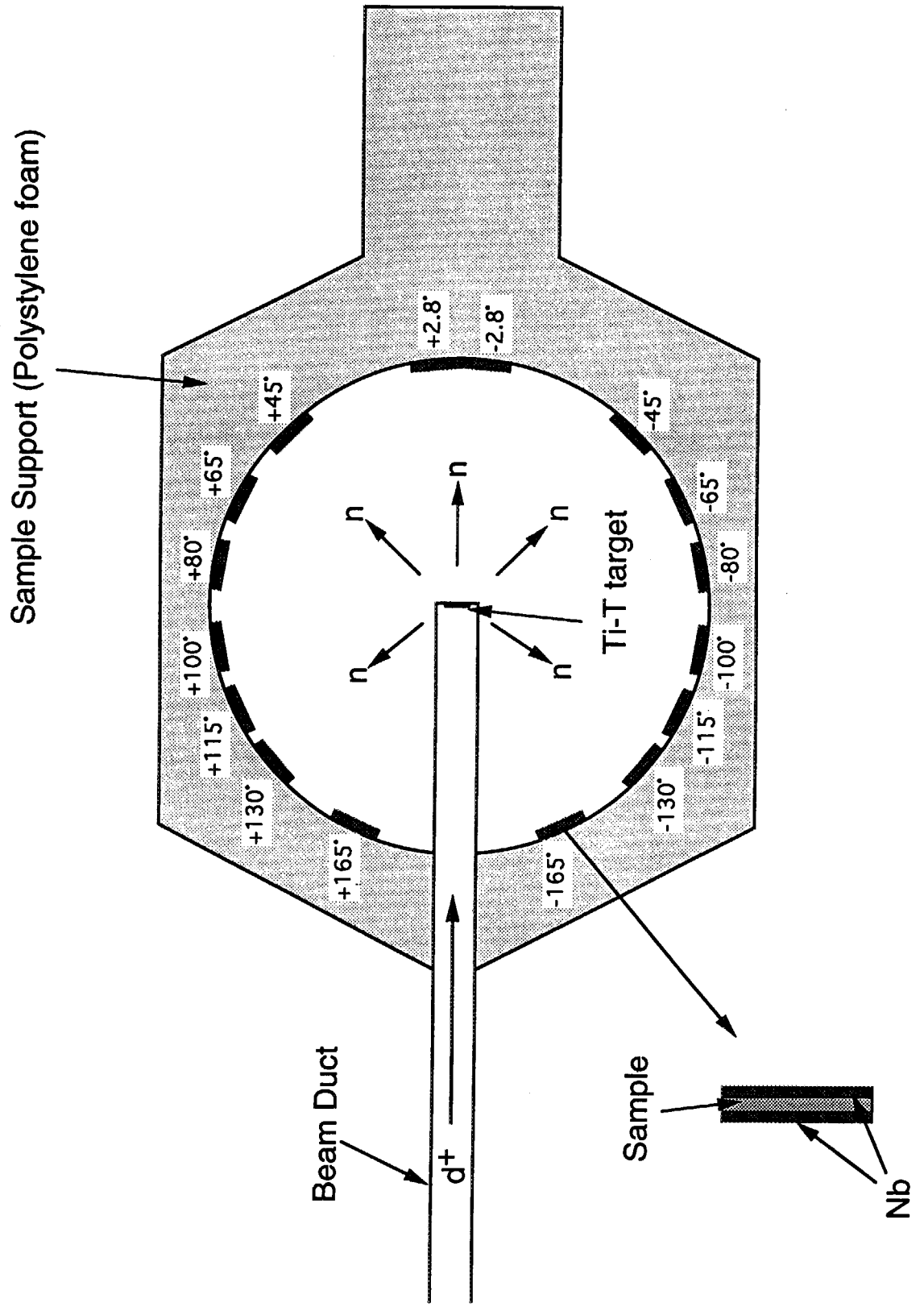

Fig. 2.1 A schematic drawing of typical irradiation setting (up-view).

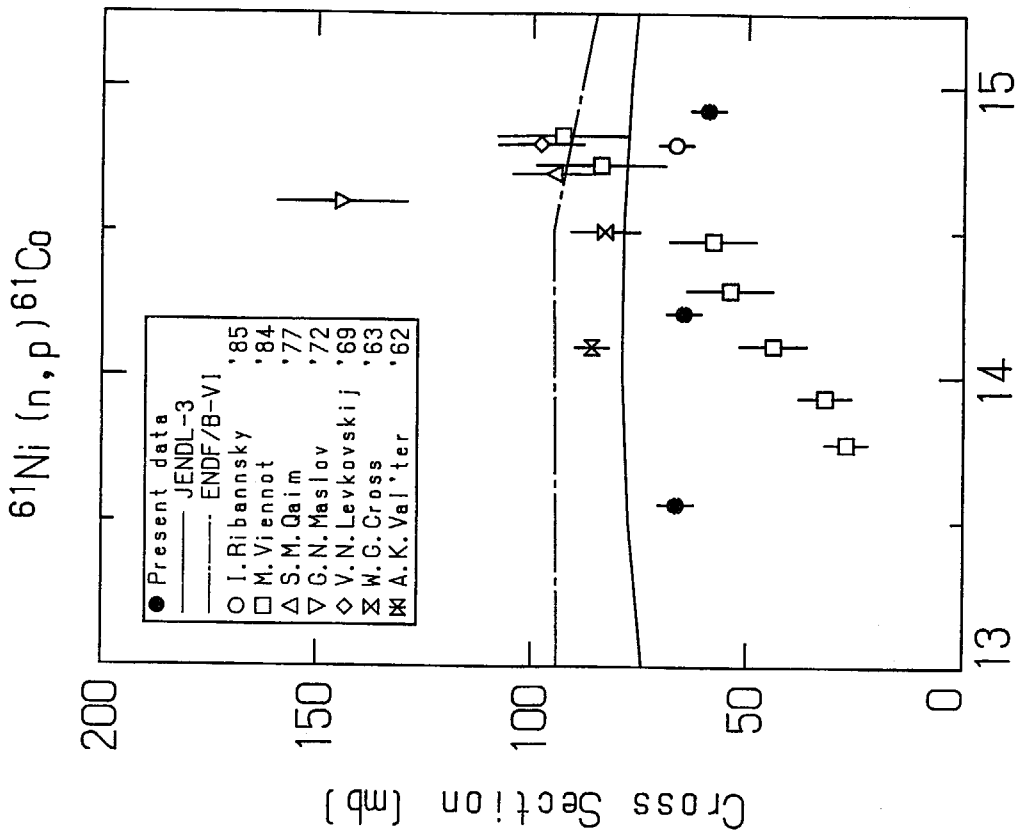

Fig. 3.2 Cross section data for ^{61}Ni (n, p) ^{61}Co.

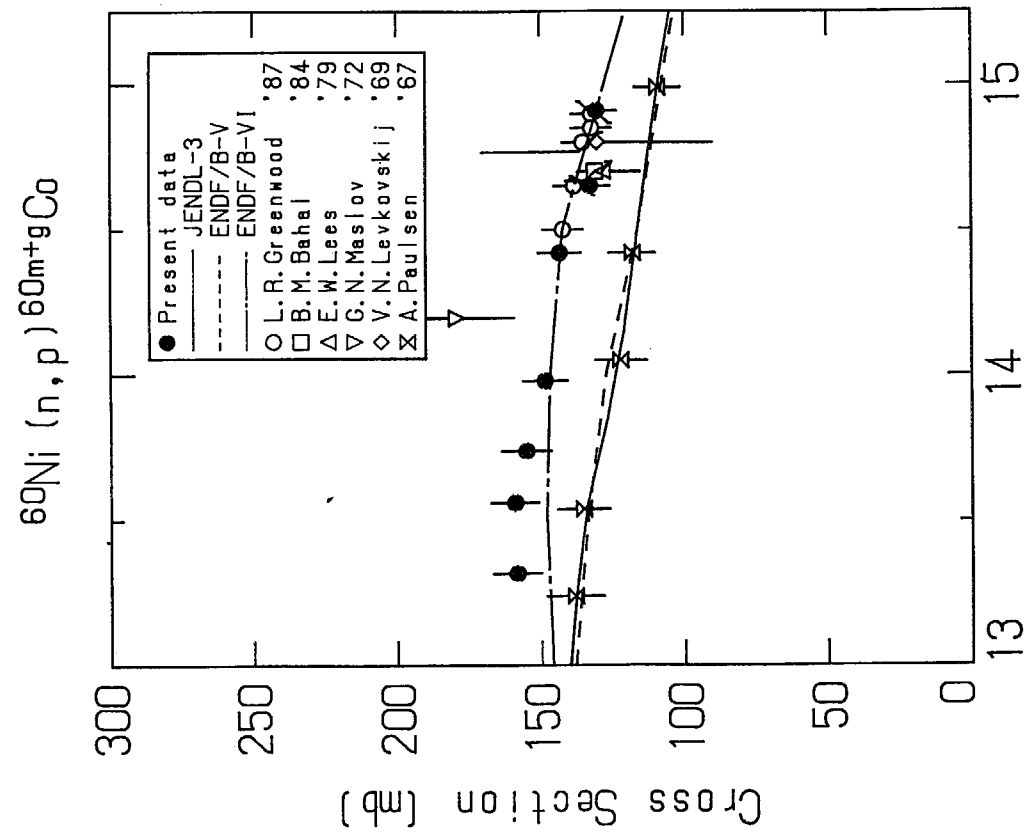

Fig. 3.1 Cross section data for ^{60}Ni (n, p) $^{60m+g}$Co.

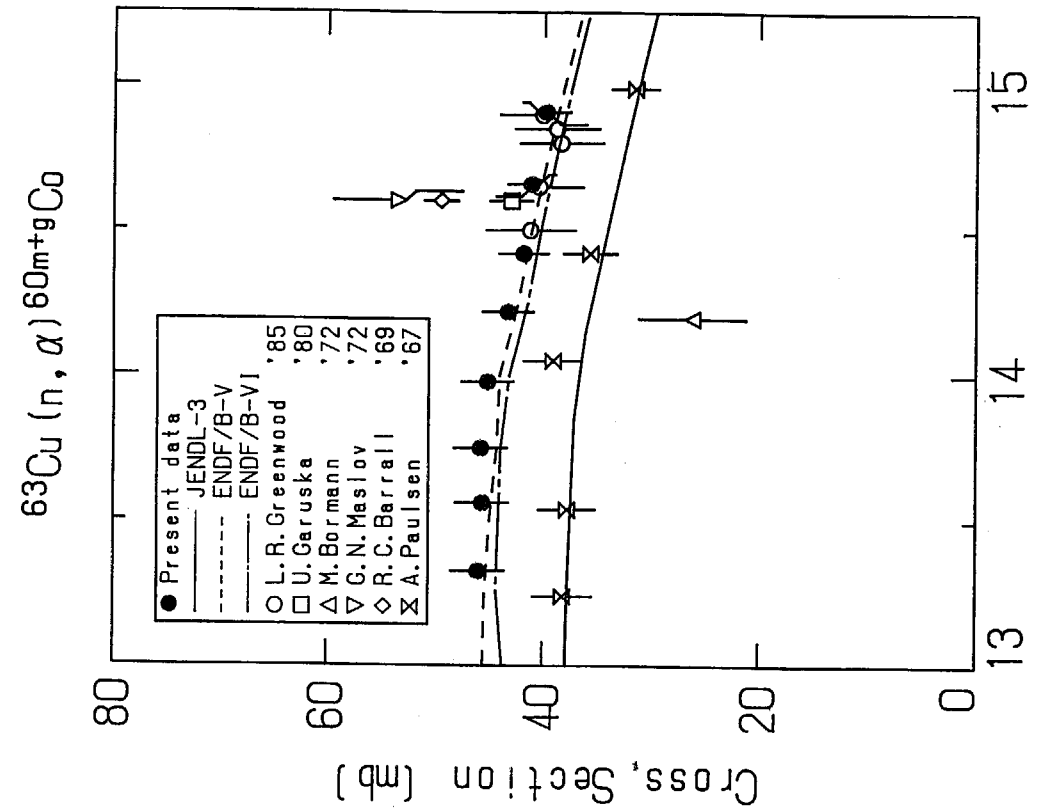

Fig. 3.4 Cross section data for ^{63}Cu (n, α) $^{60m+g}Co$.

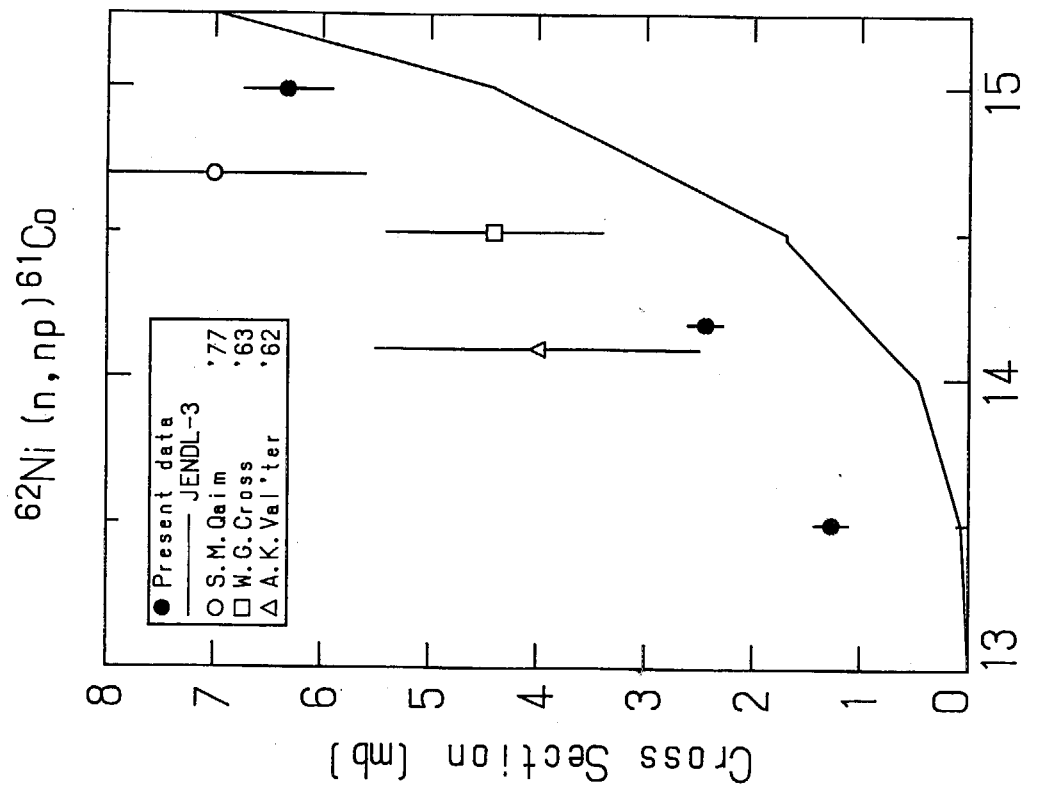

Fig. 3.3 Cross section data for ^{62}Ni (n, np) ^{61}Co.

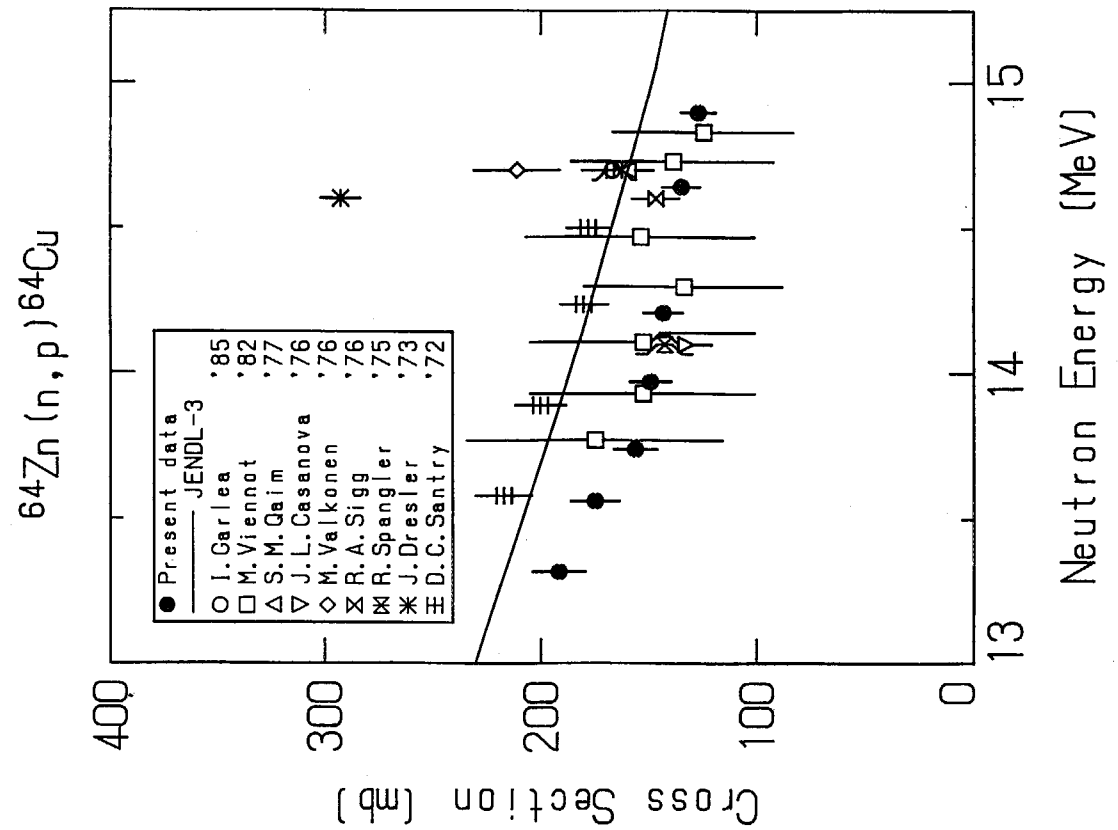

Fig. 3.6 Cross section data for ^{64}Zn (n, p) ^{64}Cu.

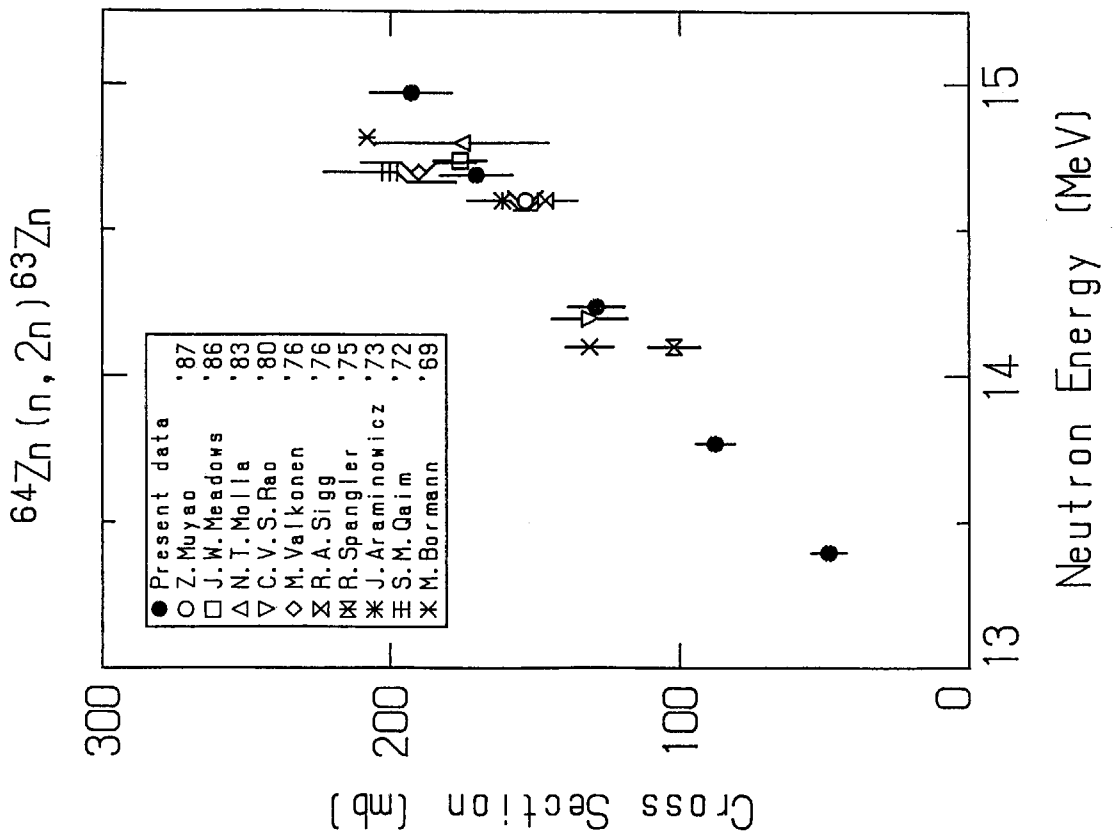

Fig. 3.5 Cross section data for ^{64}Zn (n, 2n) ^{63}Zn.

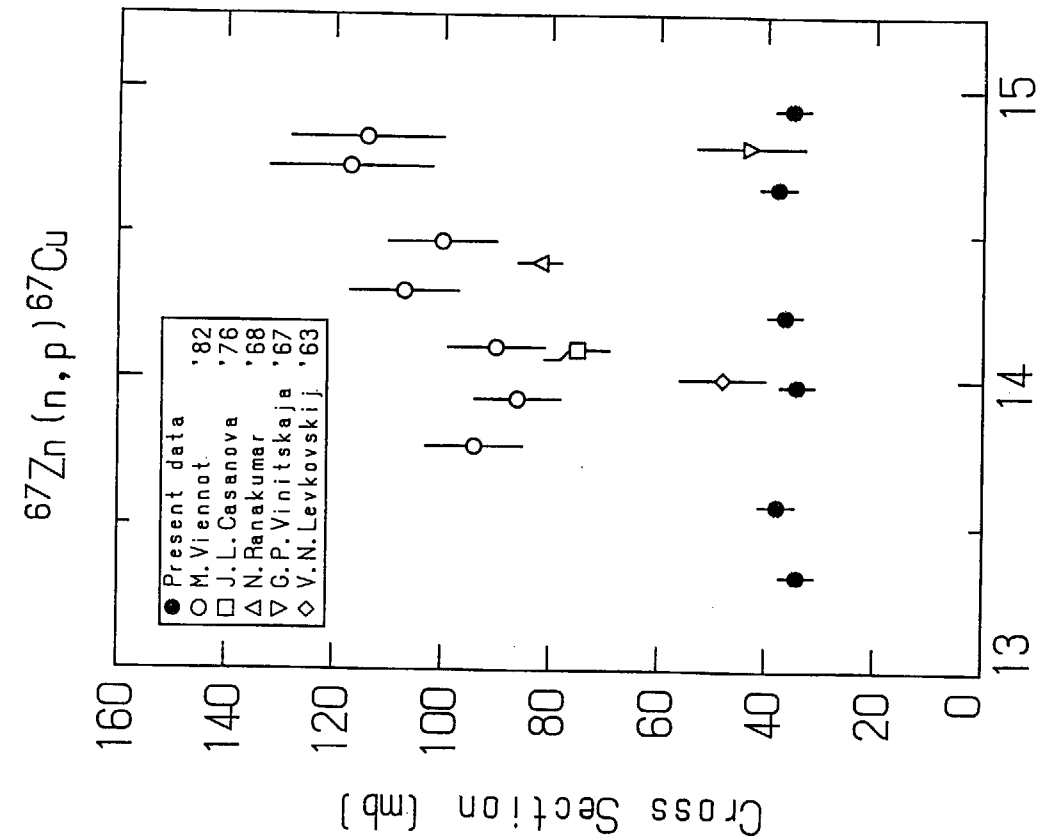

Fig. 3.8 Cross section data for ^{67}Zn (n, p) ^{67}Cu.

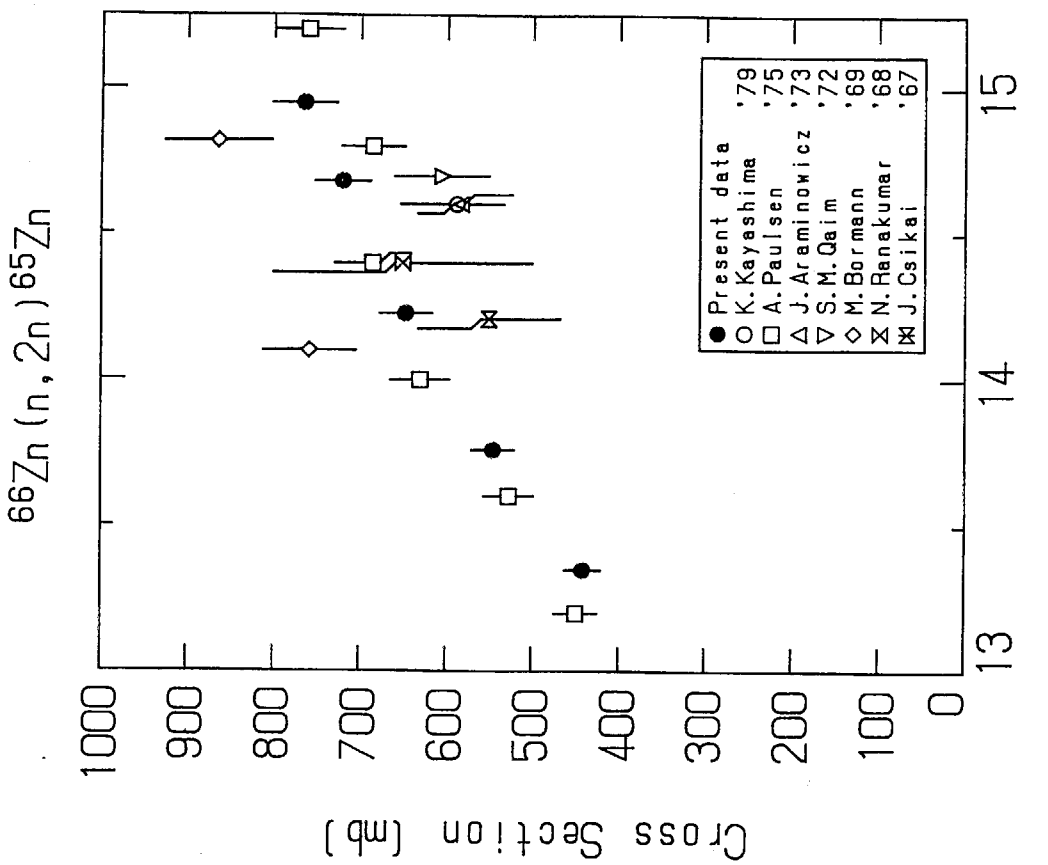

Fig. 3.7 Cross section data for ^{66}Zn (n, 2n) ^{65}Zn.

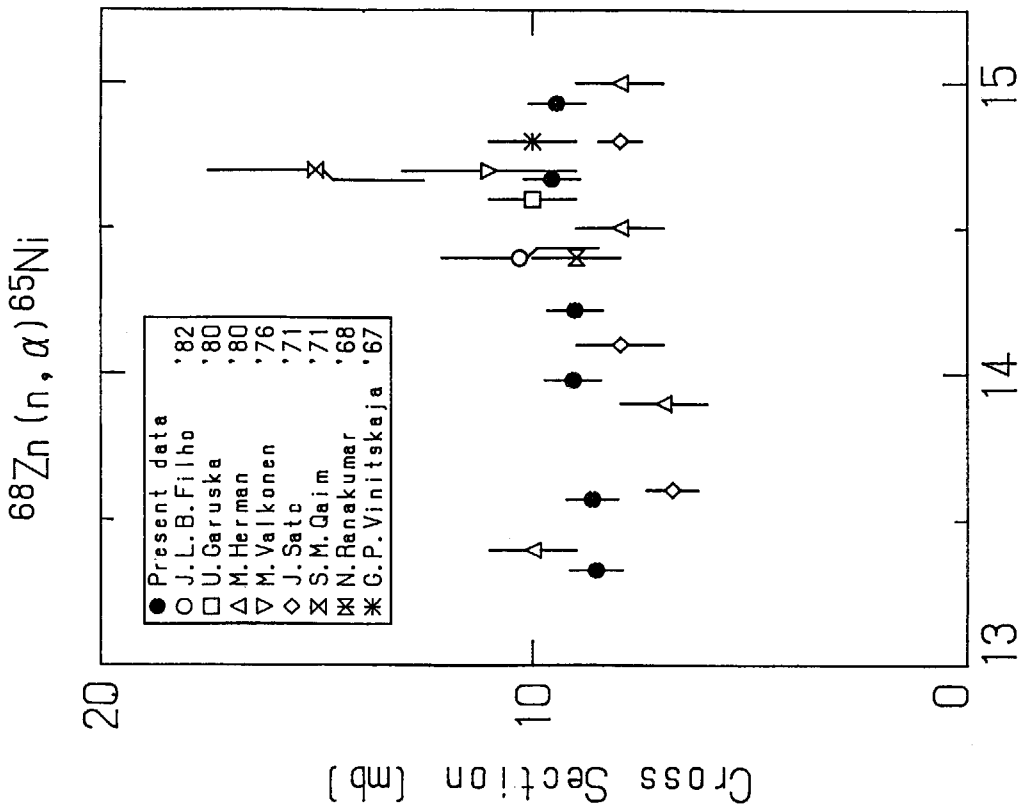

Fig. 3.10 Cross section data for ^{68}Zn (n, α) ^{65}Ni.

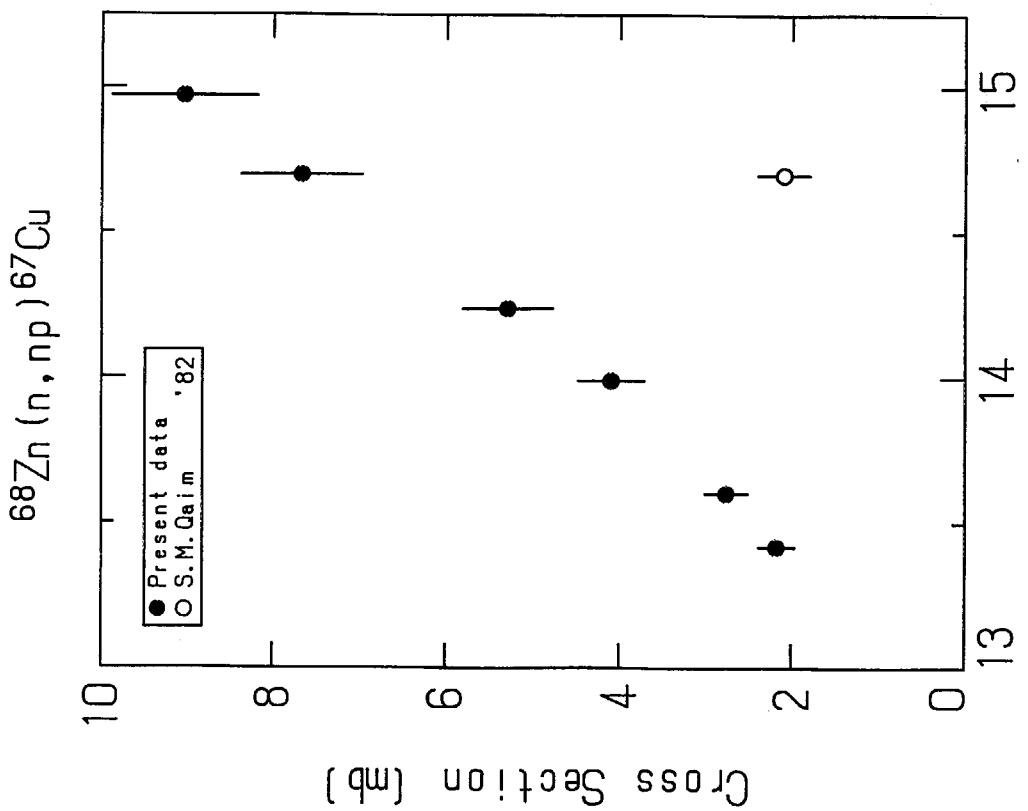

Fig. 3.9 Cross section data for ^{68}Zn (n, np) ^{67}Cu.

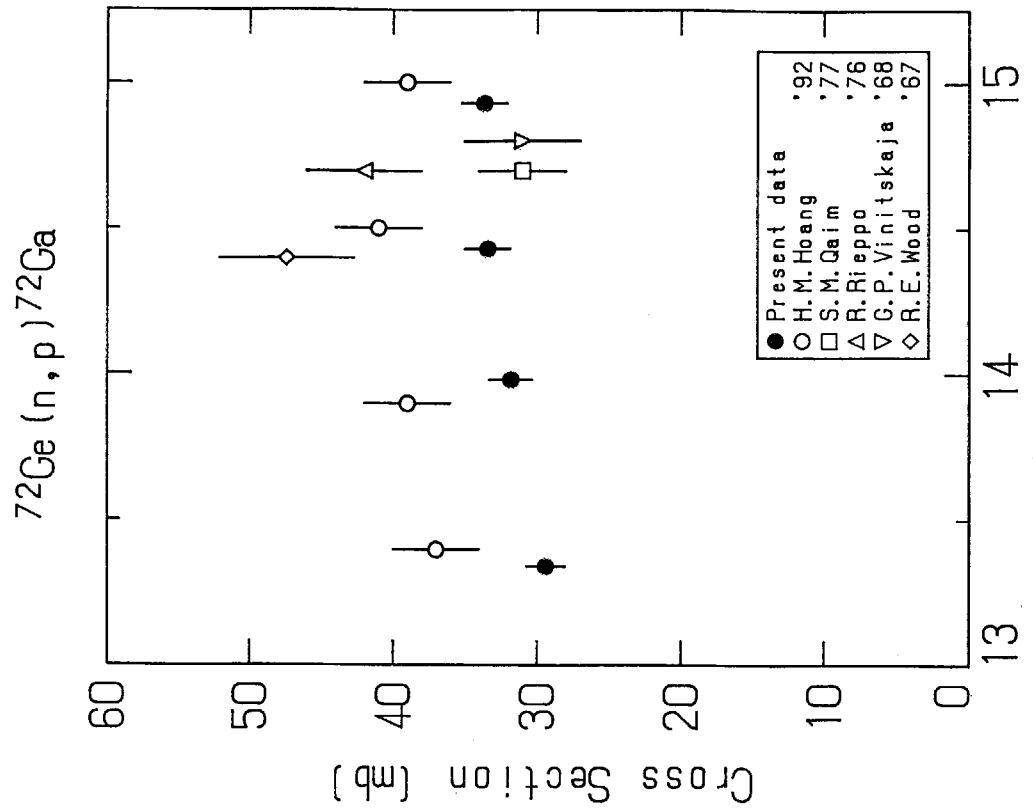

Fig. 3.12 Cross section data for ^{72}Ge (n, p) ^{72}Ga.

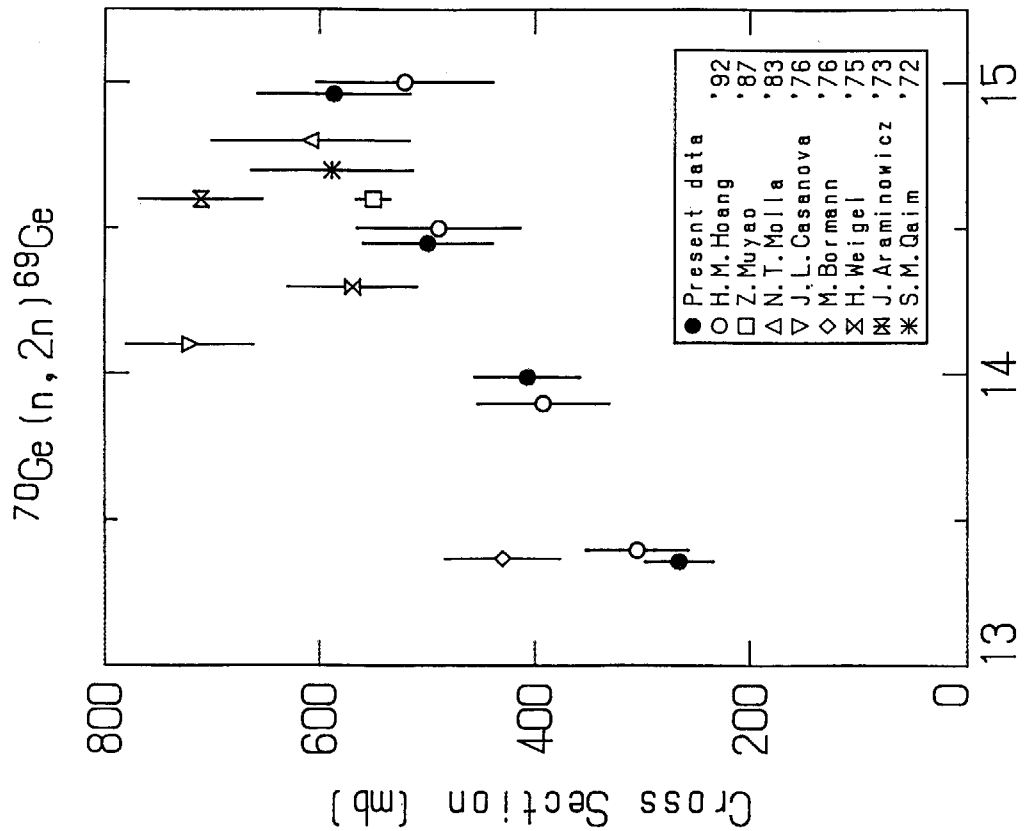

Fig. 3.11 Cross section data for ^{70}Ge (n, 2n) ^{69}Ge.

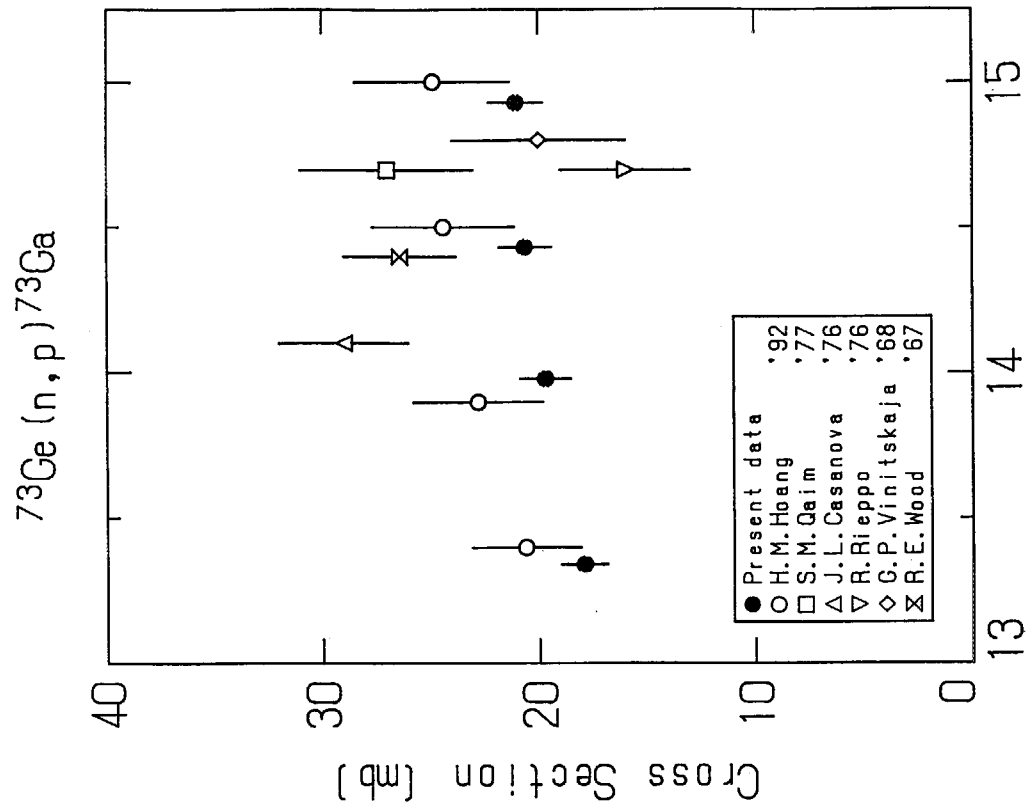

Fig. 3.14 Cross section data for ^{73}Ge (n, p) ^{73}Ga.

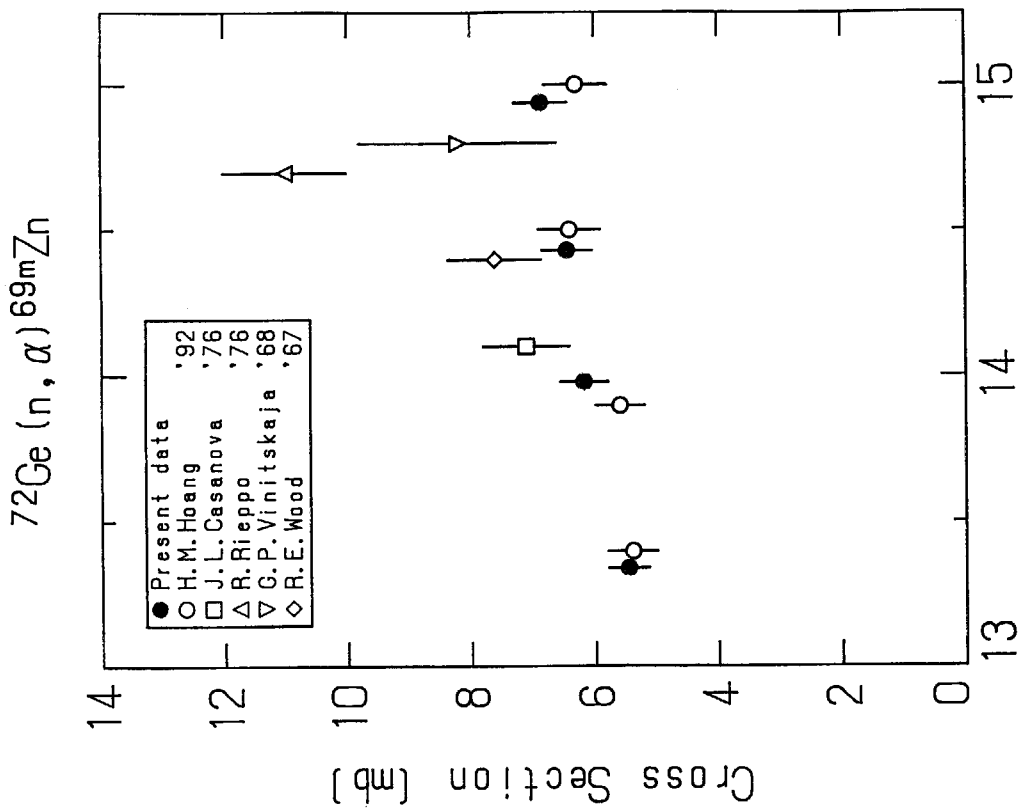

Fig. 3.13 Cross section data for ^{72}Ge (n, α) ^{69m}Zn.

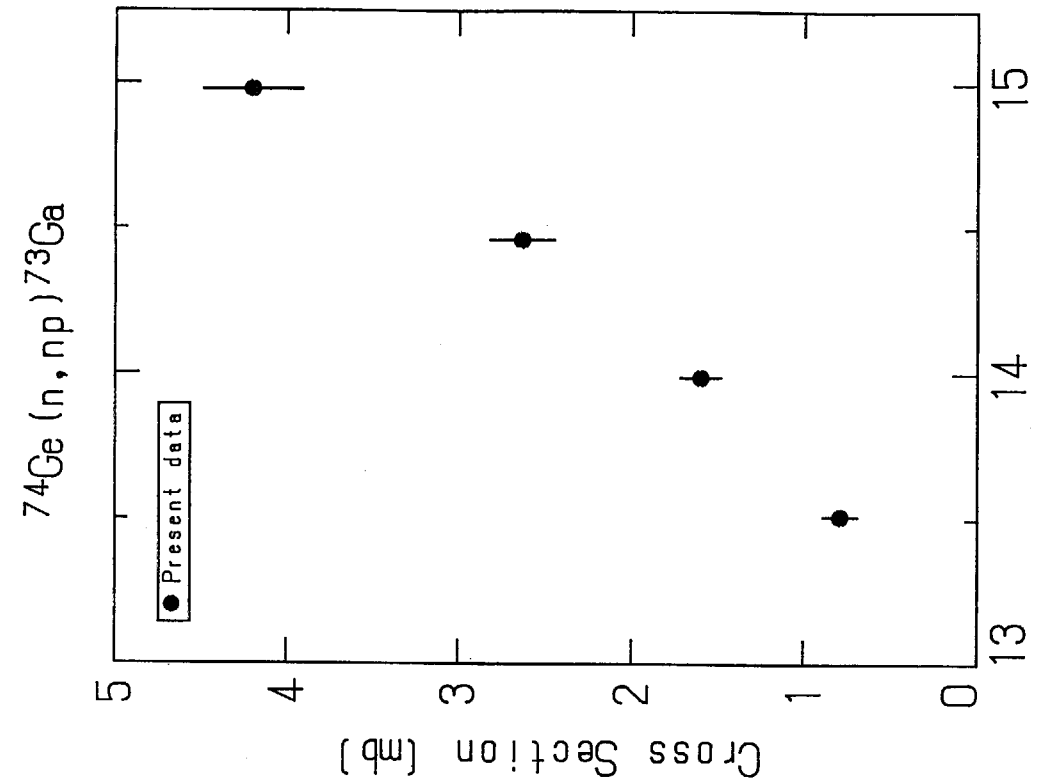

Fig. 3.16 Cross section data for ^{74}Ge (n, np) ^{73}Ga.

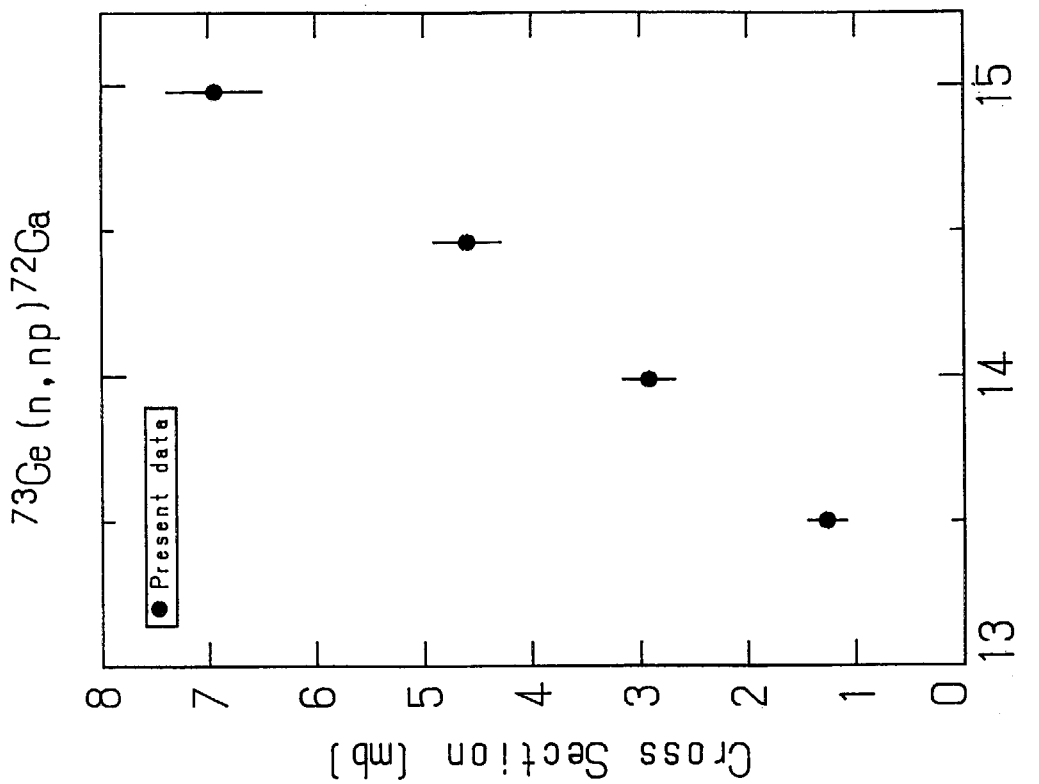

Fig. 3.15 Cross section data for ^{73}Ge (n, np) ^{72}Ga.

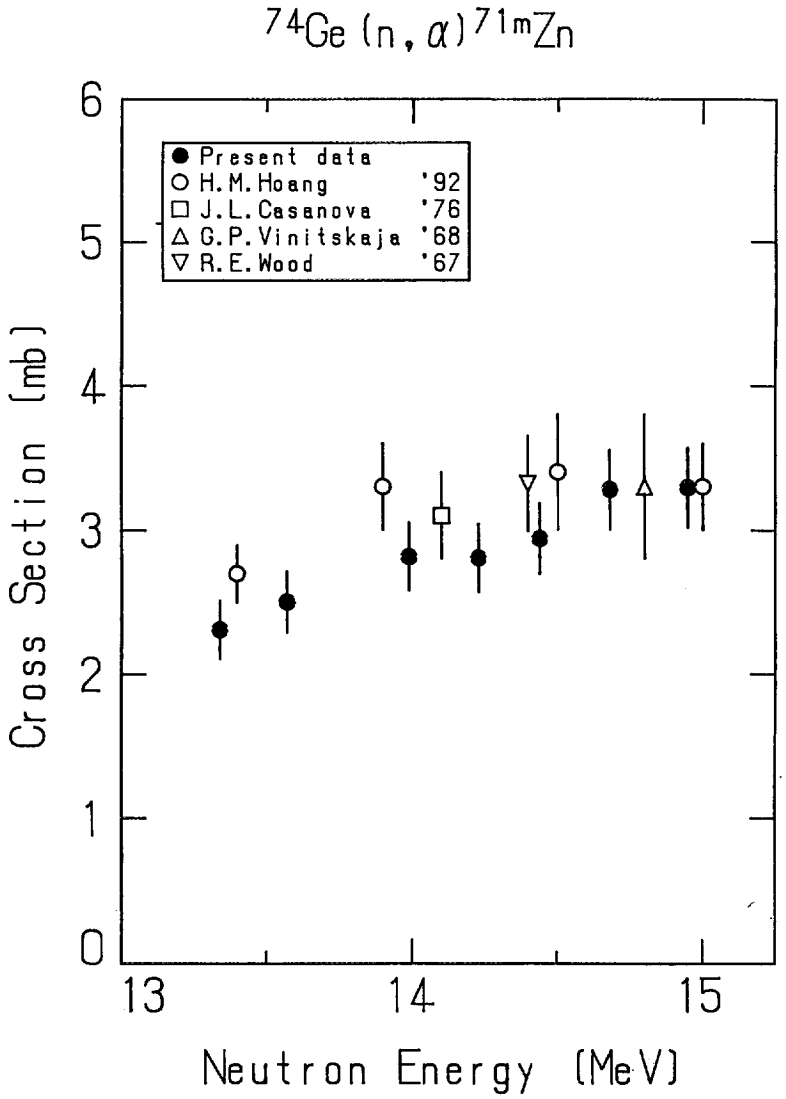

Fig. 3.17 Cross section data for ^{74}Ge (n, α) ^{71m}Zn.

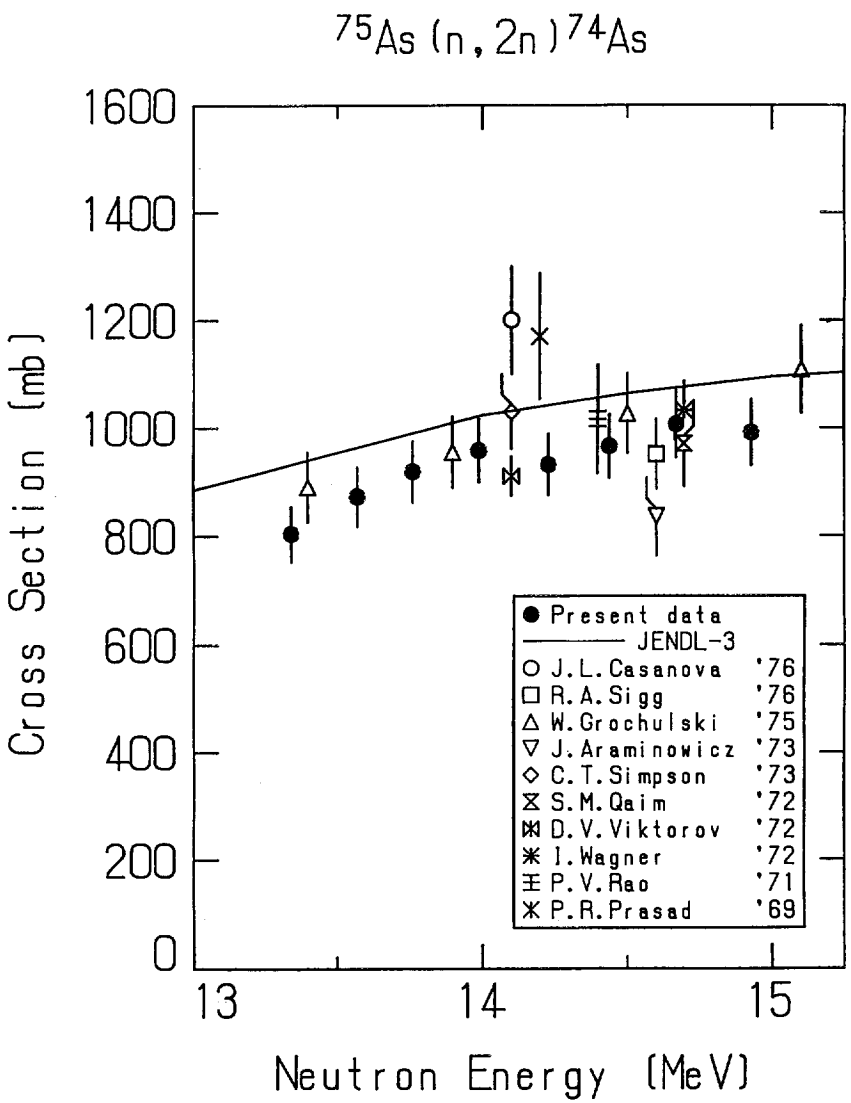

Fig. 3.18 Cross section data for ^{75}As (n, 2n) ^{74}As.

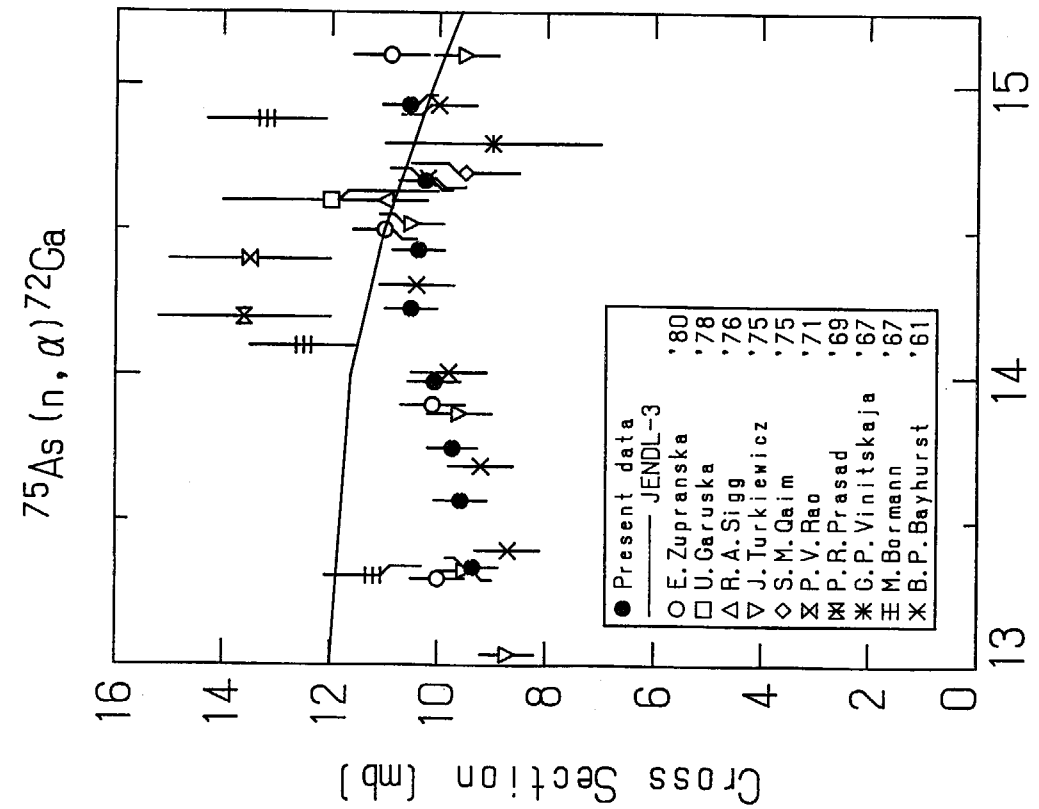

Fig. 3.20 Cross section data for ^{75}As (n, α) ^{72}Ga.

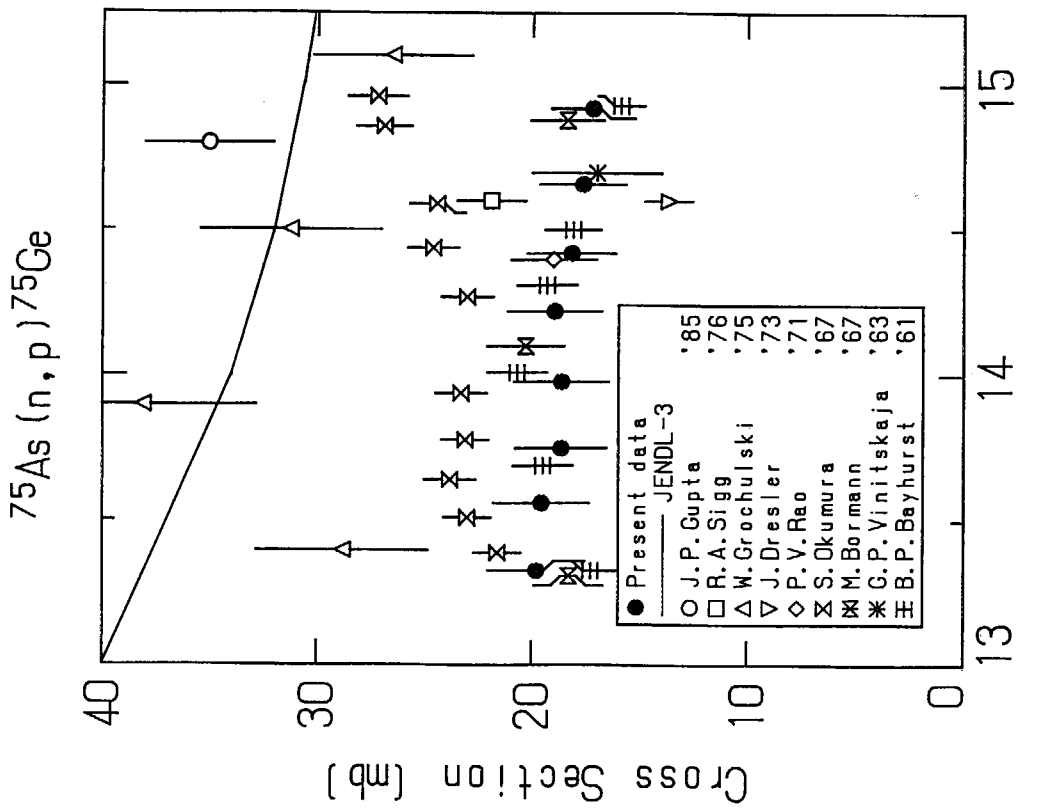

Fig. 3.19 Cross section data for ^{75}As (n, p) ^{75}Ge.

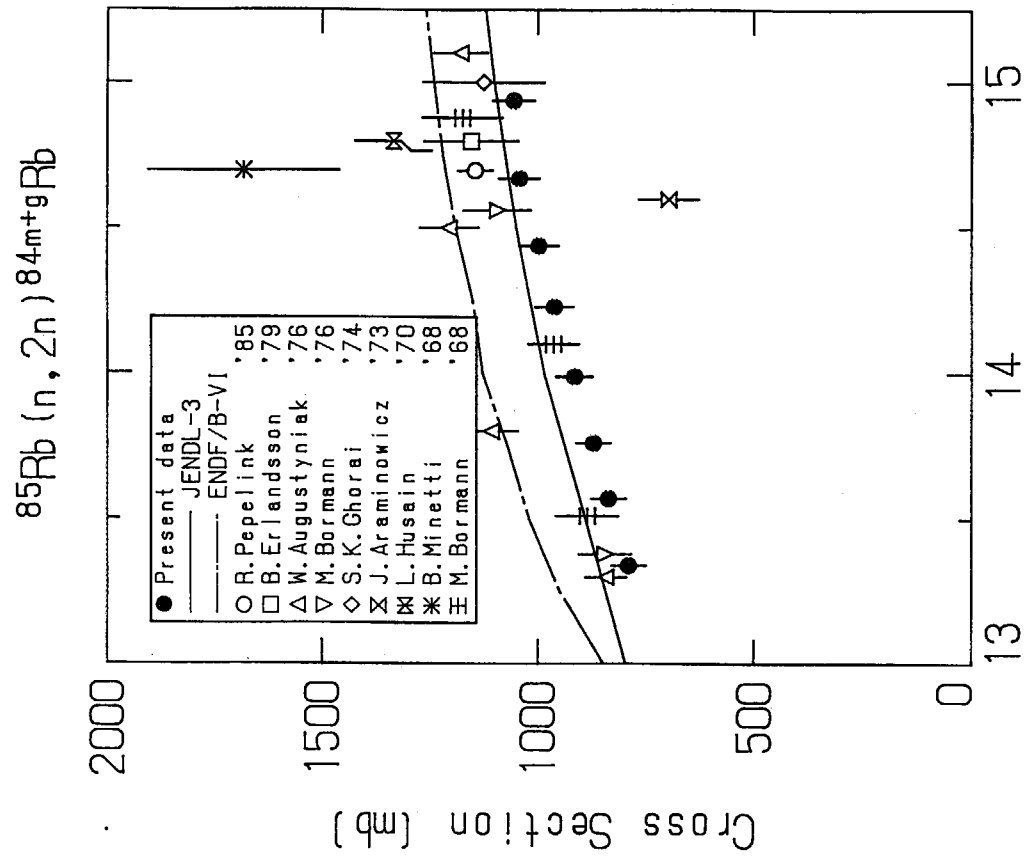

Fig. 3.22 Cross section data for ^{85}Rb (n, 2n) $^{84m+g}$Rb.

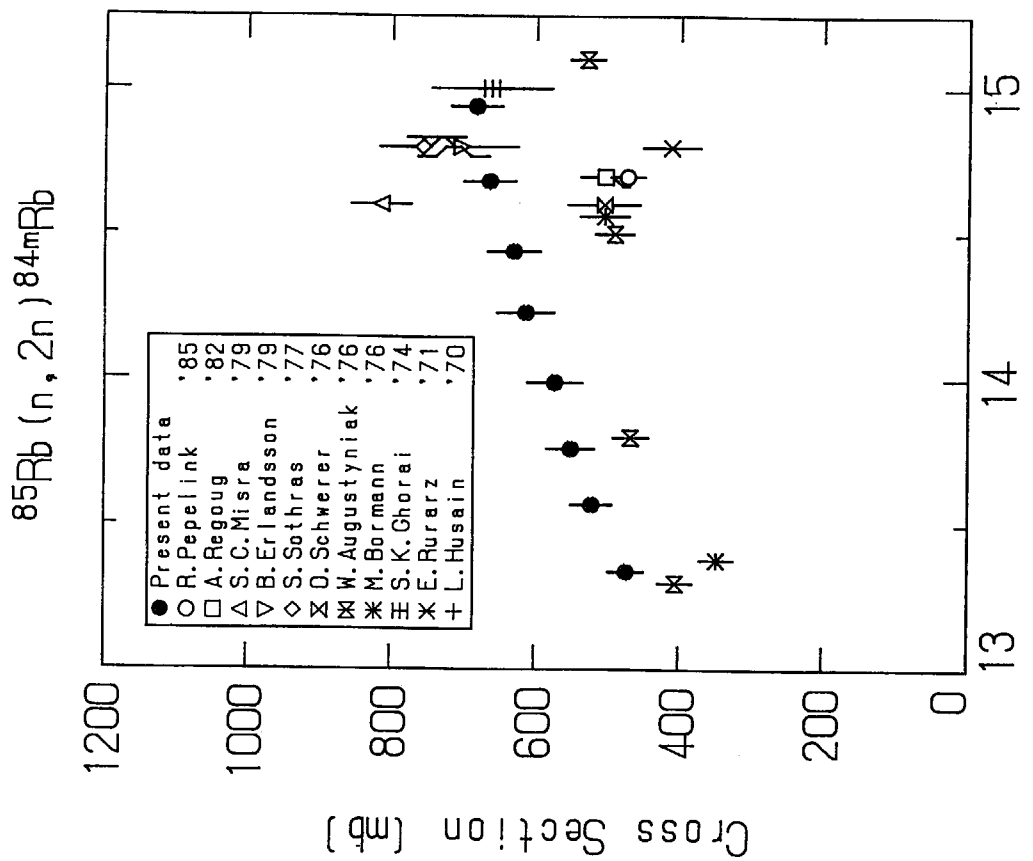

Fig. 3.21 Cross section data for ^{85}Rb (n, 2n) ^{84m}Rb.

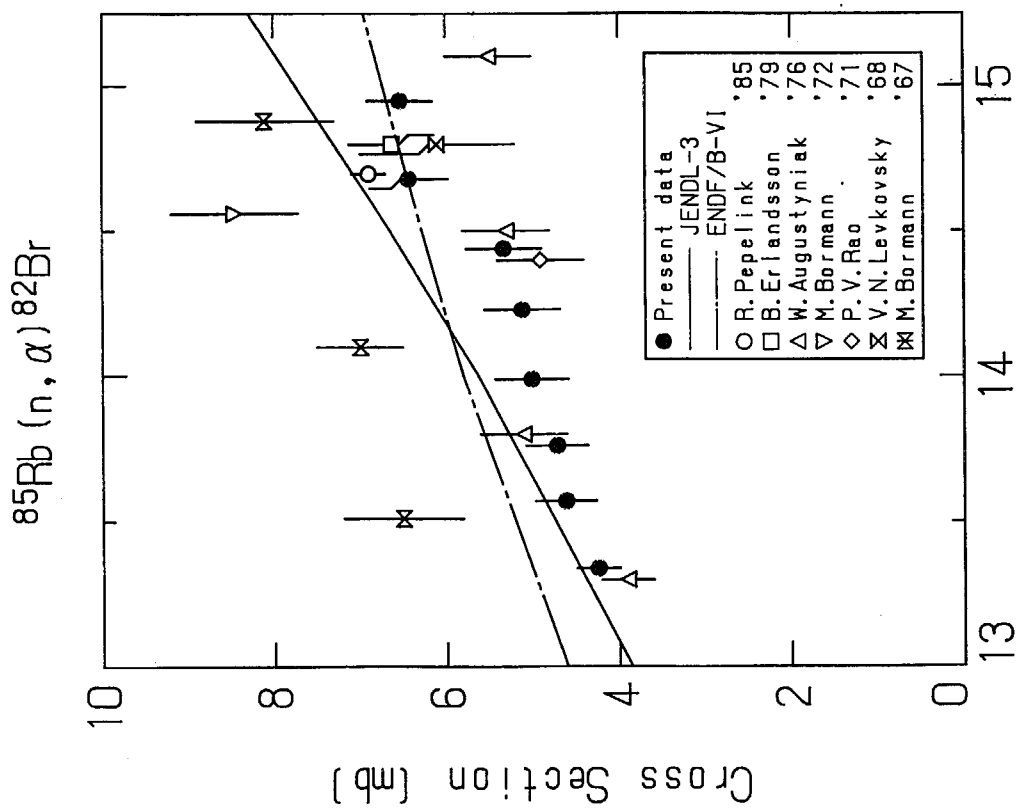

Fig. 3.24 Cross section data for ^{85}Rb (n, α) ^{82}Br.

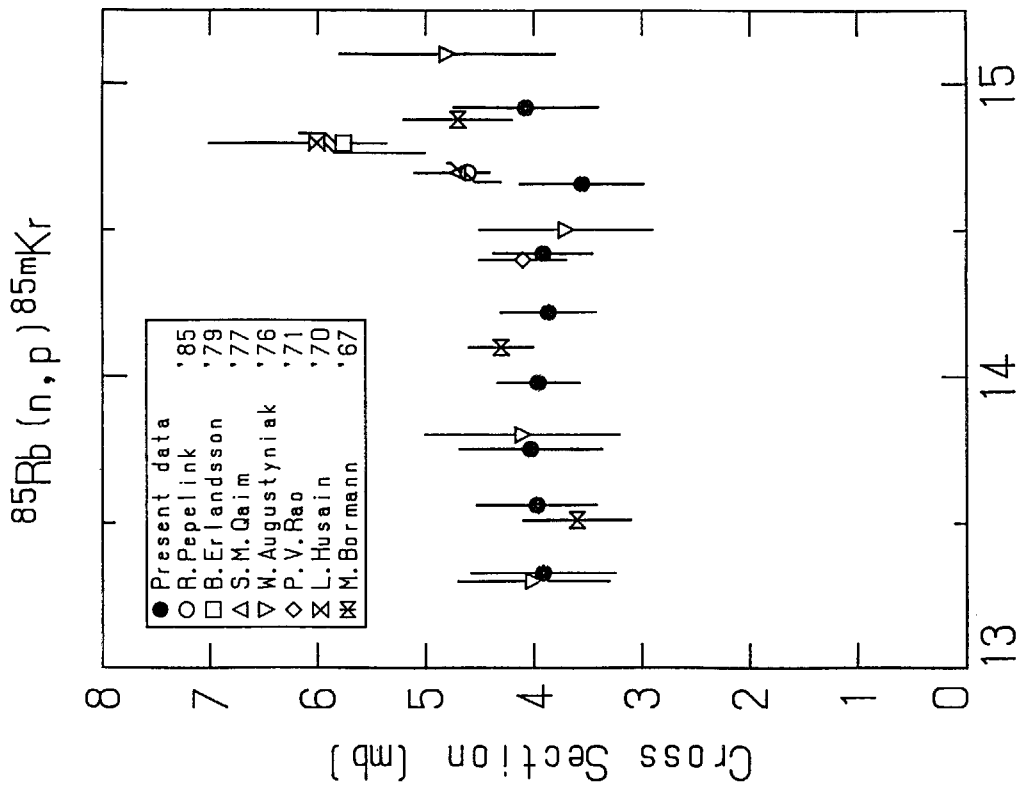

Fig. 3.23 Cross section data for ^{85}Rb (n, p) ^{85m}Kr.

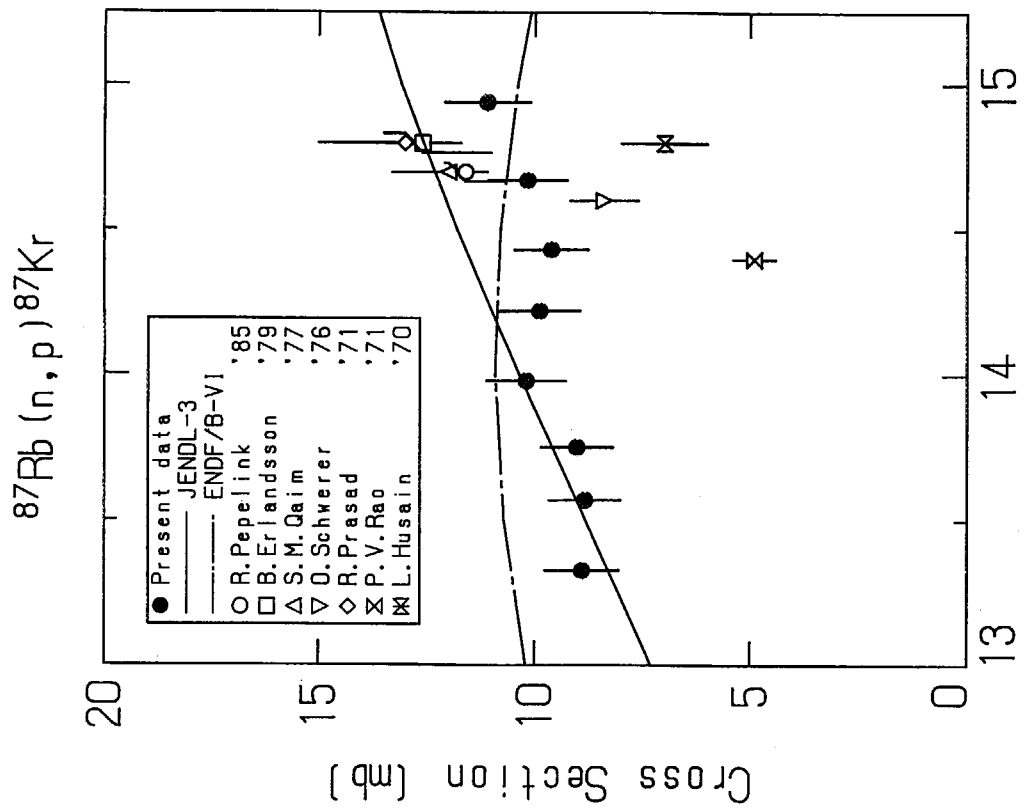

Fig. 3.26 Cross section data for ^{87}Rb (n, p) ^{87}Kr.

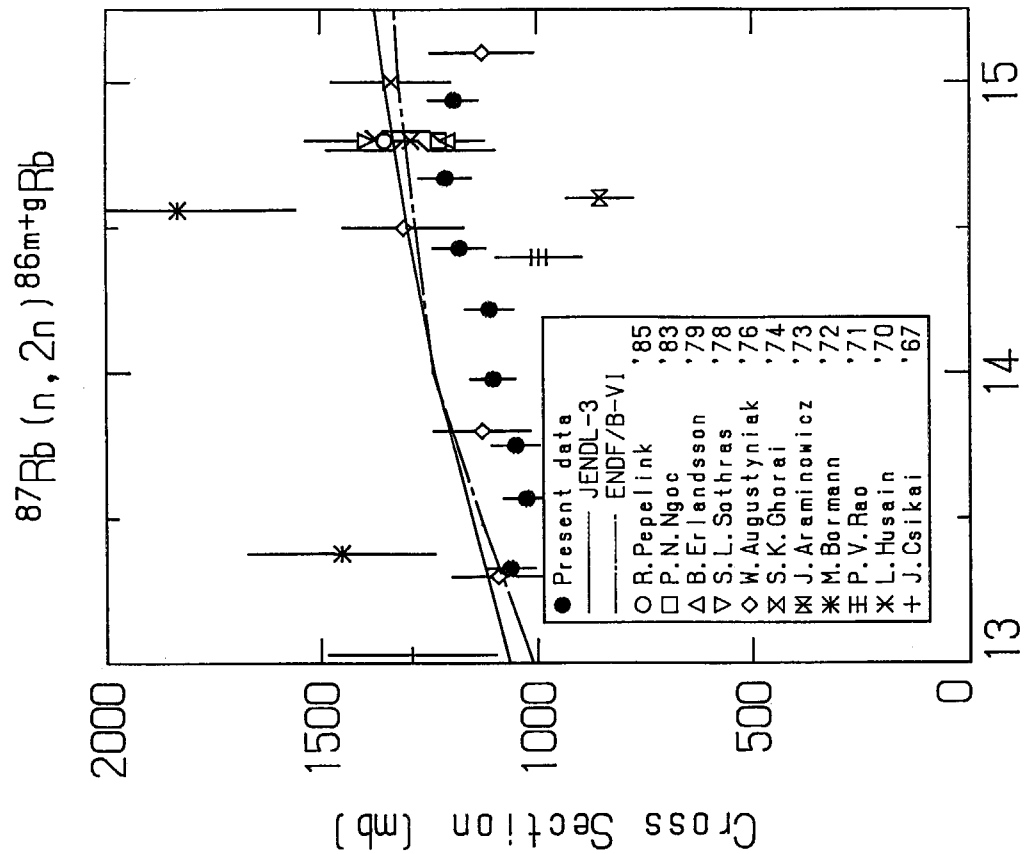

Fig. 3.25 Cross section data for ^{87}Rb (n, 2n) $^{86m+g}$Rb.

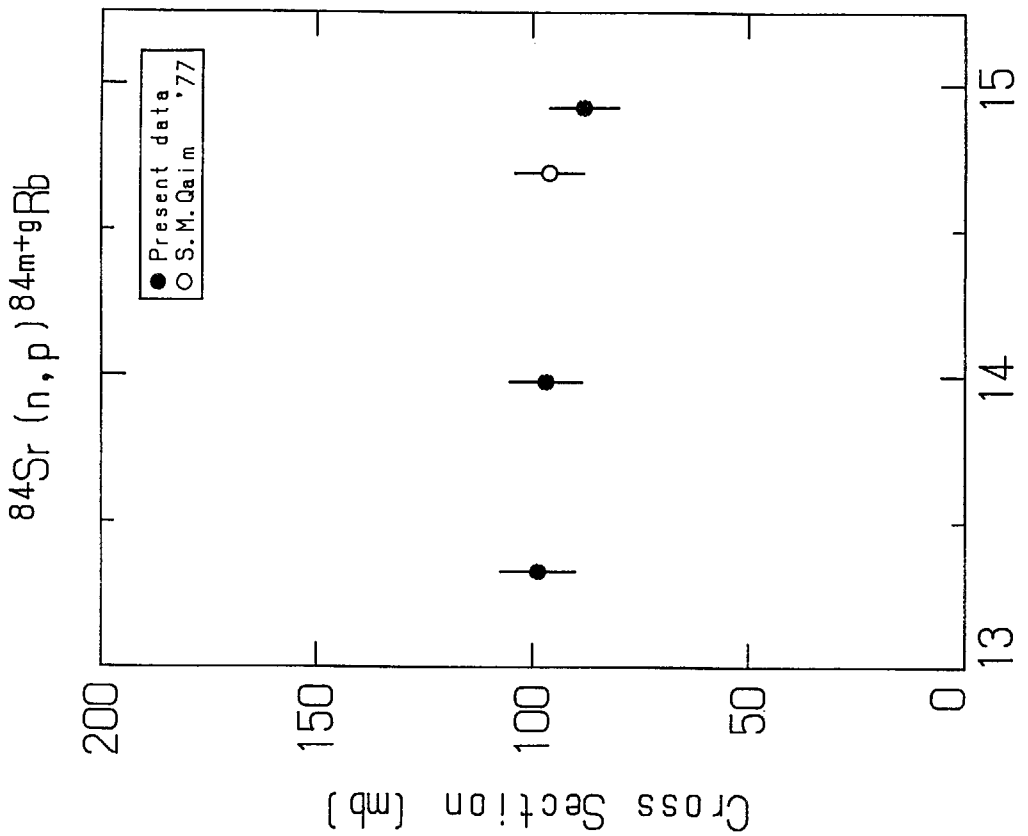

Fig. 3.28 Cross section data for ^{84}Sr (n, p) $^{84m+g}Rb$.

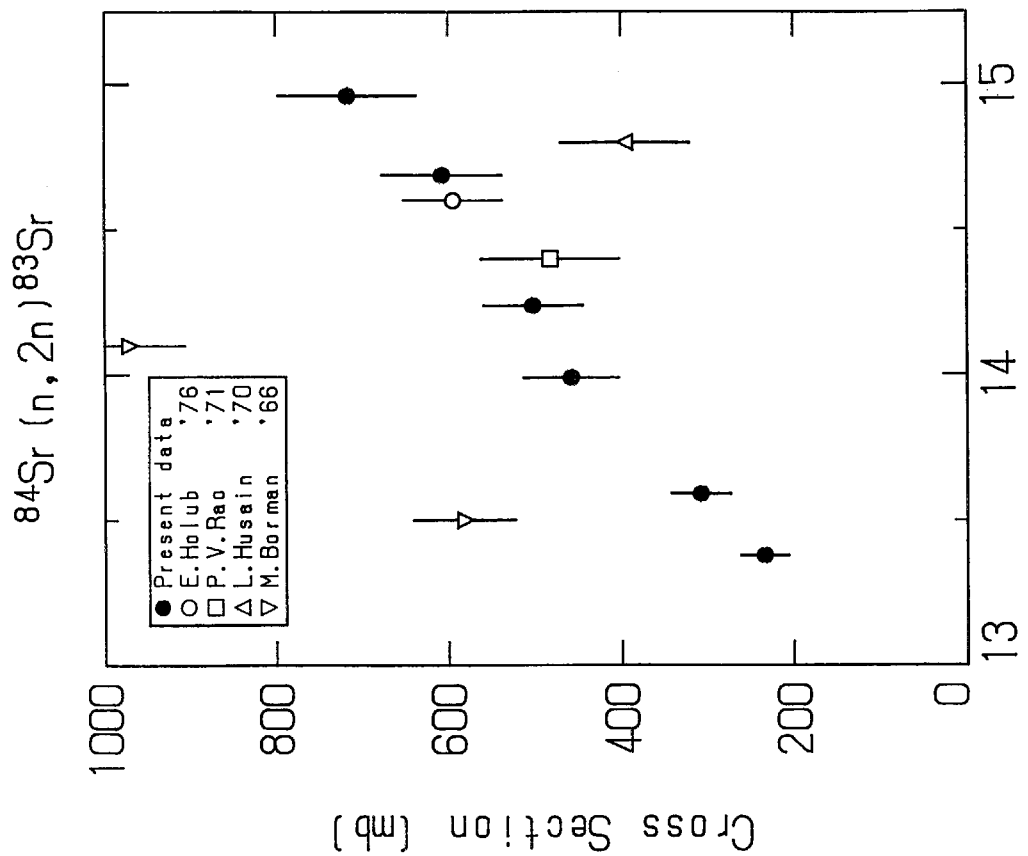

Fig. 3.27 Cross section data for ^{84}Sr (n, 2n) ^{83}Sr.

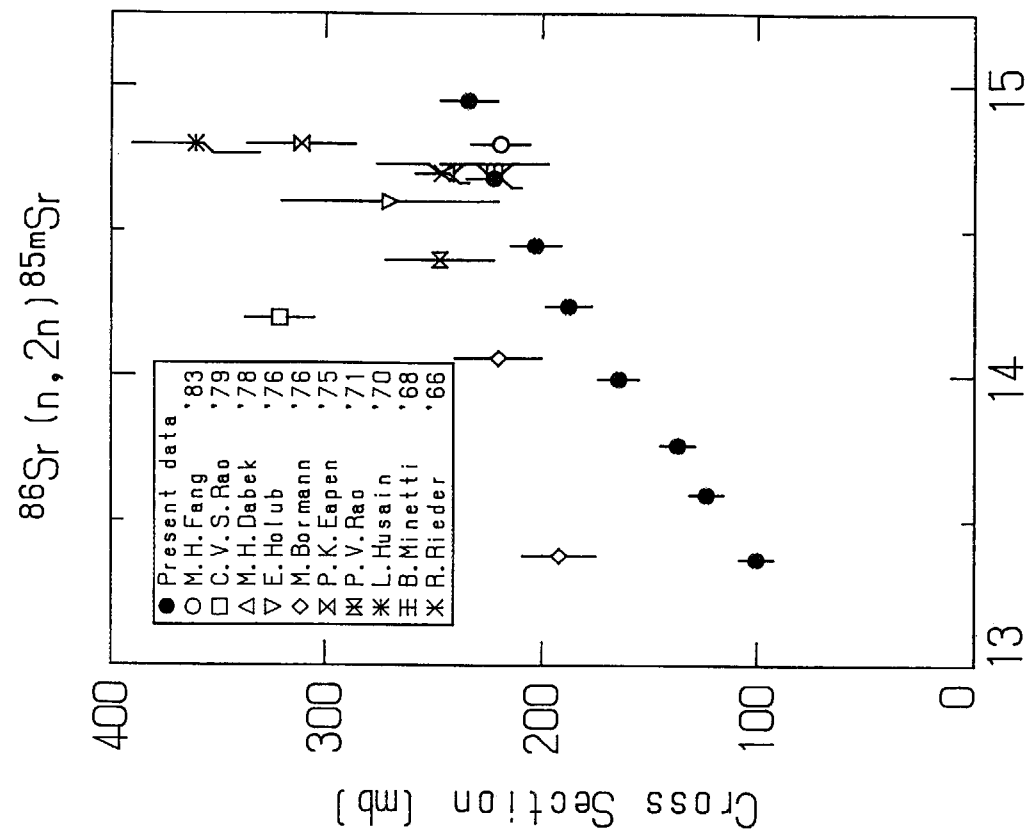

Fig. 3.30 Cross section data for ^{86}Sr (n, 2n) ^{85m}Sr.

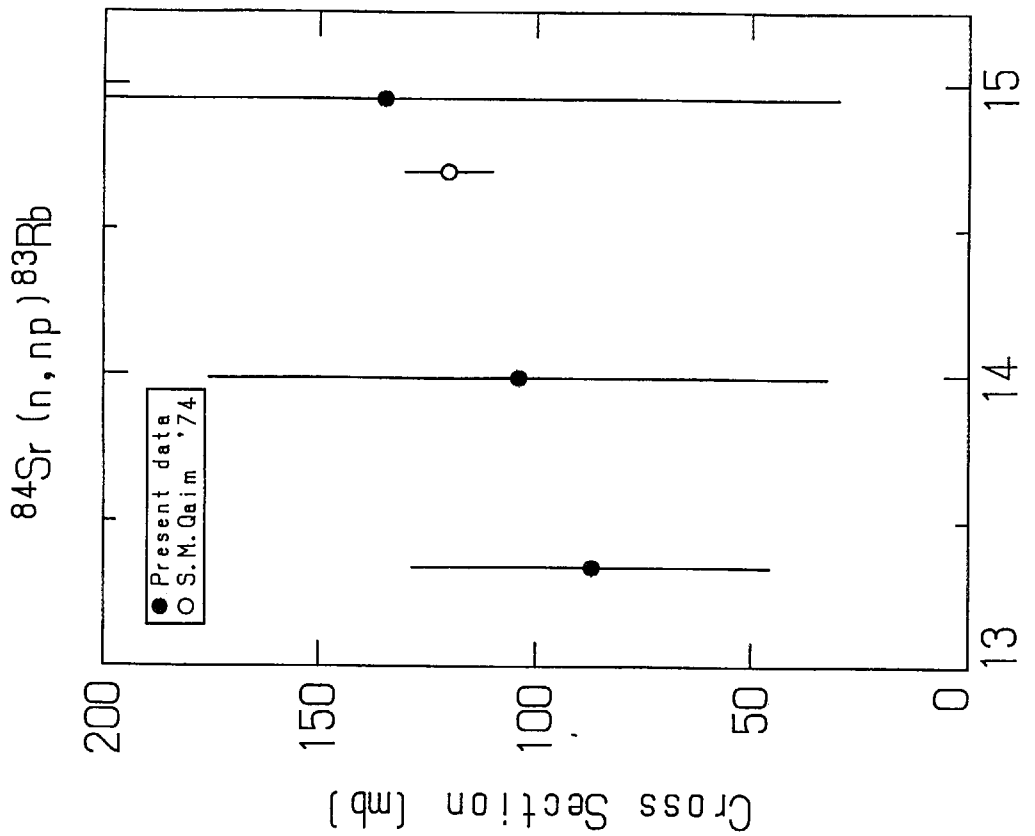

Fig. 3.29 Cross section data for ^{84}Sr (n, np) ^{83}Rb.

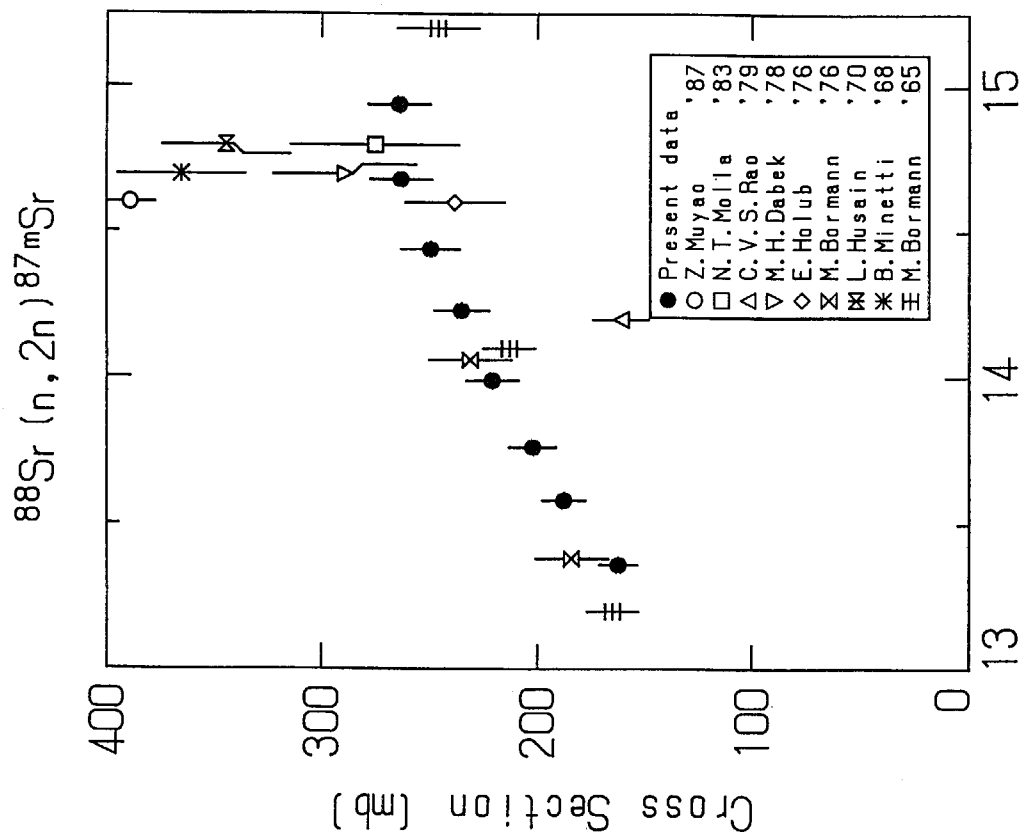

Fig. 3.32 Cross section data for ^{88}Sr (n, 2n) ^{87m}Sr.

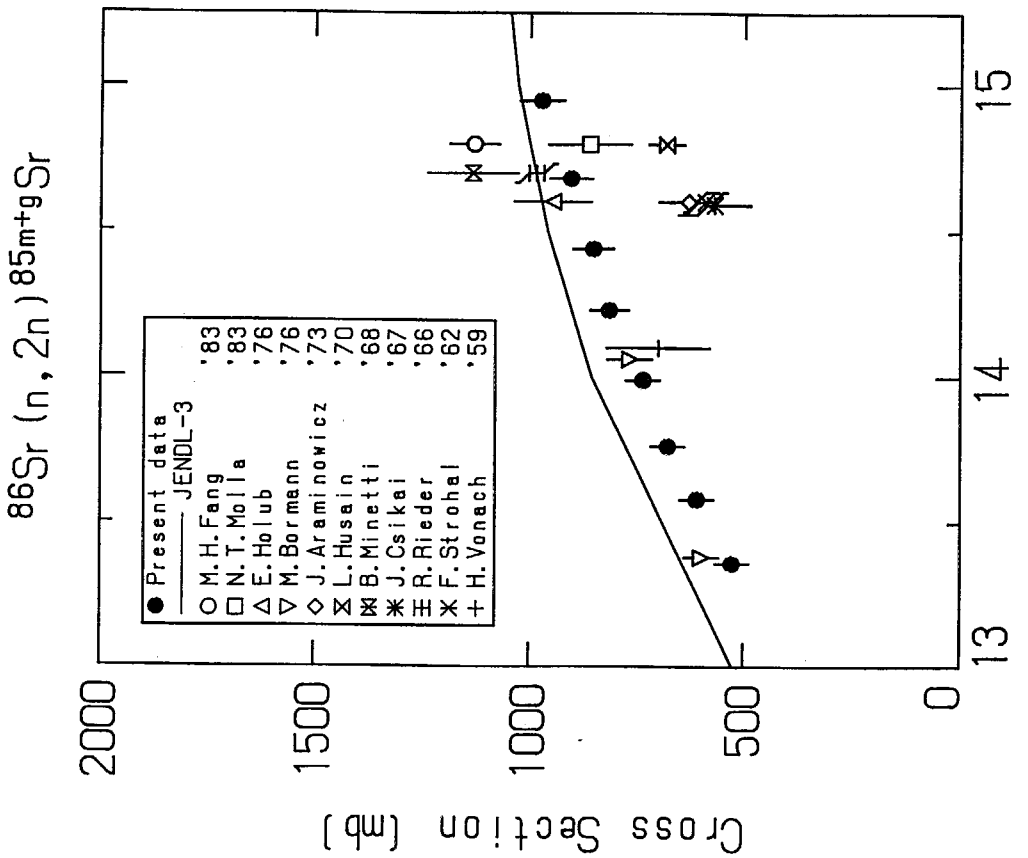

Fig. 3.31 Cross section data for ^{86}Sr (n, 2n) $^{85m+g}Sr$.

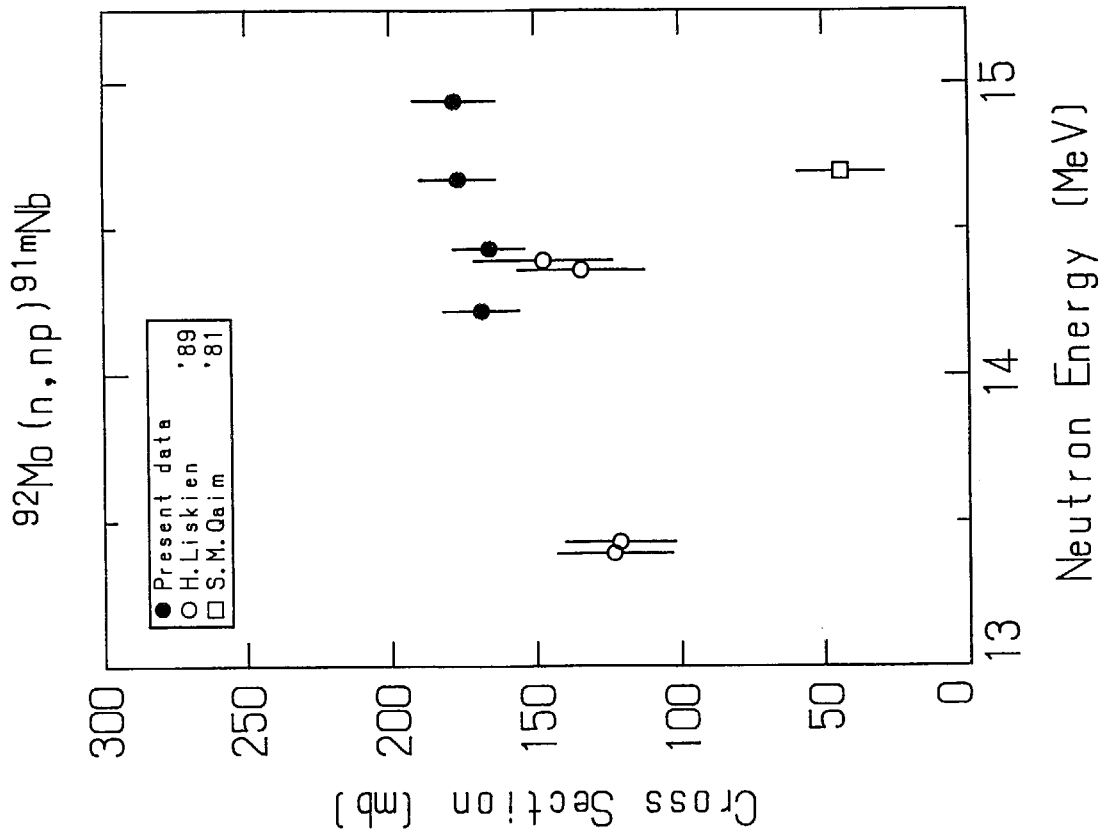

Fig. 3.34 Cross section data for ^{92}Mo (n, np) ^{91m}Nb.

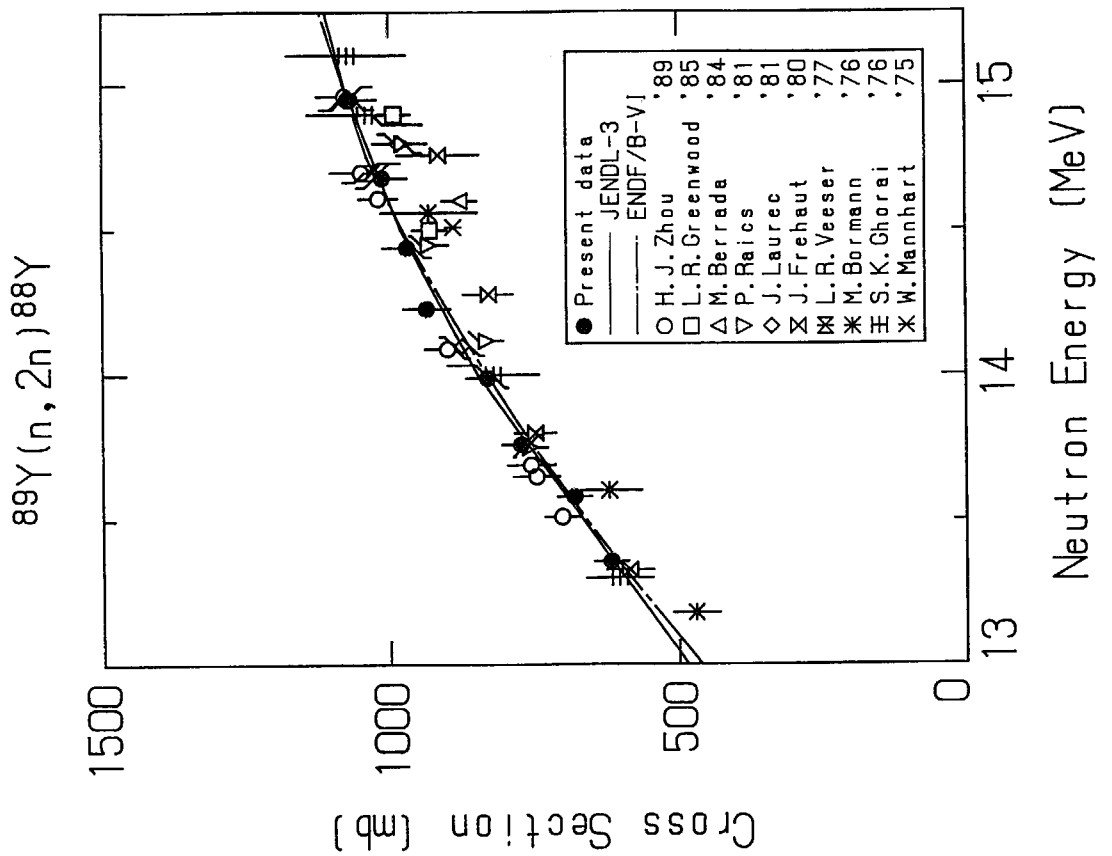

Fig. 3.33 Cross section data for ^{89}Y (n, 2n) ^{88}Y.

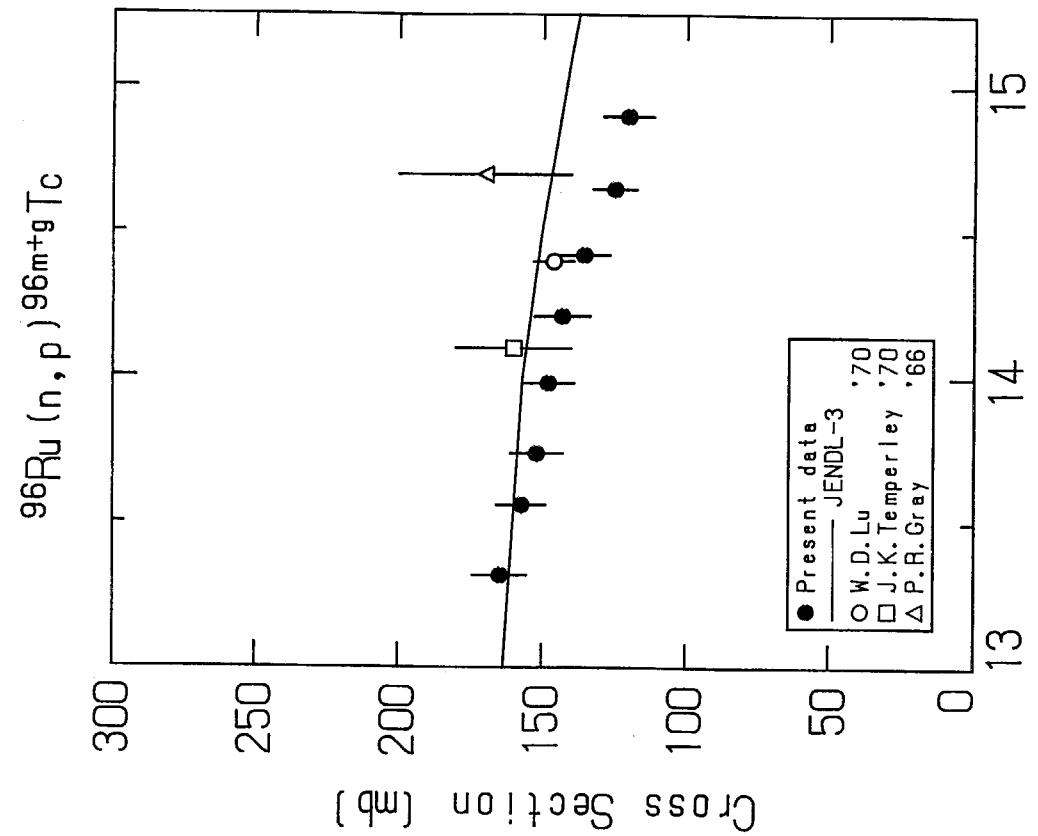

Fig. 3.36 Cross section data for ^{96}Ru (n, p) $^{96m+g}$Tc.

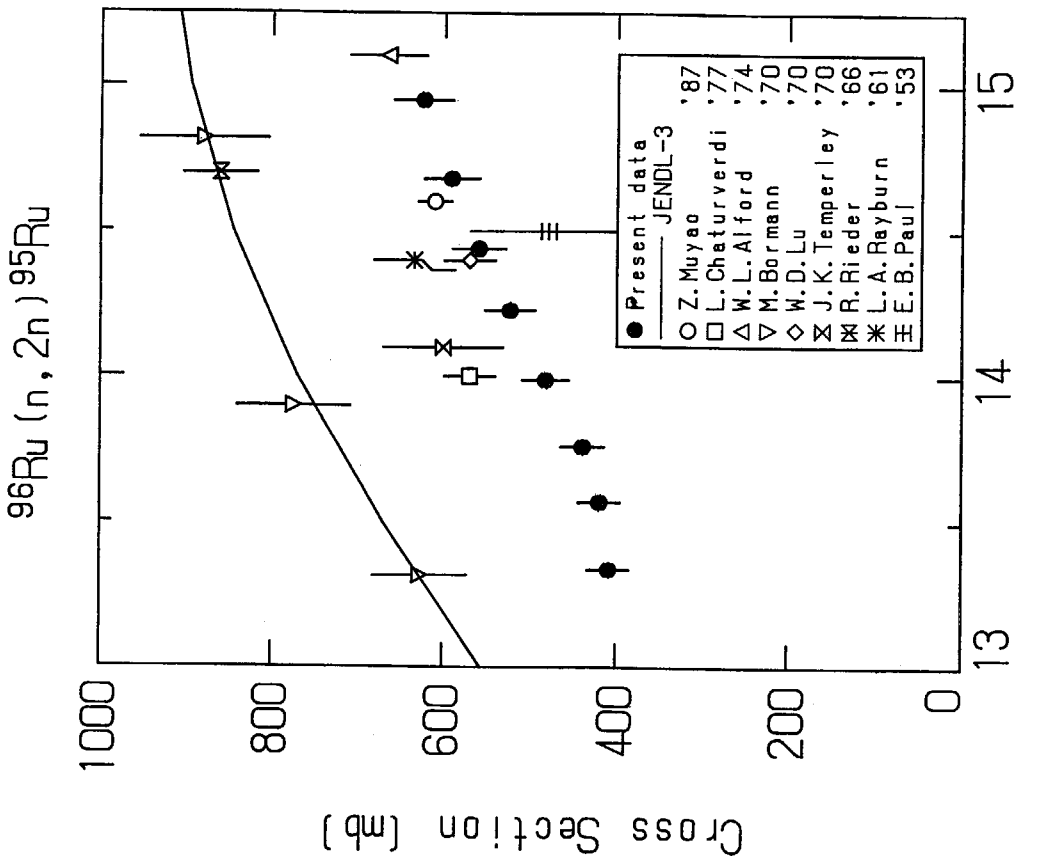

Fig. 3.35 Cross section data for ^{96}Ru (n, 2n) ^{95}Ru.

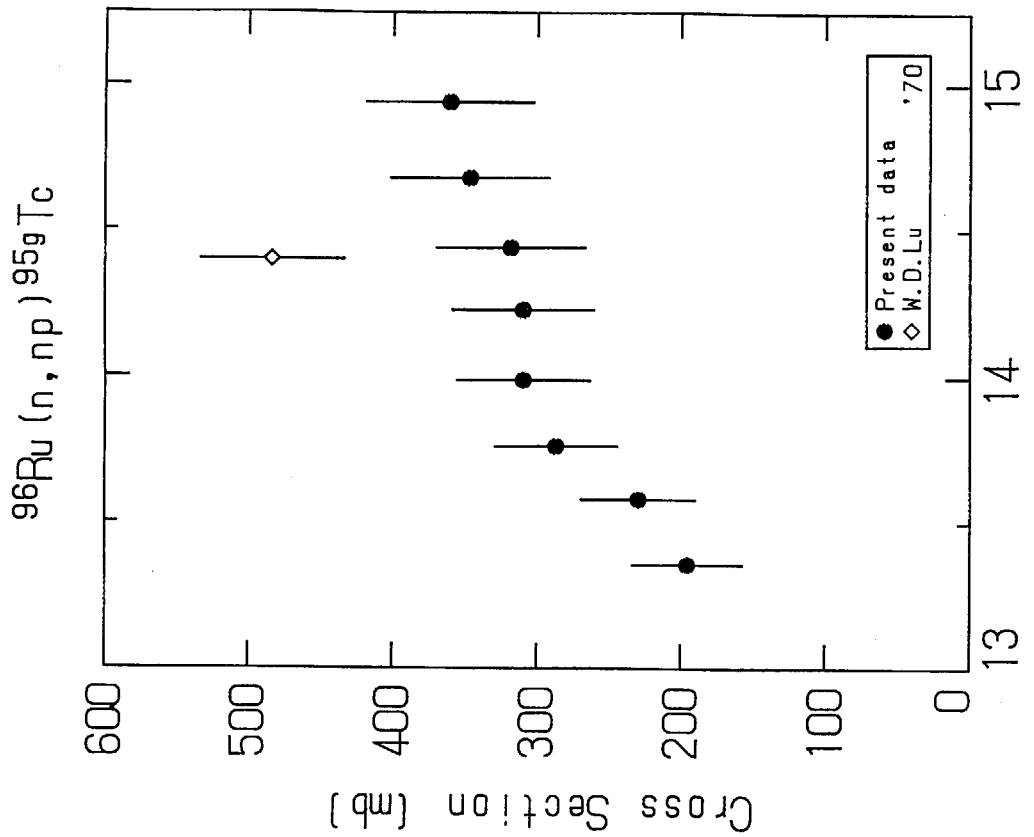

Fig. 3.38 Cross section data for ^{96}Ru (n, np) ^{95g}Tc.

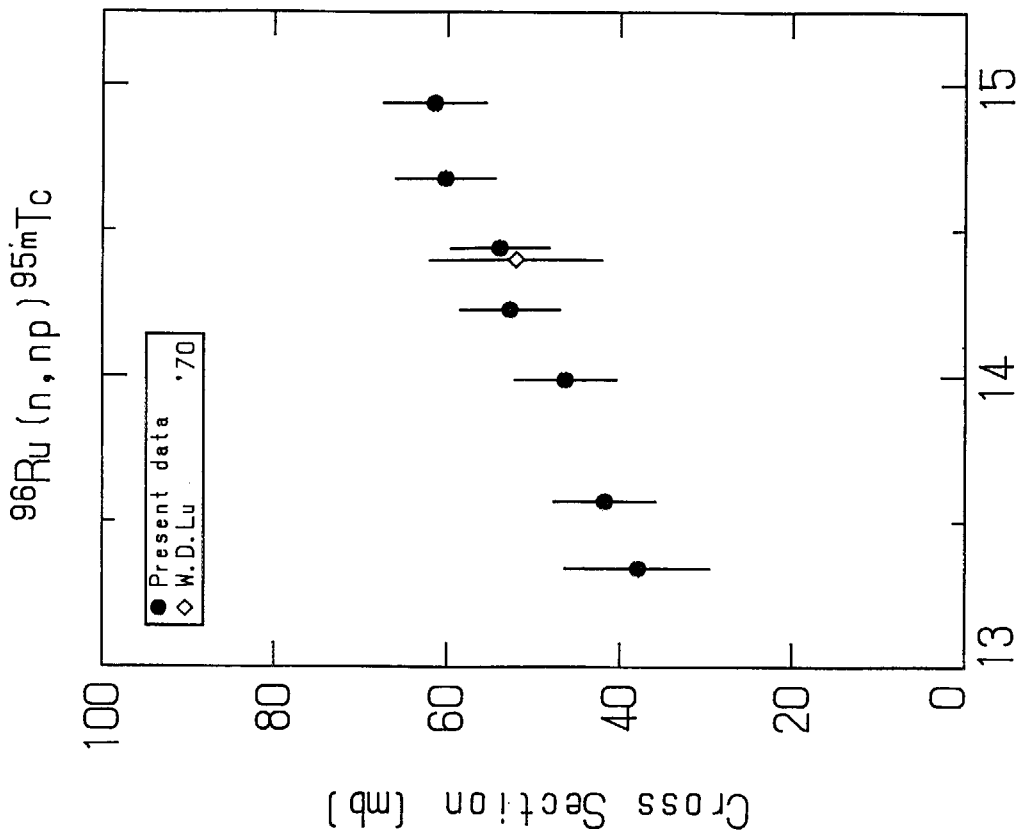

Fig. 3.37 Cross section data for ^{96}Ru (n, np) ^{95m}Tc.

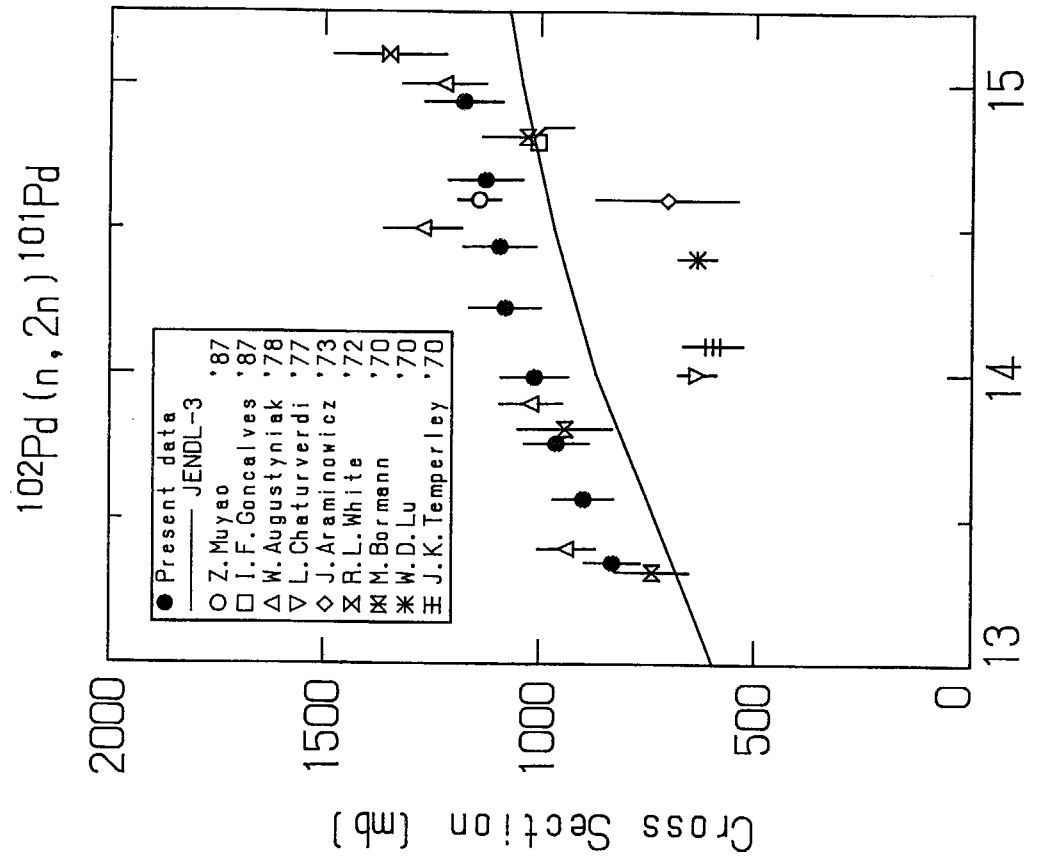

Fig. 3.40 Cross section data for ^{102}Pd (n, 2n) ^{101}Pd.

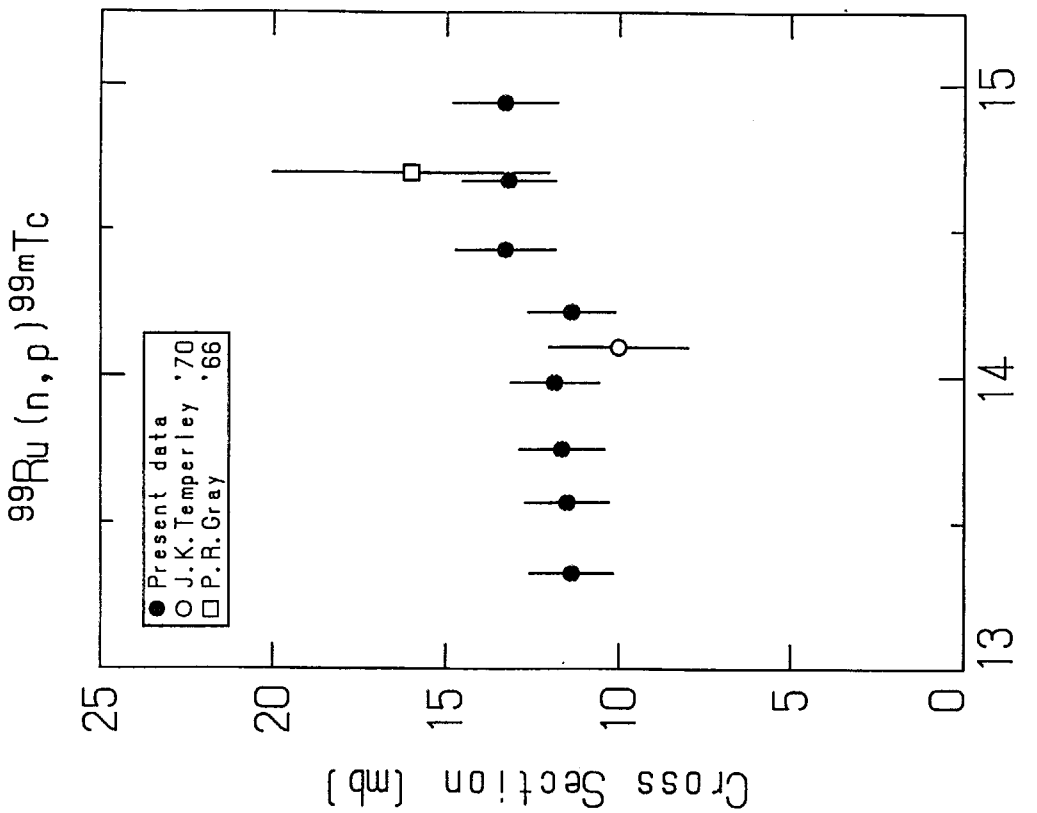

Fig. 3.39 Cross section data for ^{99}Ru (n, p) ^{99m}Tc.

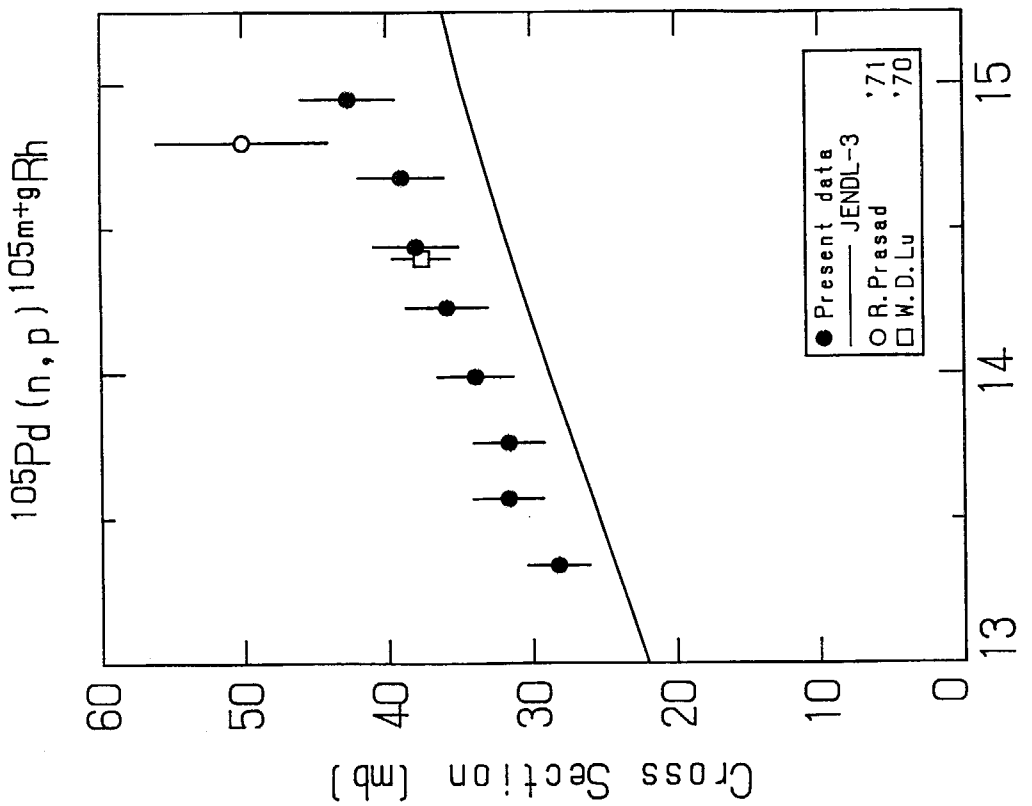

Fig. 3.42 Cross section data for ^{105}Pd (n, p) $^{105m+g}$Rh.

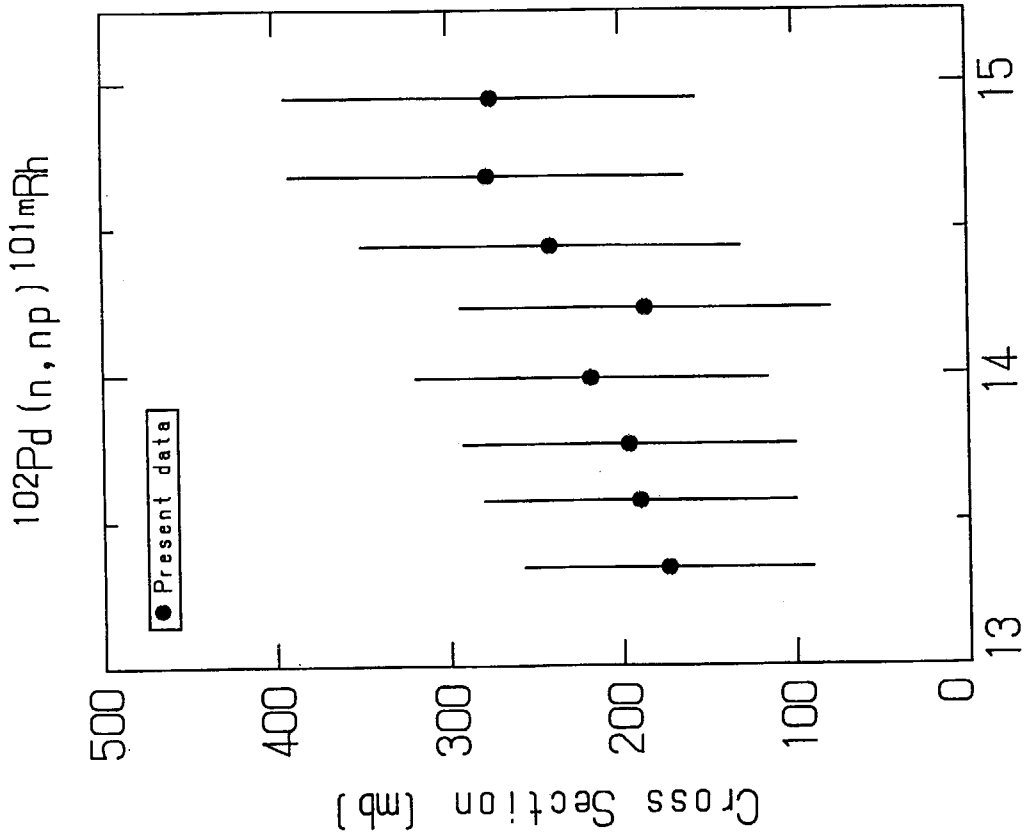

Fig. 3.41 Cross section data for ^{102}Pd (n, np) ^{101m}Rh.

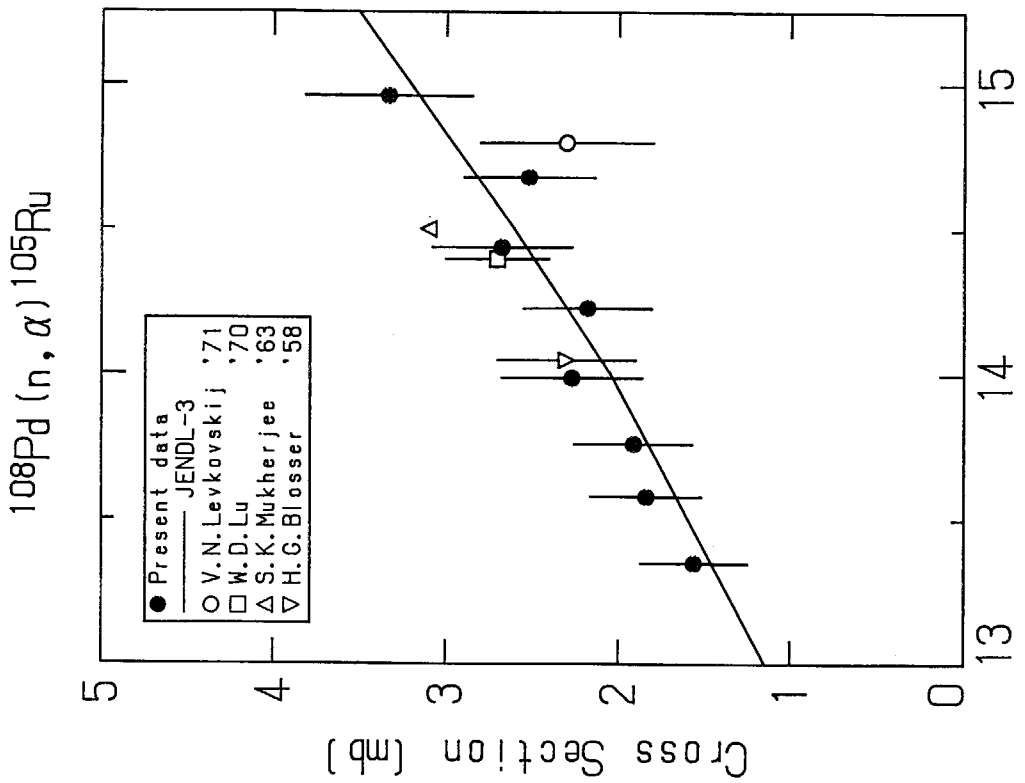

Fig. 3.44 Cross section data for ^{108}Pd (n, α) ^{105}Ru.

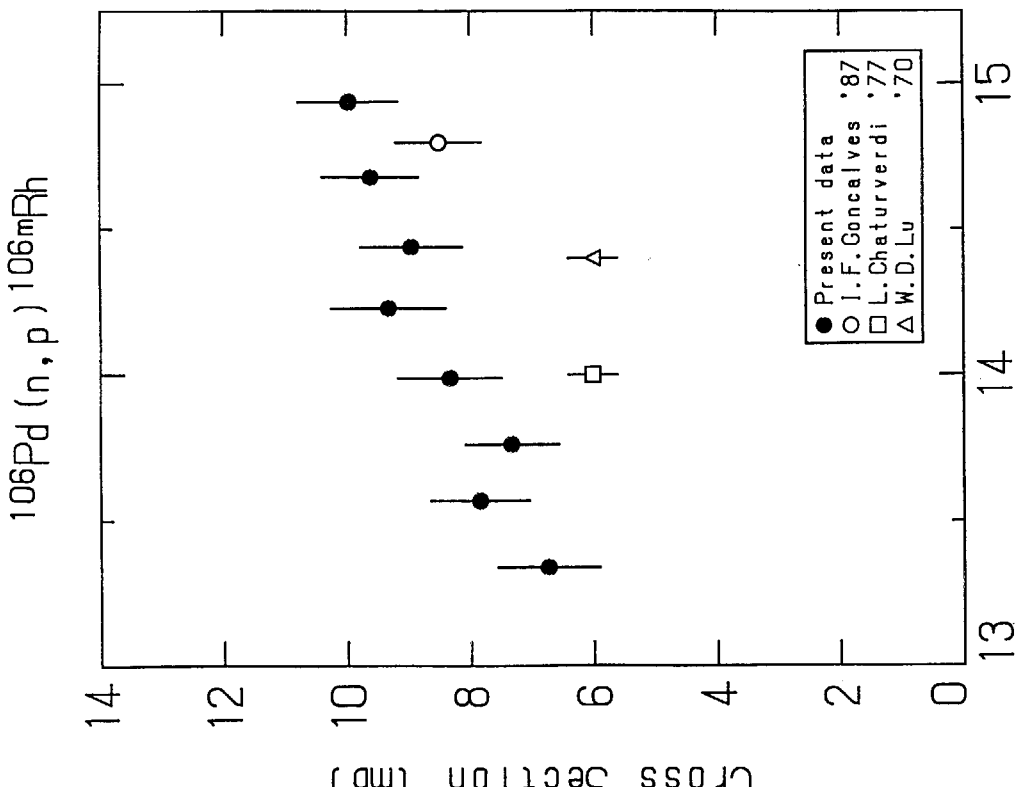

Fig. 3.43 Cross section data for ^{106}Pd (n, p) ^{106m}Rh.

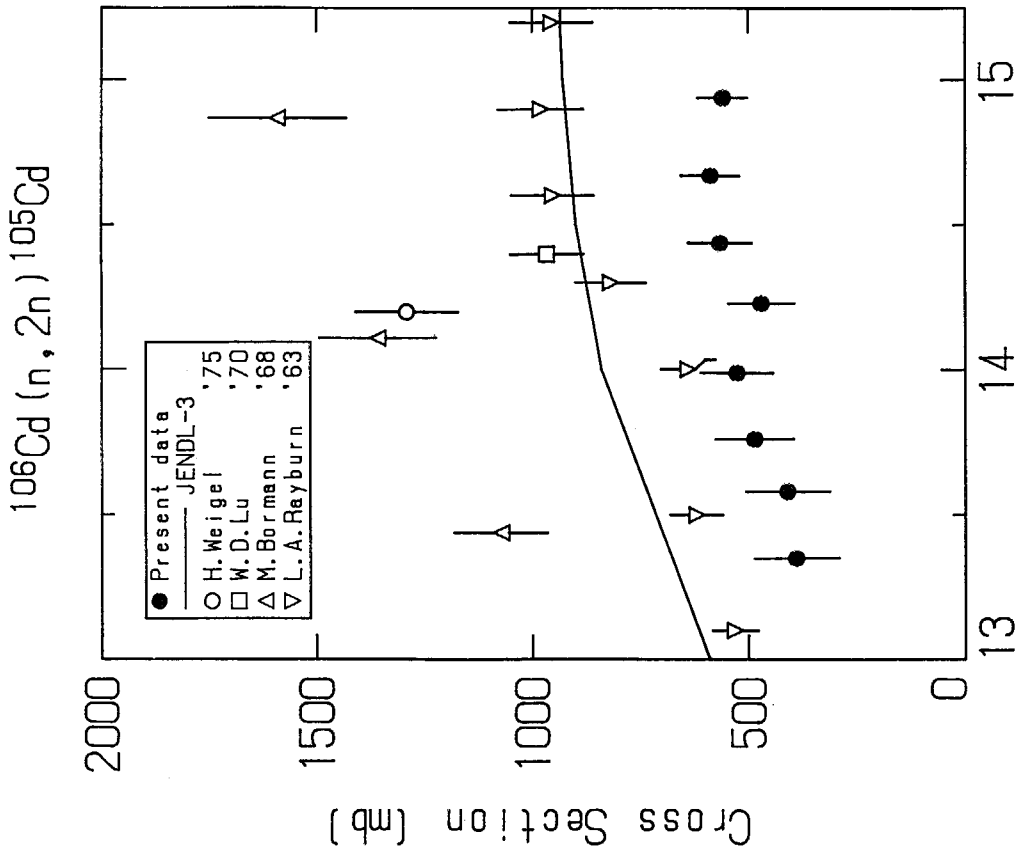

Fig. 3.46 Cross section data for ^{106}Cd (n, 2n) ^{105}Cd.

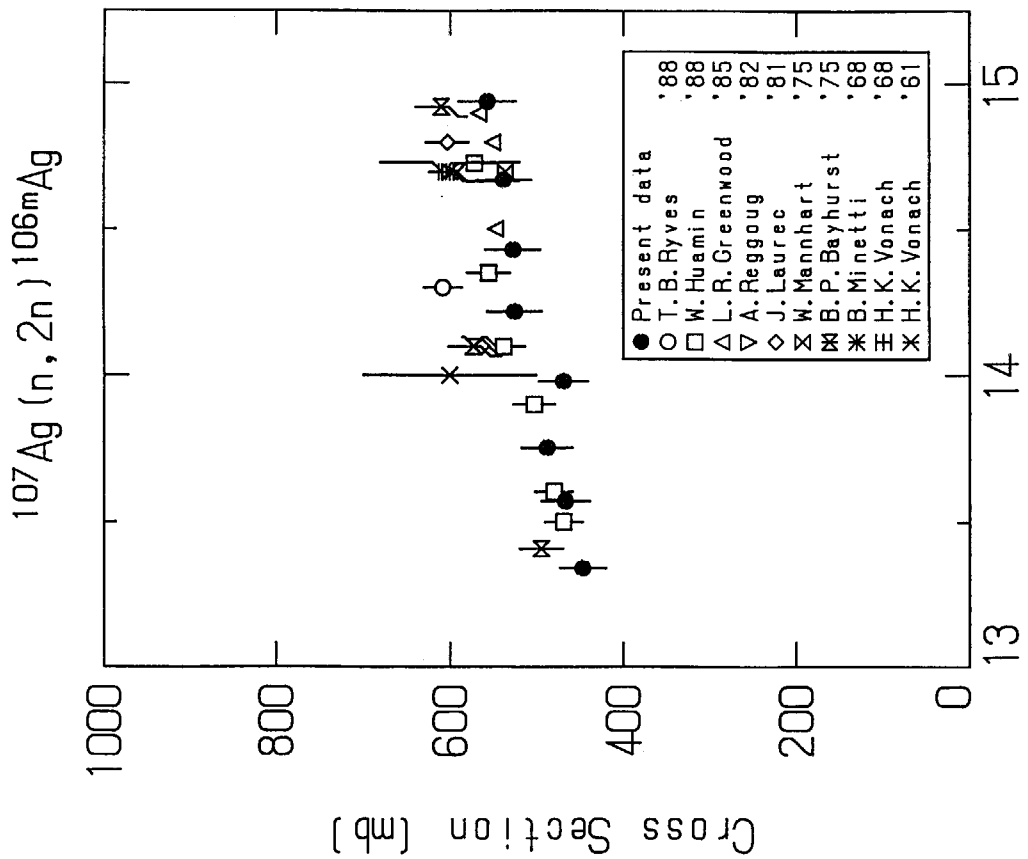

Fig. 3.45 Cross section data for ^{107}Ag (n, 2n) ^{106m}Ag.

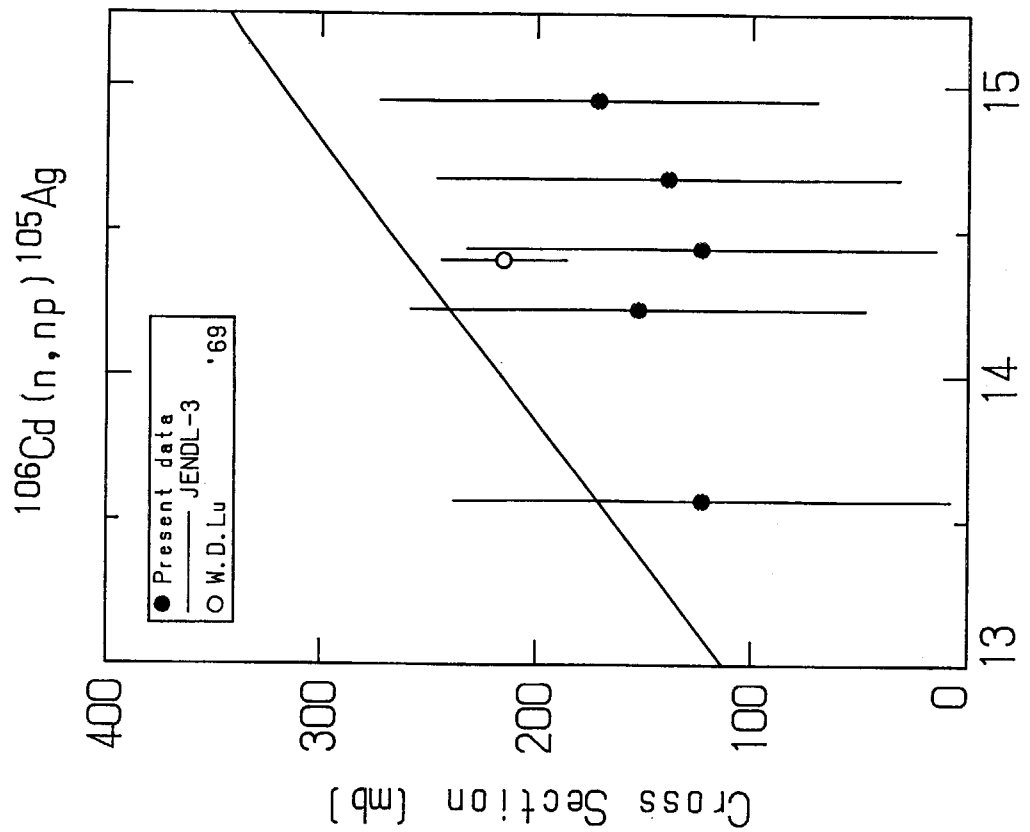

Fig. 3.48 Cross section data for ^{106}Cd (n, np) ^{105}Ag.

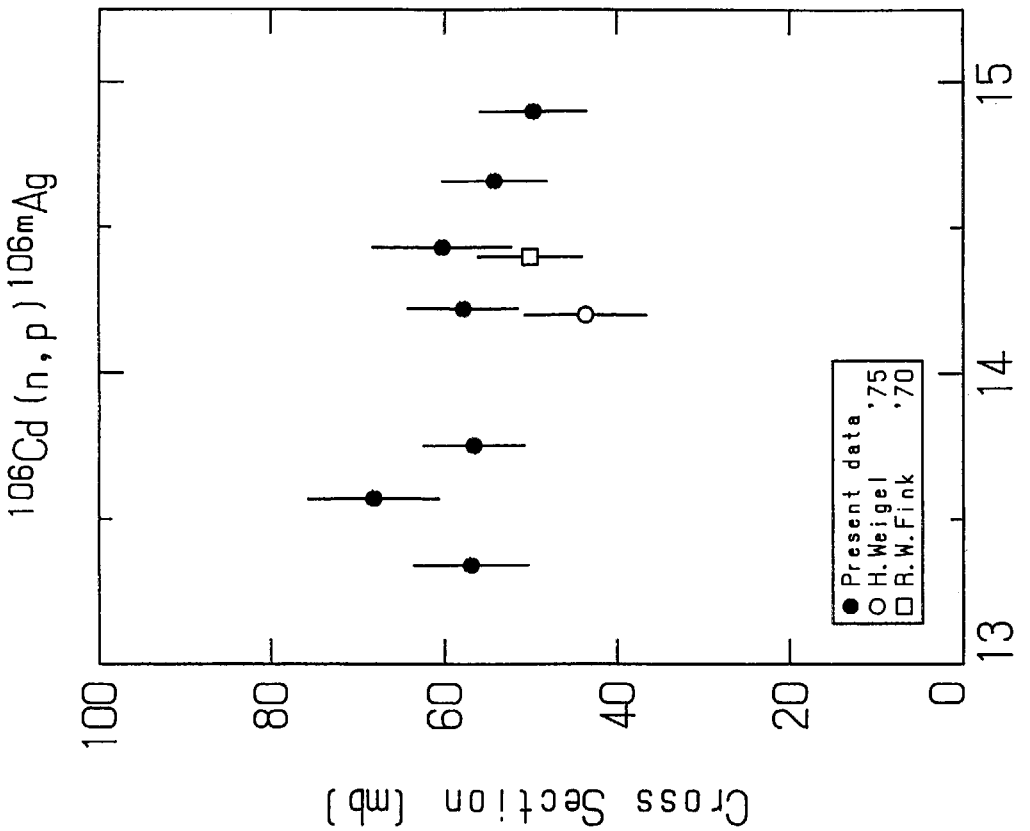

Fig. 3.47 Cross section data for ^{106}Cd (n, p) ^{106m}Ag.

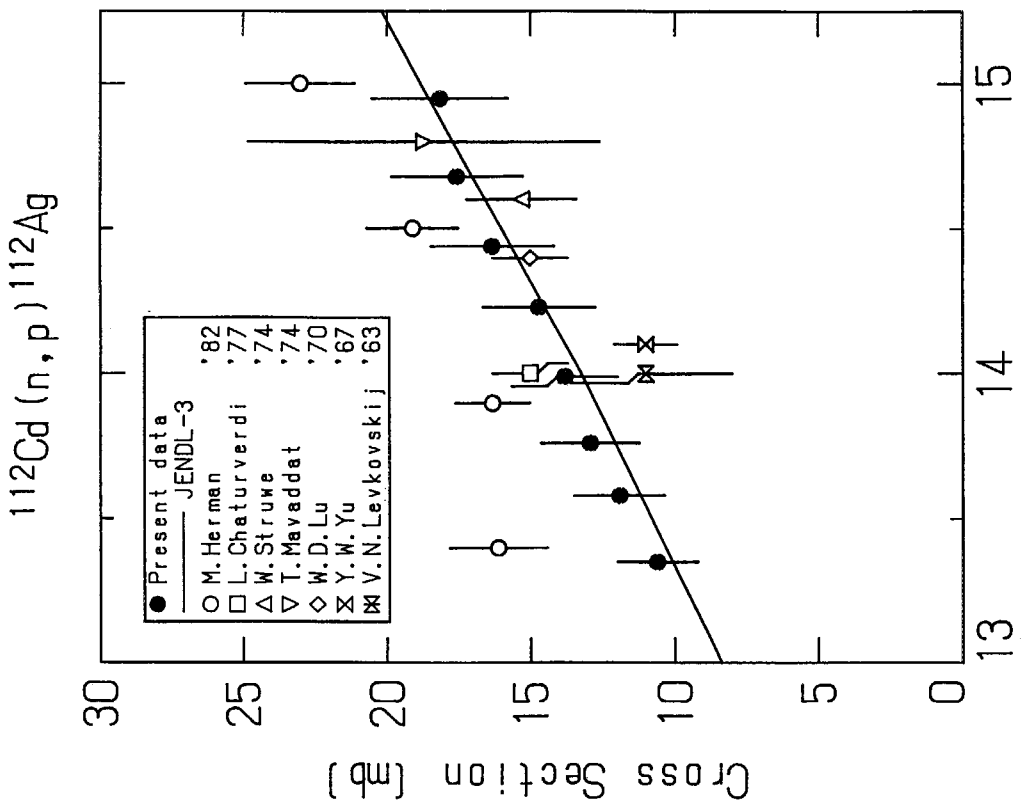

Fig. 3.50 Cross section data for ^{112}Cd (n, p) ^{112}Ag.

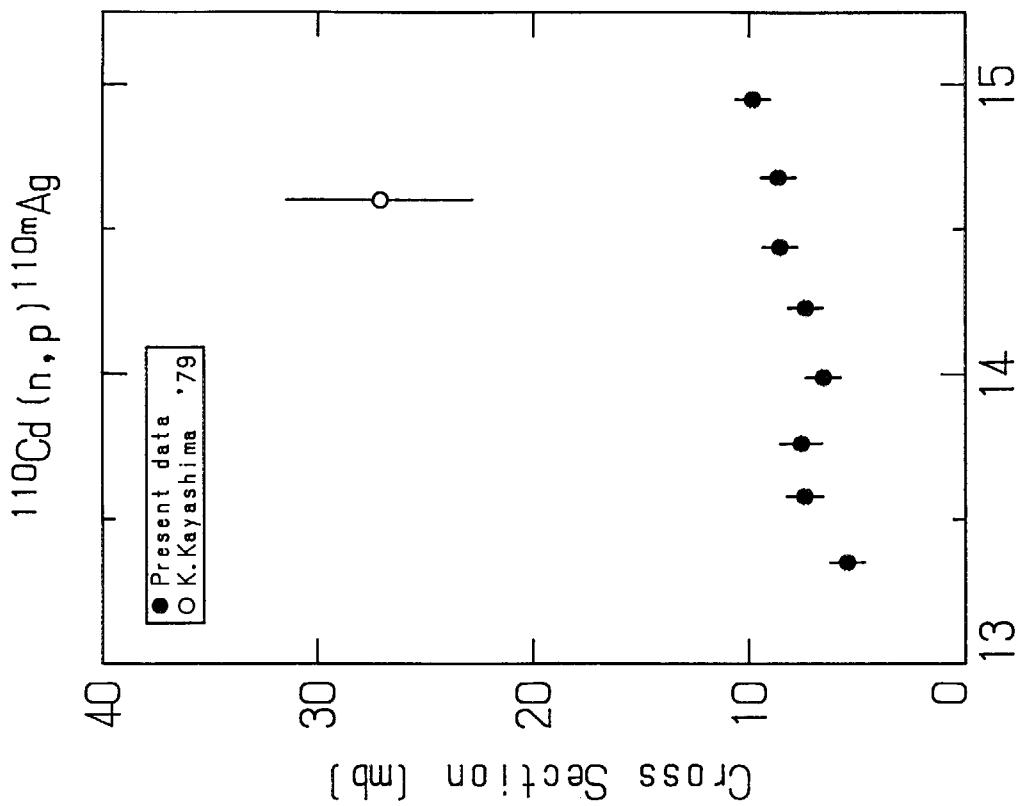

Fig. 3.49 Cross section data for ^{110}Cd (n, p) ^{110m}Ag.

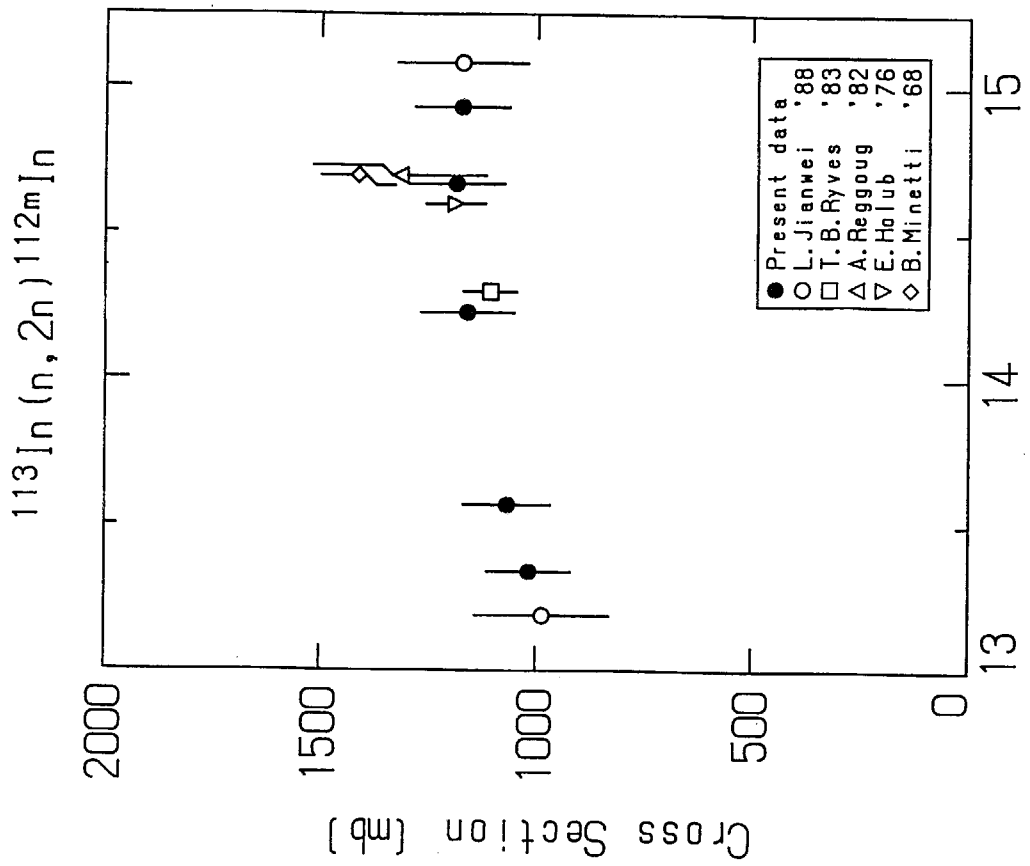

Fig. 3.52 Cross section data for ^{113}In (n, 2n) ^{112m}In.

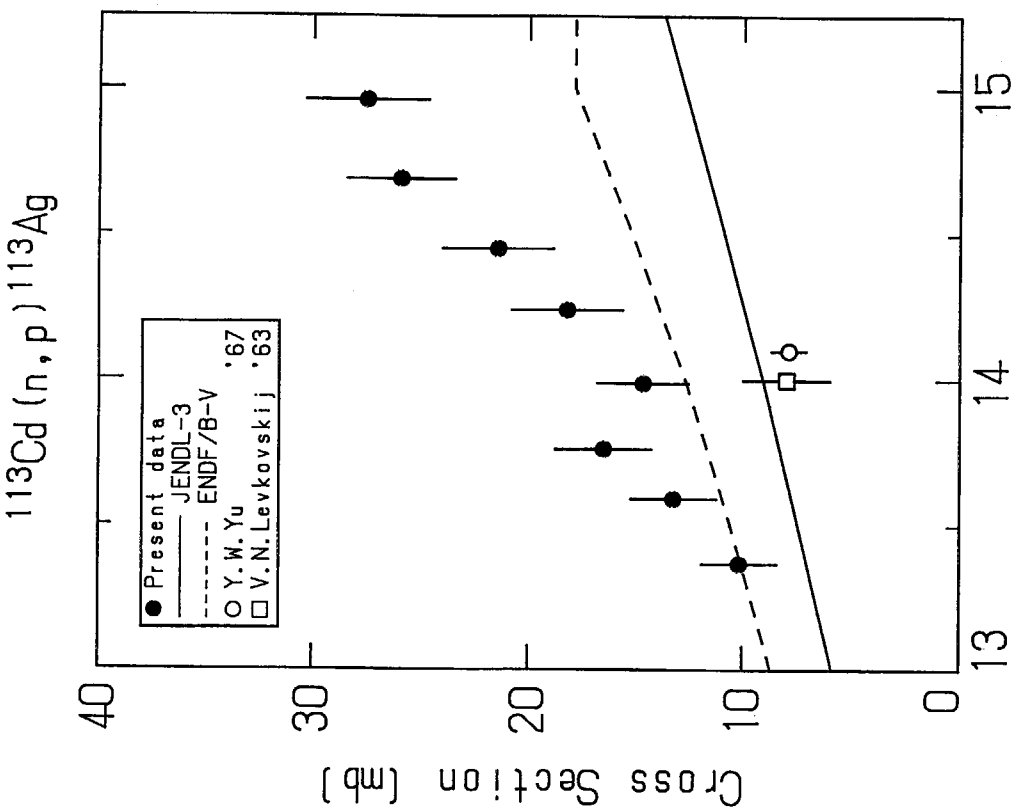

Fig. 3.51 Cross section data for ^{113}Cd (n, p) ^{113}Ag.

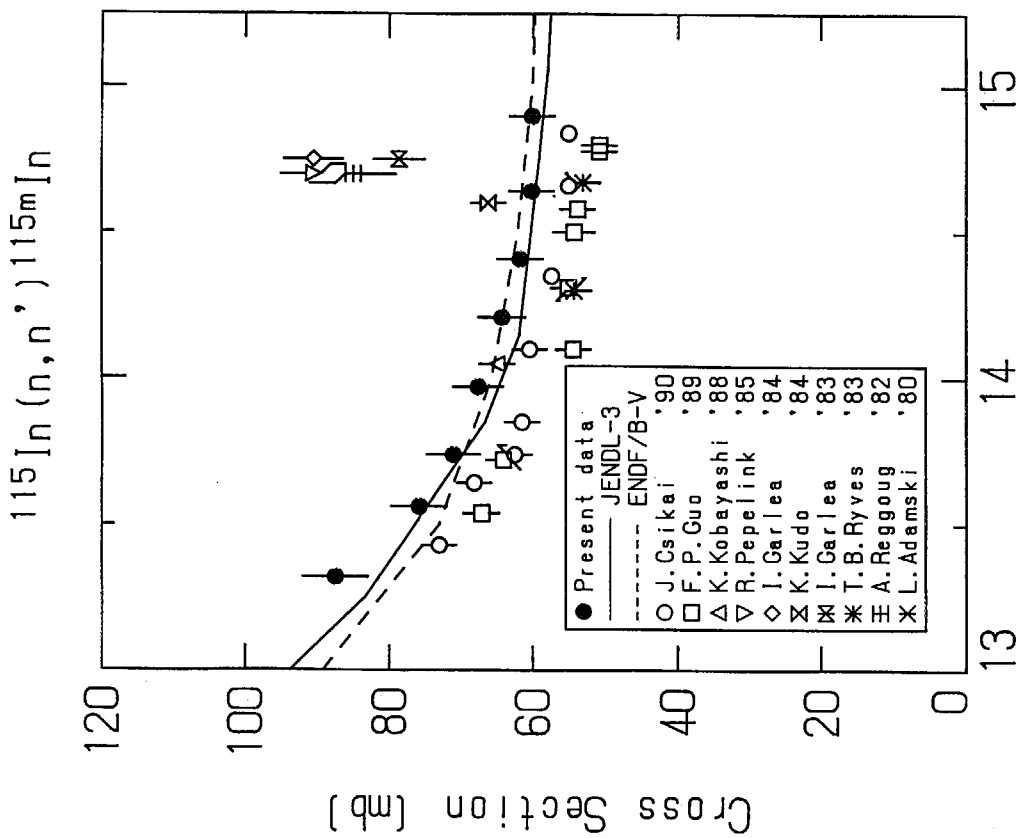

Fig. 3.54 Cross section data for ^{115}In (n, n′) ^{115m}In.

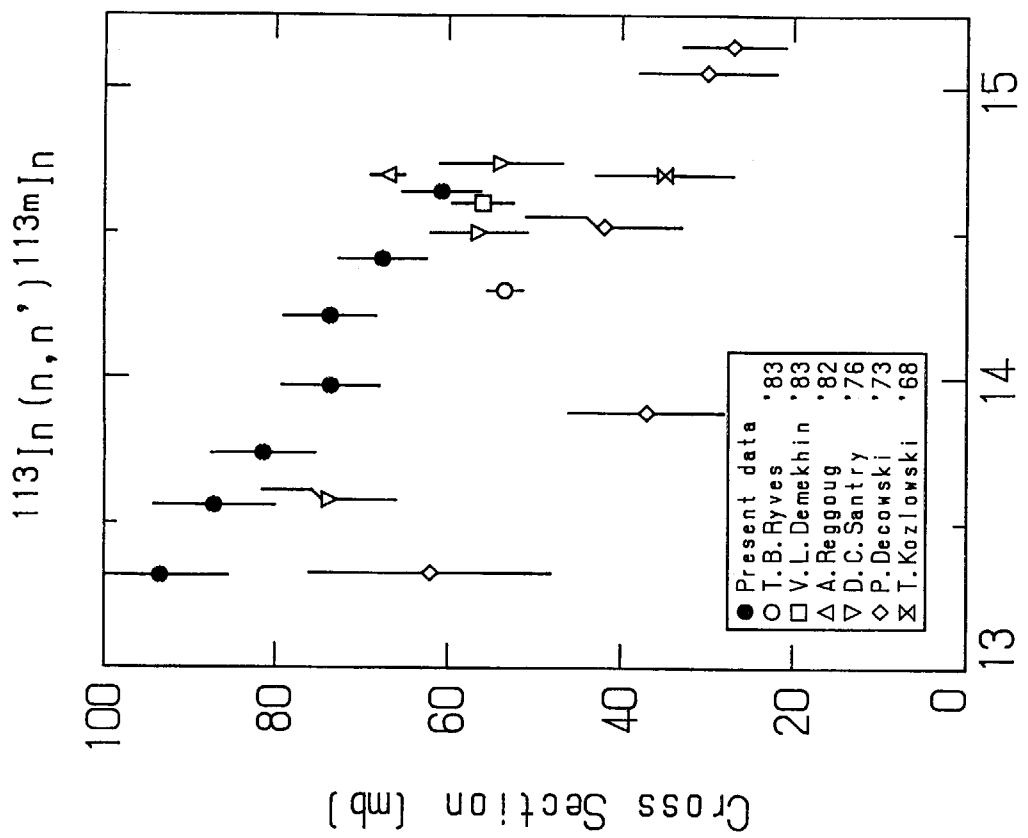

Fig. 3.53 Cross section data for ^{113}In (n, n′) ^{113m}In.

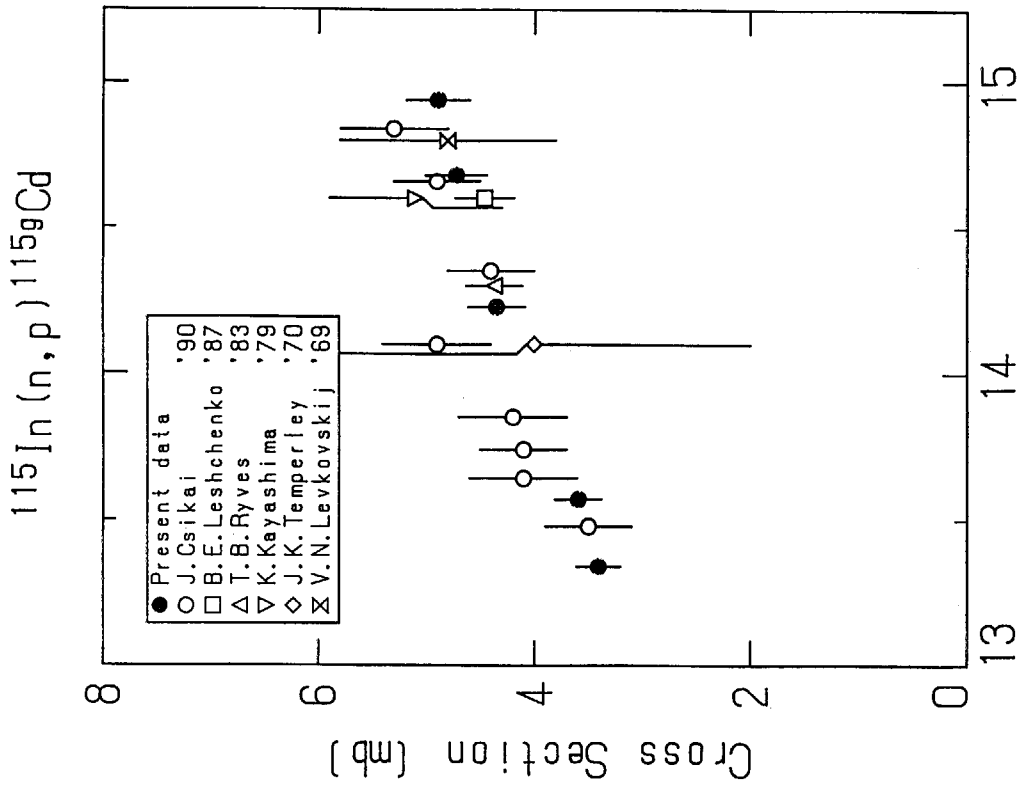

Fig. 3.56 Cross section data for ^{115}In (n, p) ^{115g}Cd.

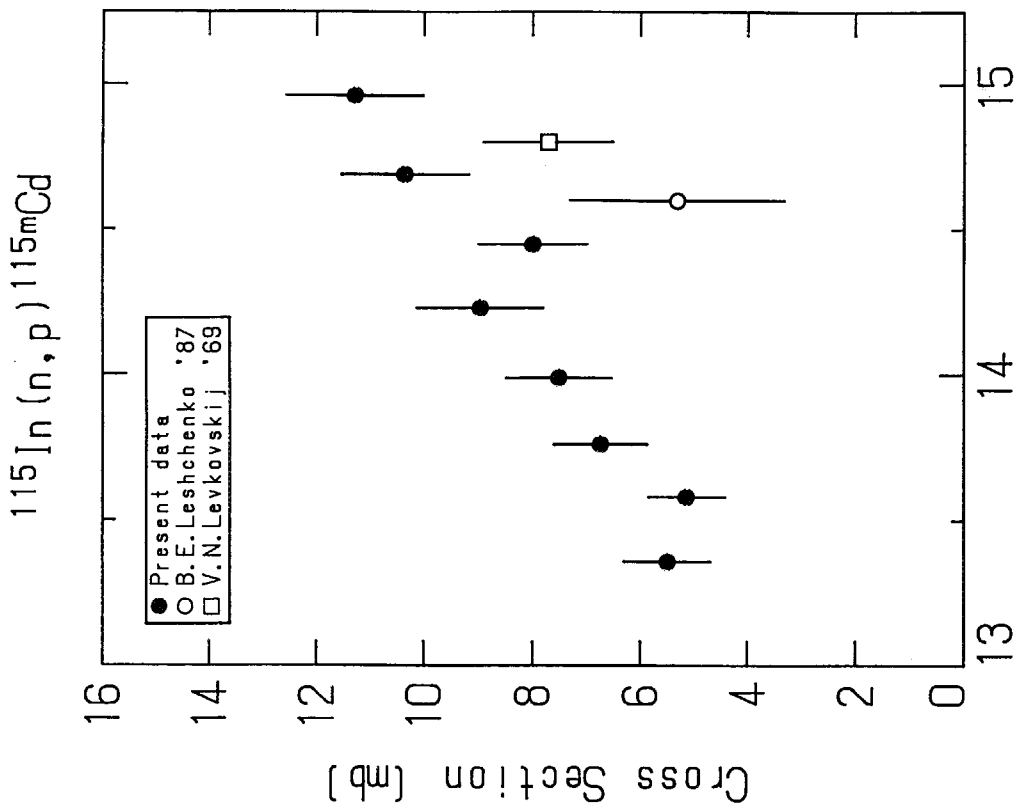

Fig. 3.55 Cross section data for ^{115}In (n, p) ^{115m}Cd.

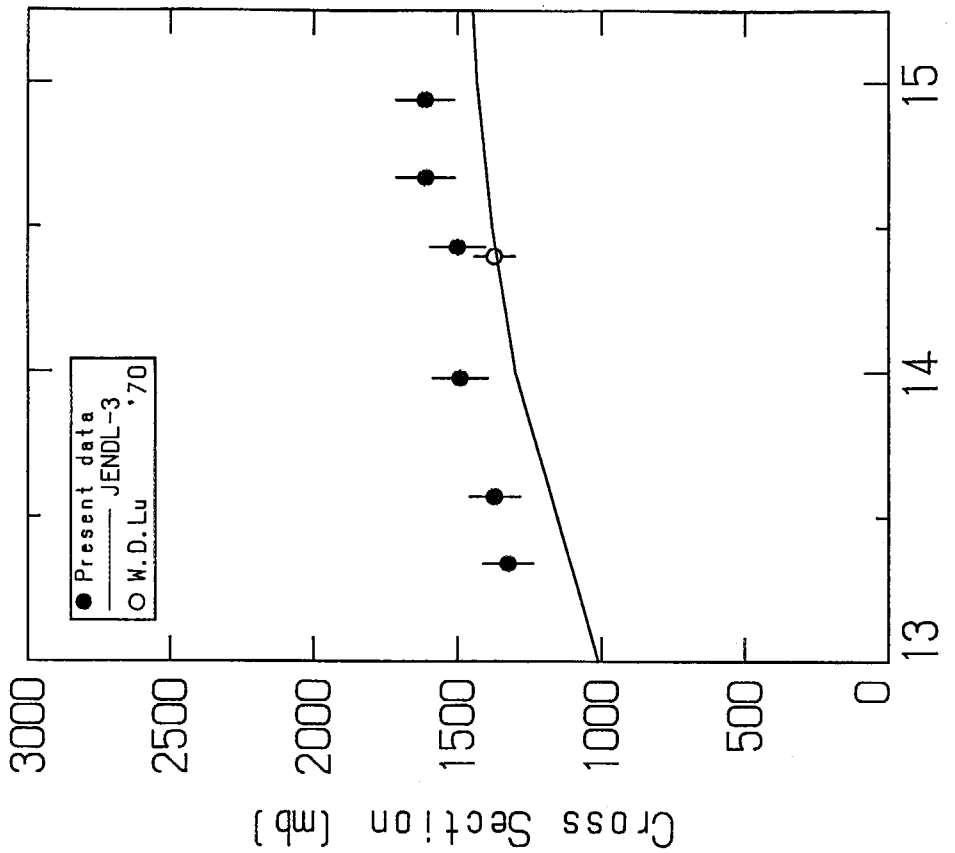

Fig. 3.58 Cross section data for ^{130}Ba (n, 2n) $^{129m+g}$Ba.

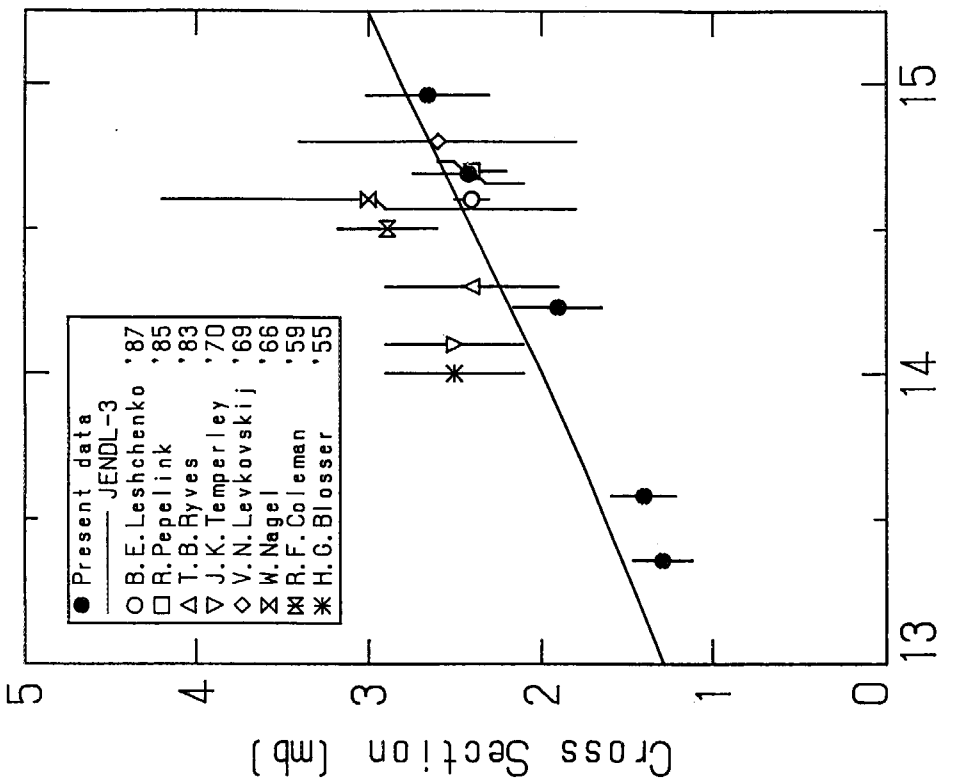

Fig. 3.57 Cross section data for ^{115}In (n, α) ^{112}Ag.

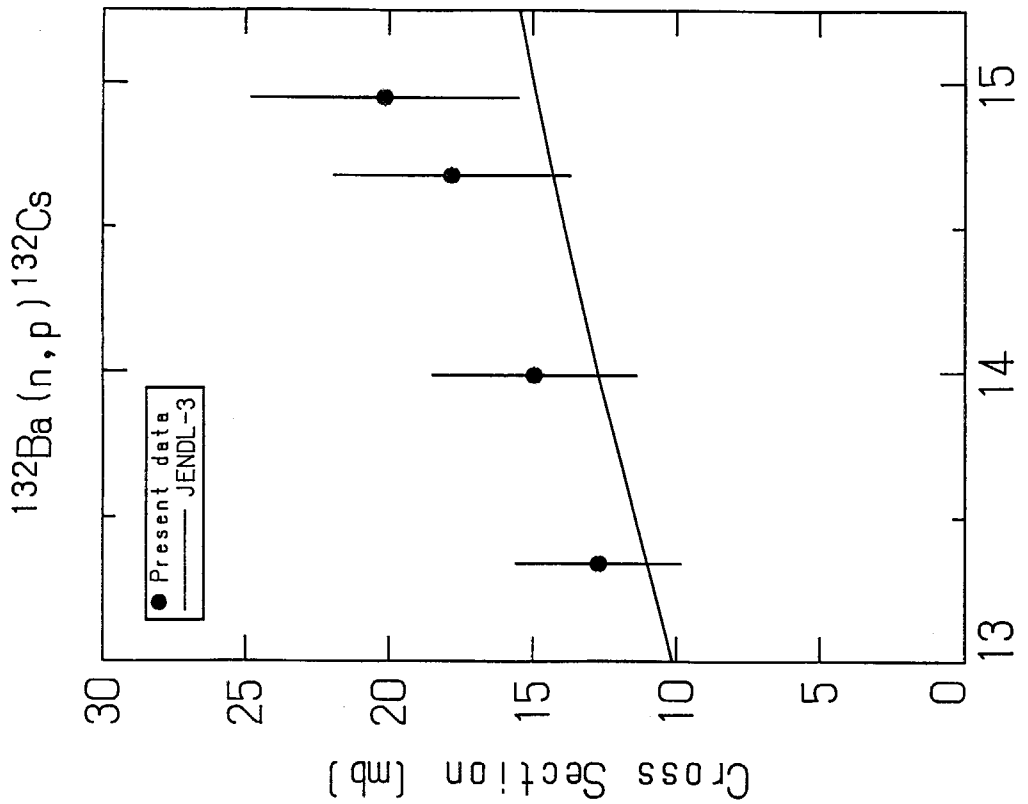

Fig. 3.60 Cross section data for ^{132}Ba (n, p) ^{132}Cs.

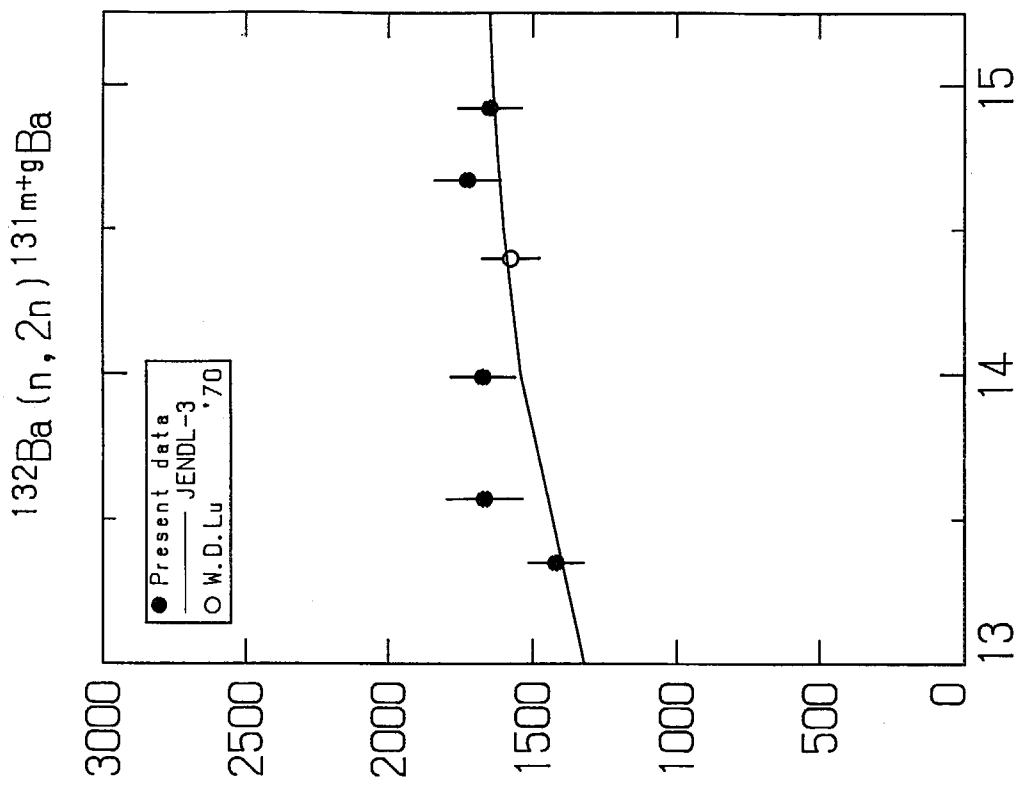

Fig. 3.59 Cross section data for ^{132}Ba (n, 2n) $^{131m+g}$Ba.

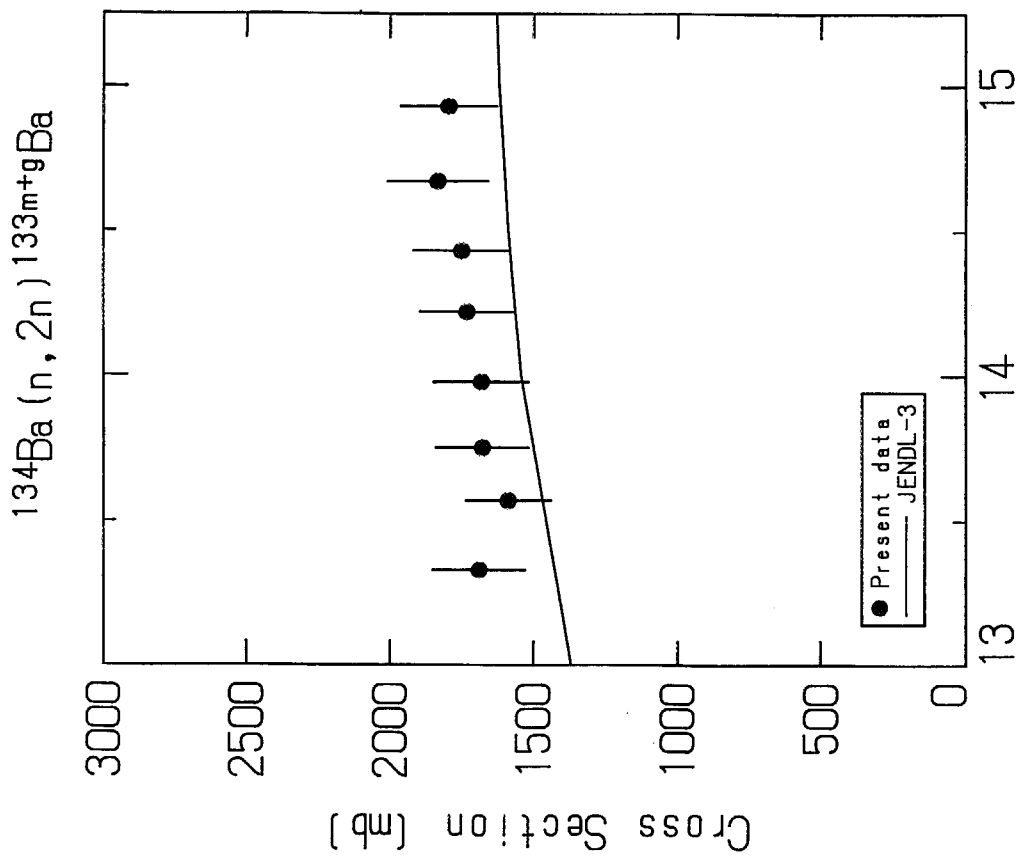

Fig. 3.62 Cross section data for ^{134}Ba (n, 2n) $^{133m+g}$Ba.

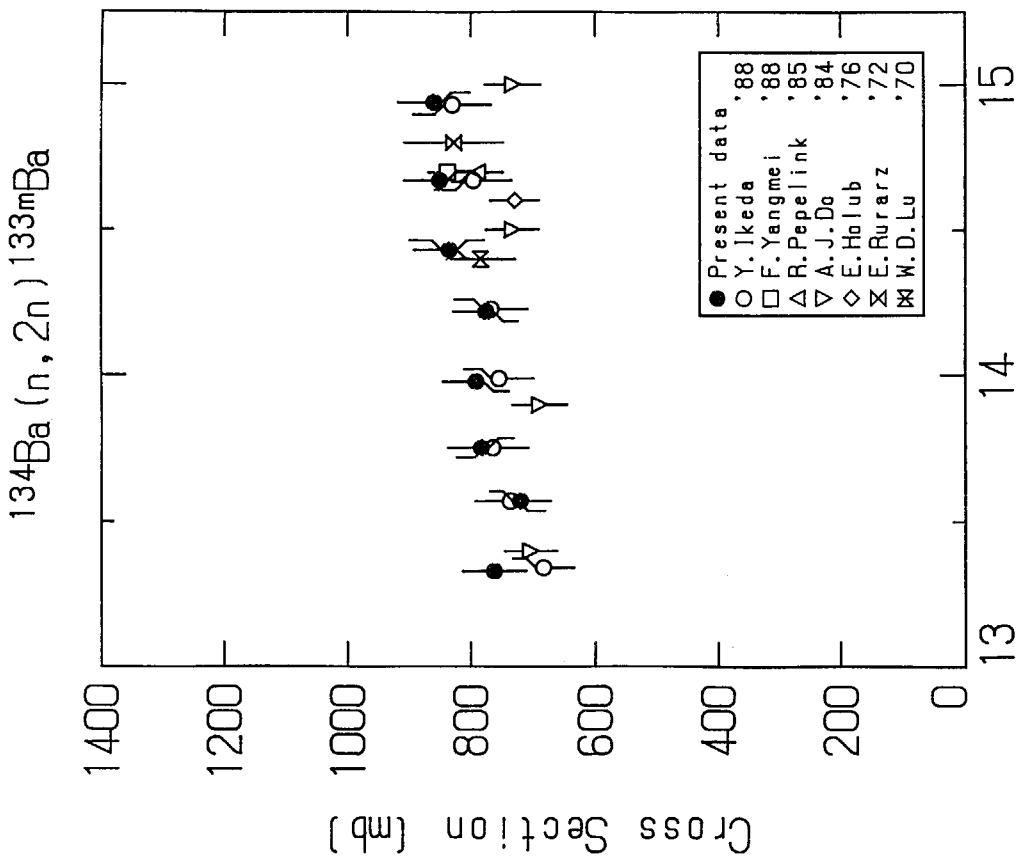

Fig. 3.61 Cross section data for ^{134}Ba (n, 2n) ^{133m}Ba.

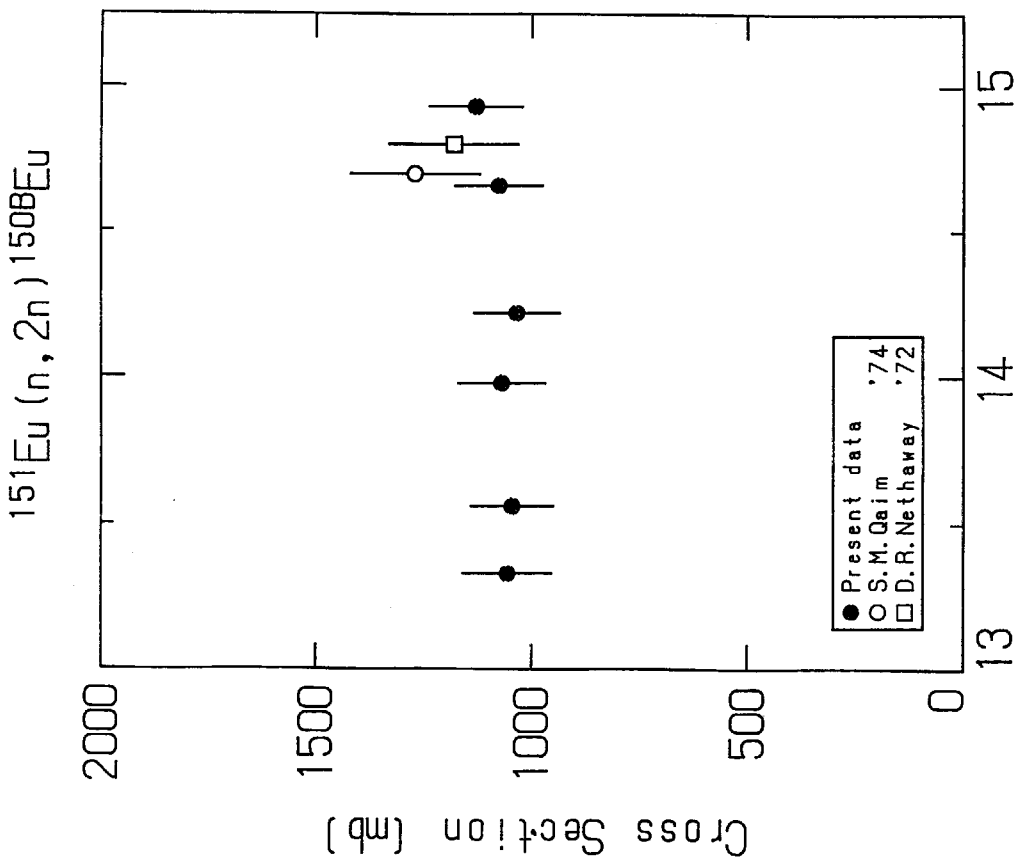

Fig. 3.64 Cross section data for ^{151}Eu (n, 2n) ^{150B}Eu.

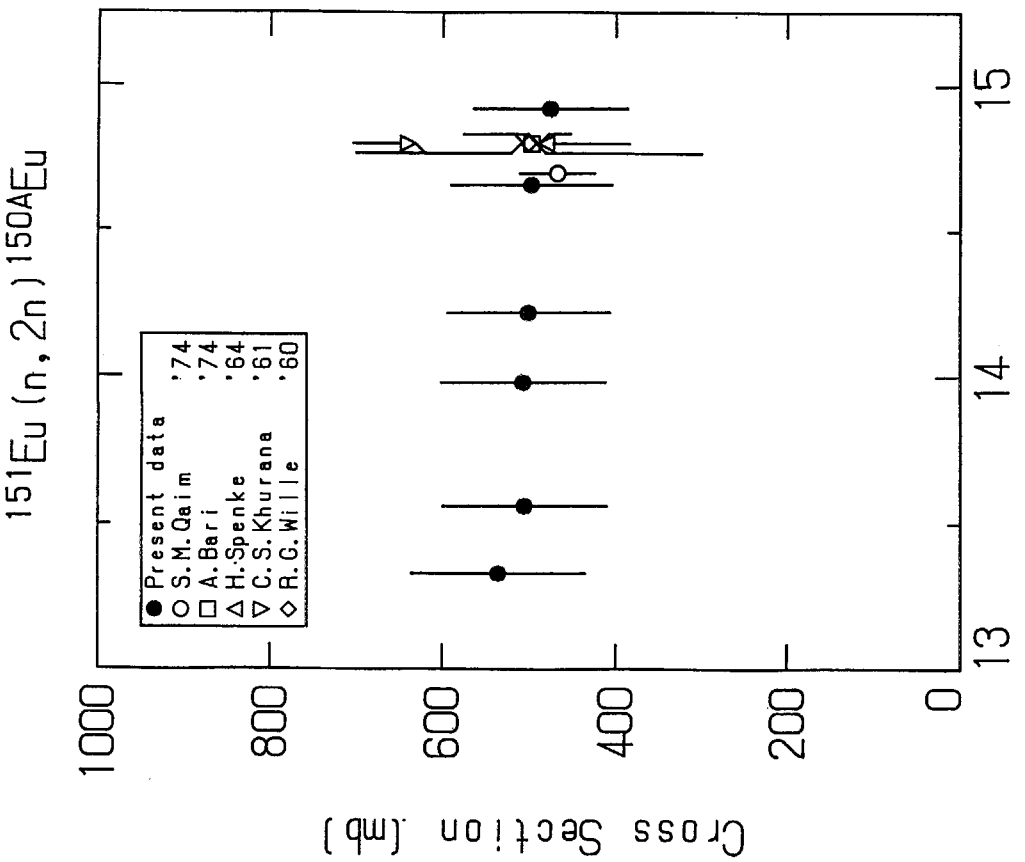

Fig. 3.63 Cross section data for ^{151}Eu (n, 2n) ^{130A}Eu.

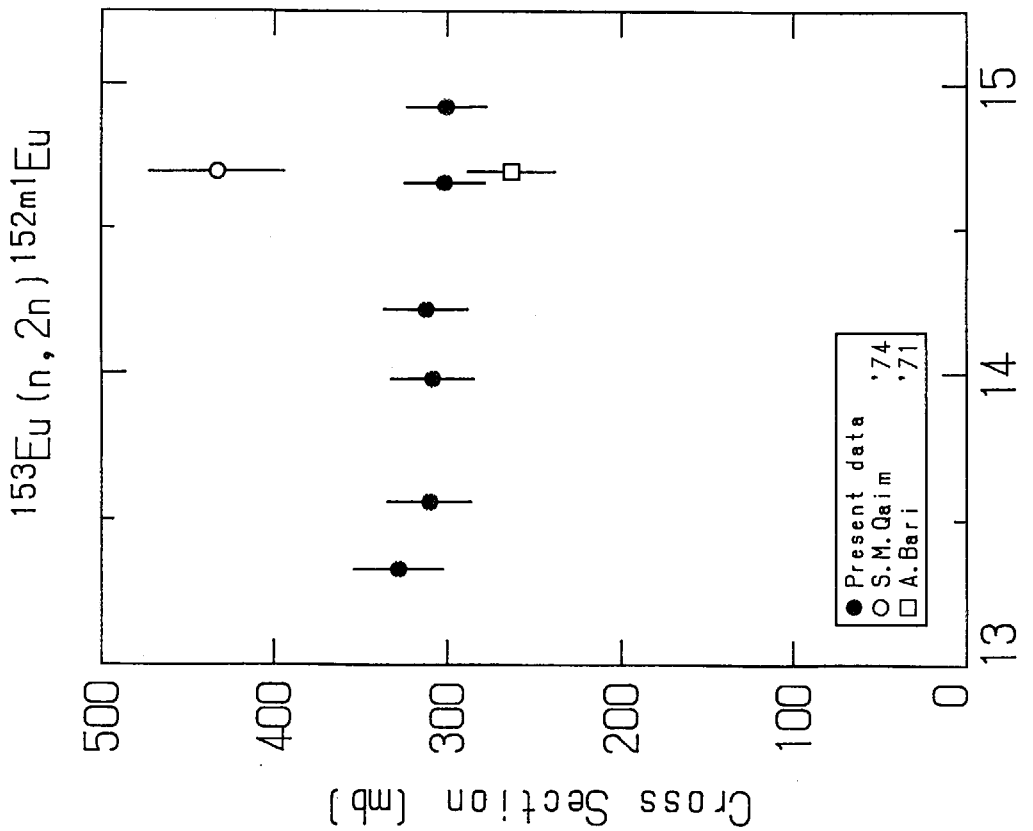

Fig. 3.66 Cross section data for ^{153}Eu (n, 2n) ^{152m1}Eu.

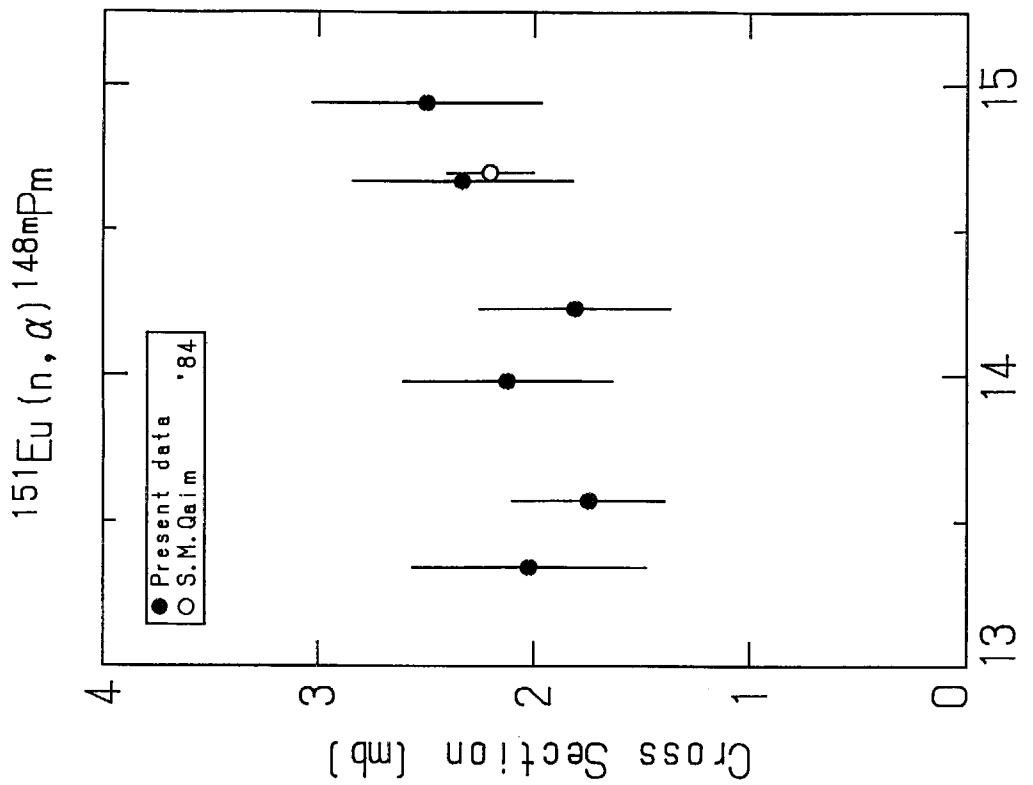

Fig. 3.65 Cross section data for ^{151}Eu (n, α) ^{148m}Pm.

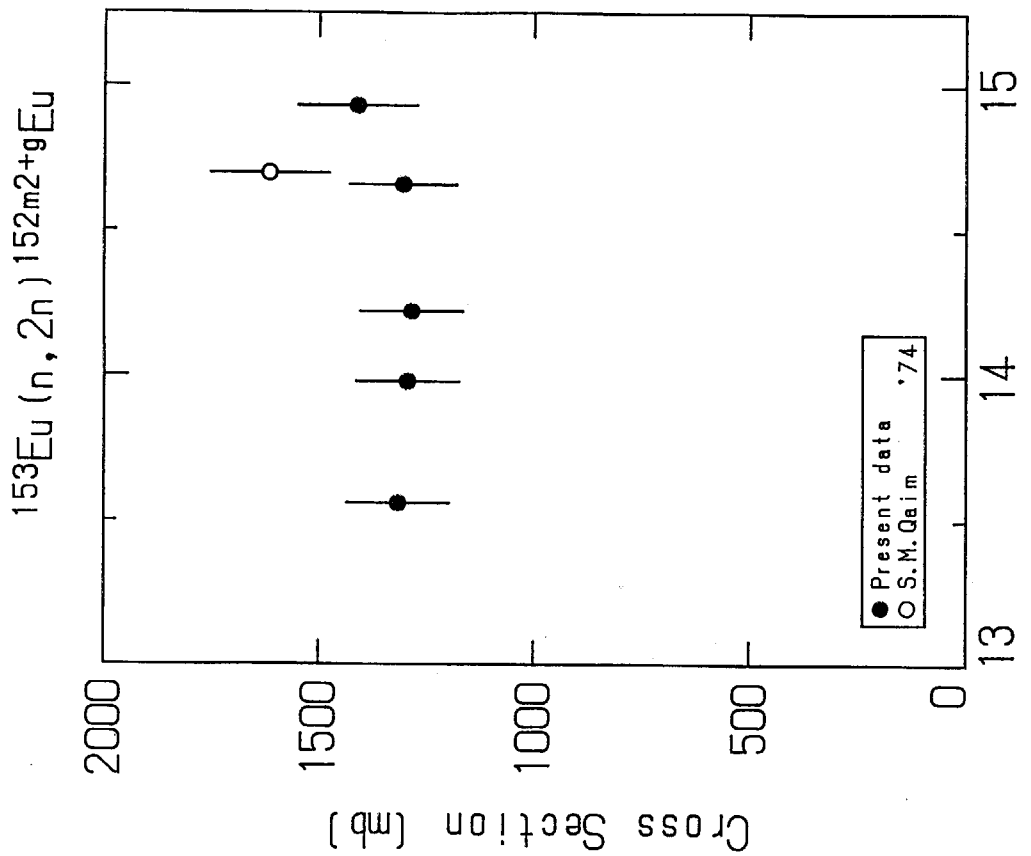

Fig. 3.68 Cross section data for ^{153}Eu (n, 2n) $^{152m2+g}$Eu.

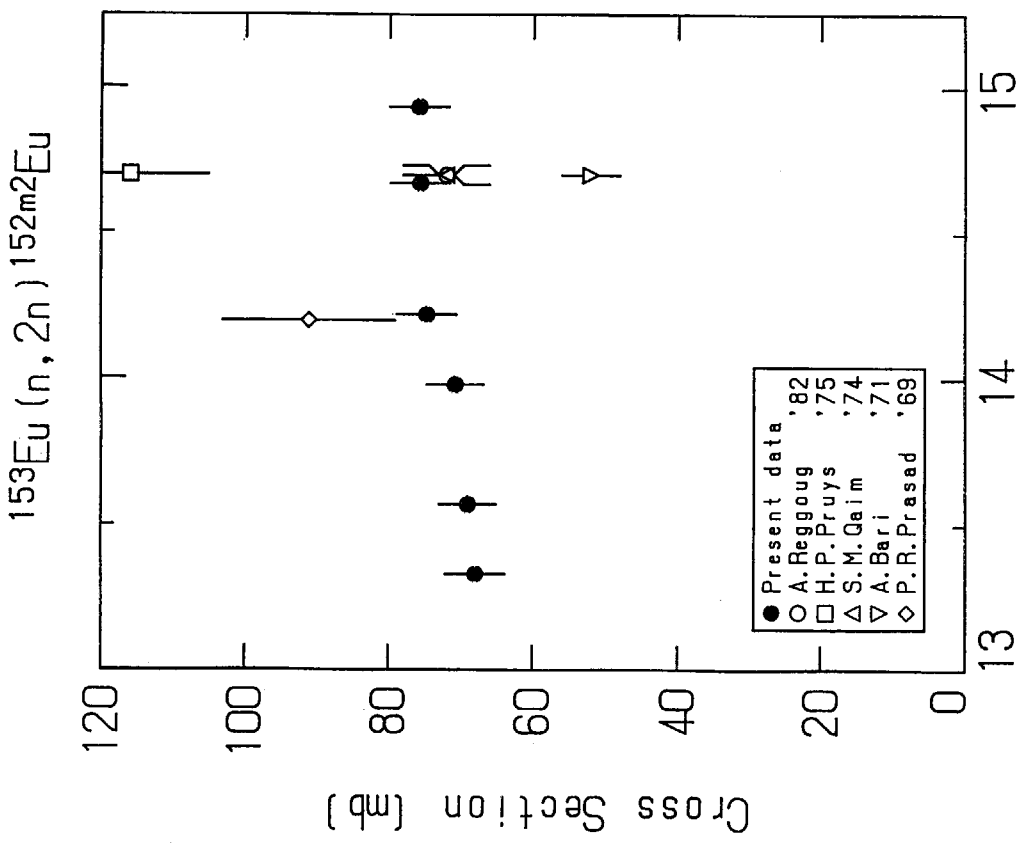

Fig. 3.67 Cross section data for ^{153}Eu (n, 2n) ^{152m2}Eu.

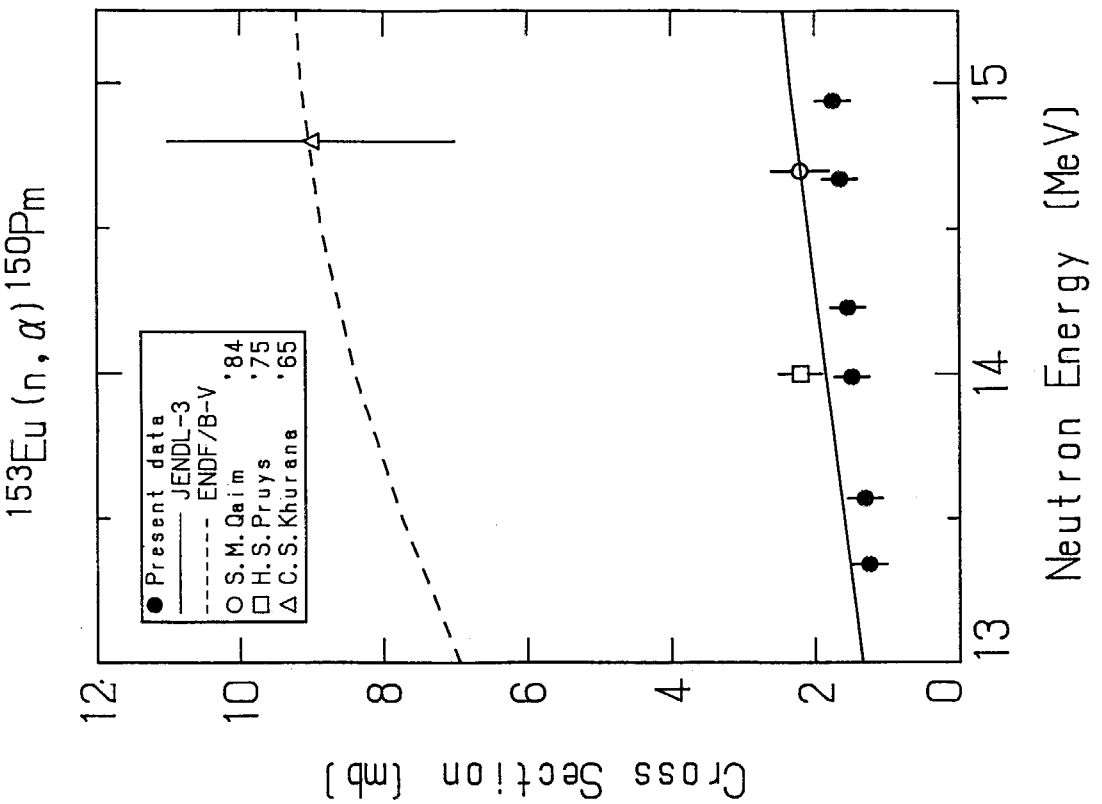

Fig. 3.70 Cross section data for ^{153}Eu (n, α) ^{150}Pm.

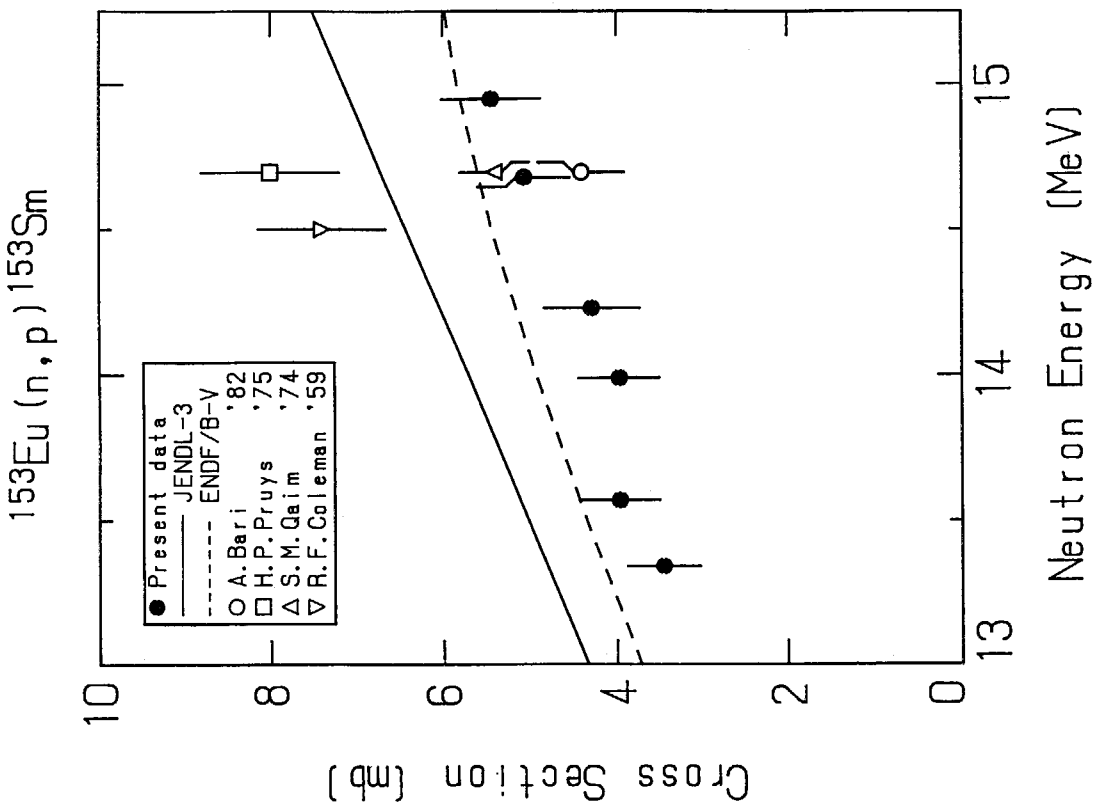

Fig. 3.69 Cross section data for ^{153}Eu (n, p) ^{153}Sm.

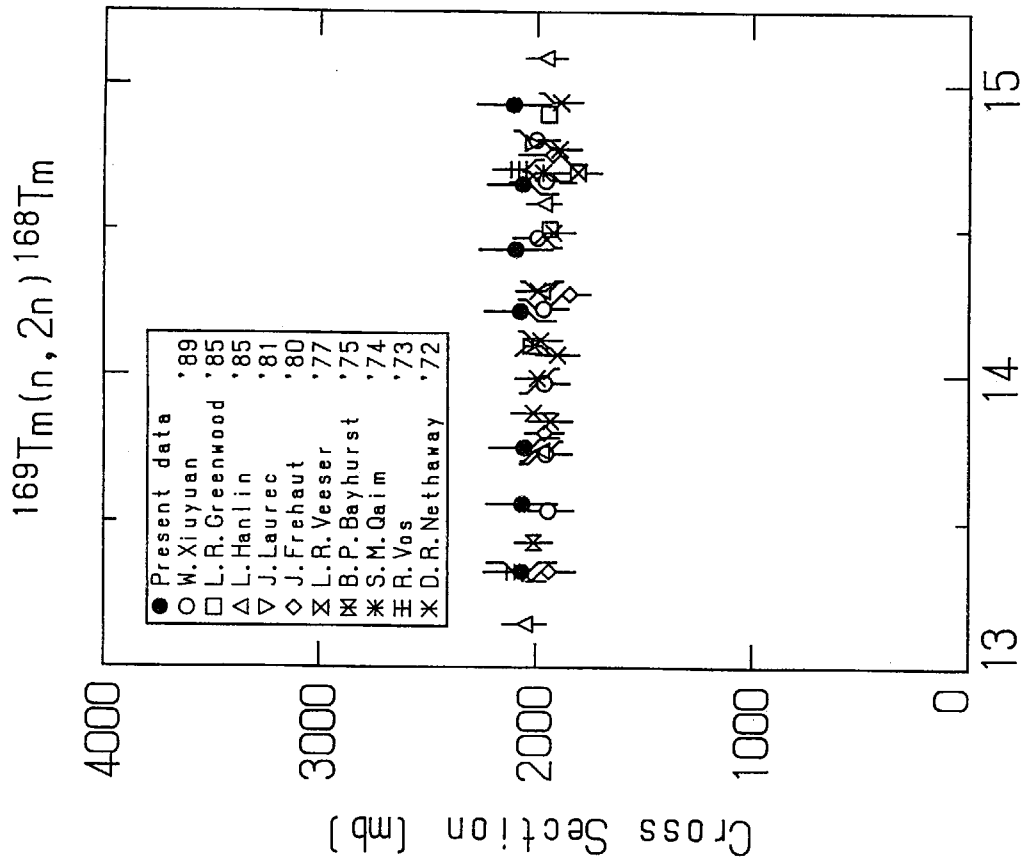

Fig. 3.72 Cross section data for ^{169}Tm (n, 2n) ^{168}Tm.

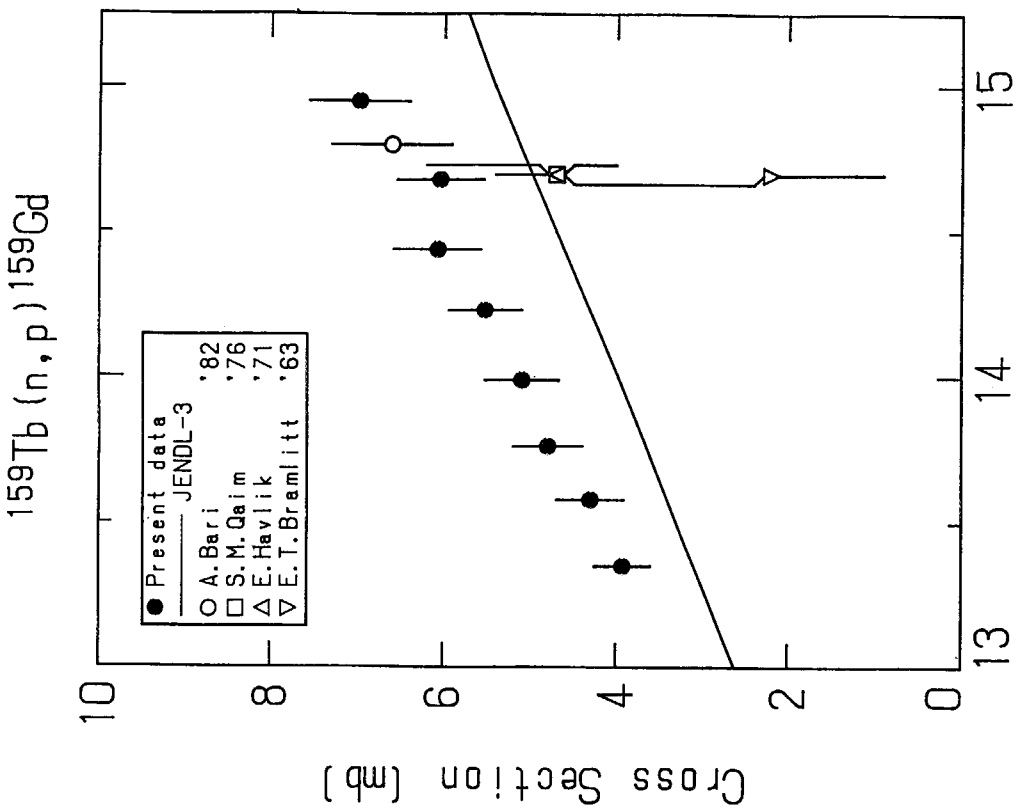

Fig. 3.71 Cross section data for ^{159}Tb (n, p) ^{159}Gd.

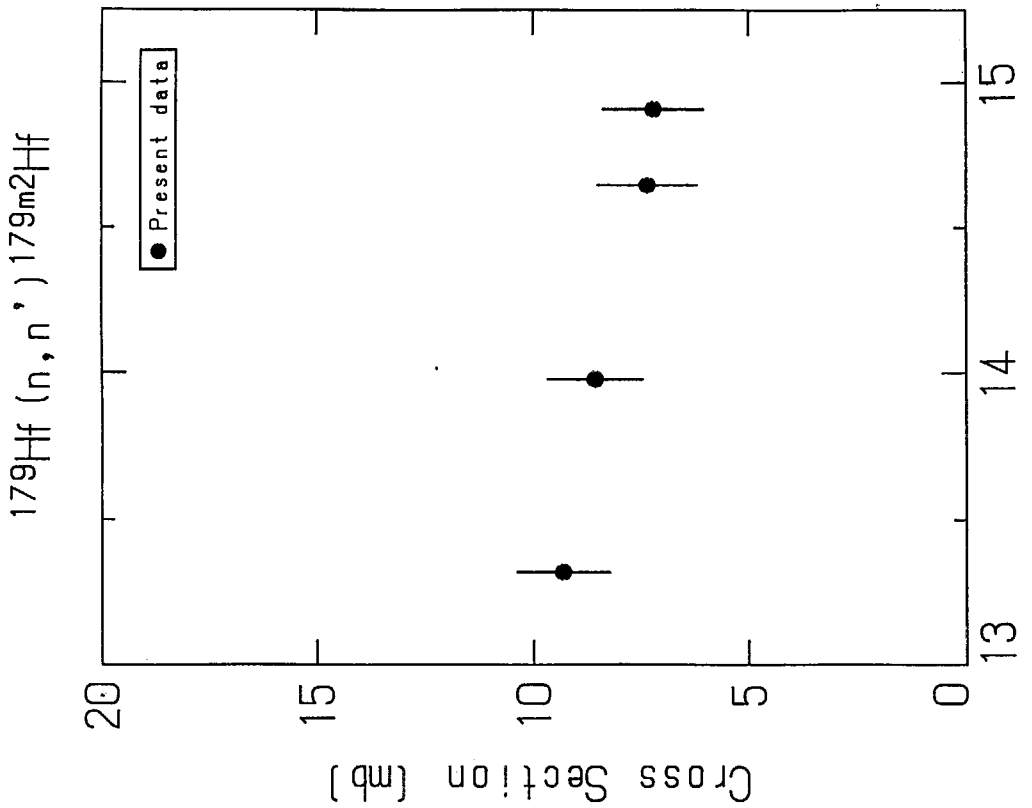

Fig. 3.74 Cross section data for ^{179}Hf (n, n') ^{179m2}Hf.

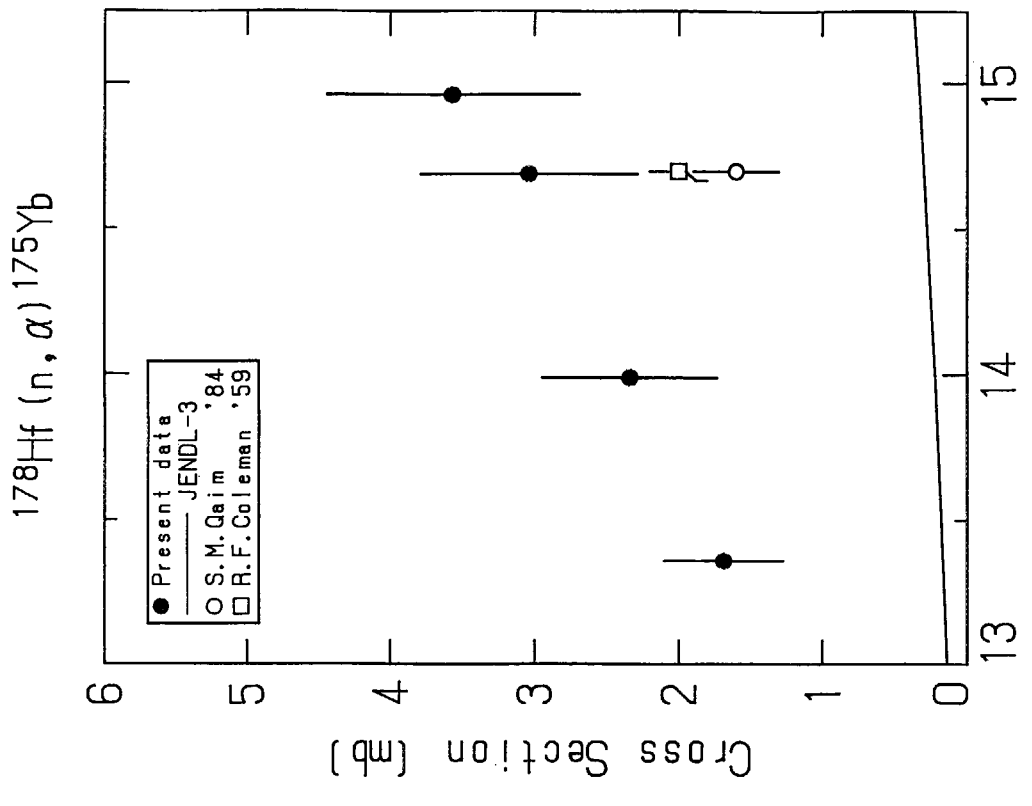

Fig. 3.73 Cross section data for ^{178}Hf (n, α) ^{175}Yb.

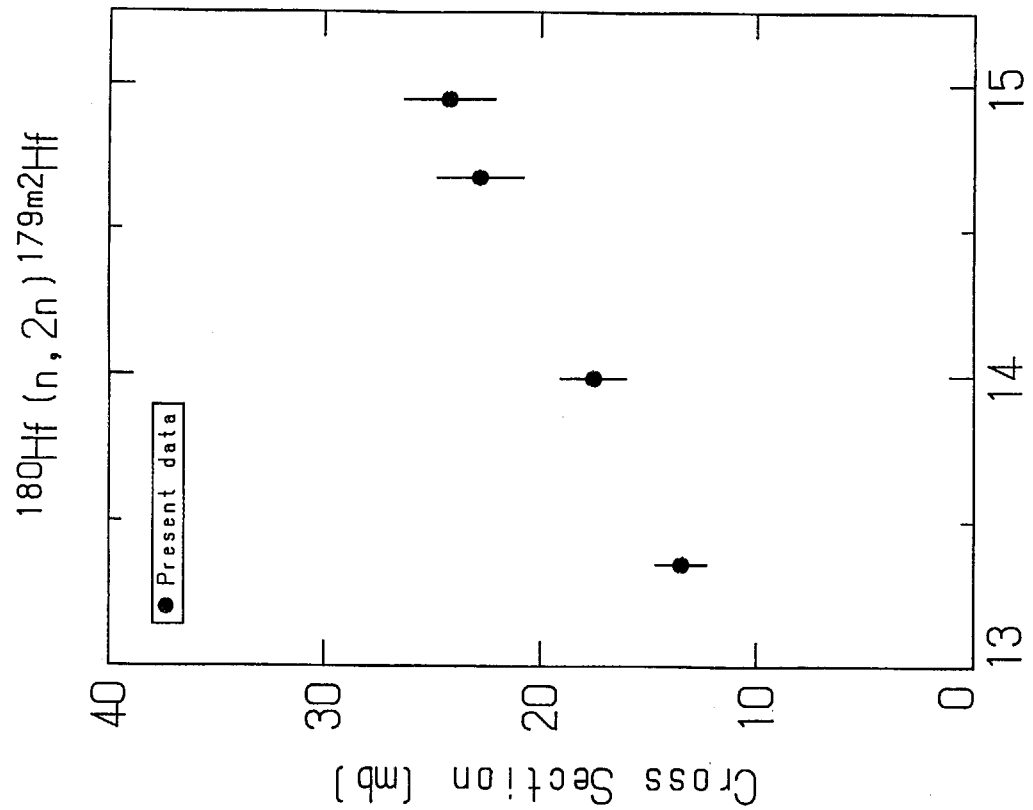

Fig. 3.76 Cross section data for ^{180}Hf (n, 2n) ^{179m2}Hf.

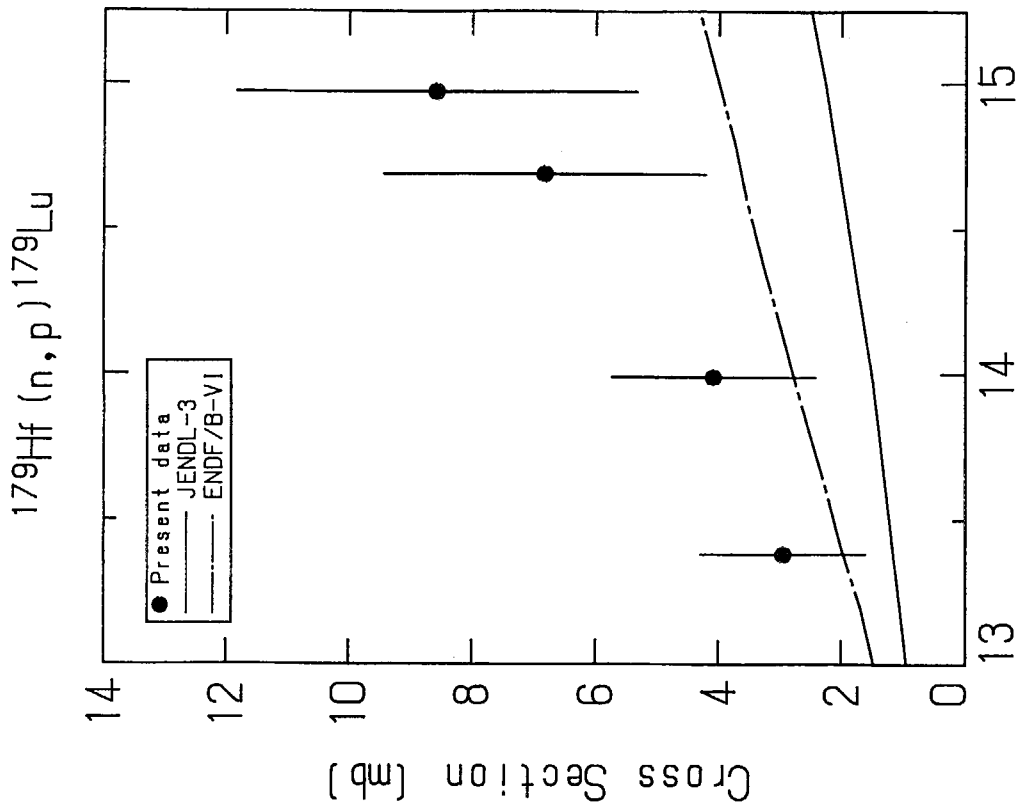

Fig. 3.75 Cross section data for ^{179}Hf (n, p) ^{179}Lu.

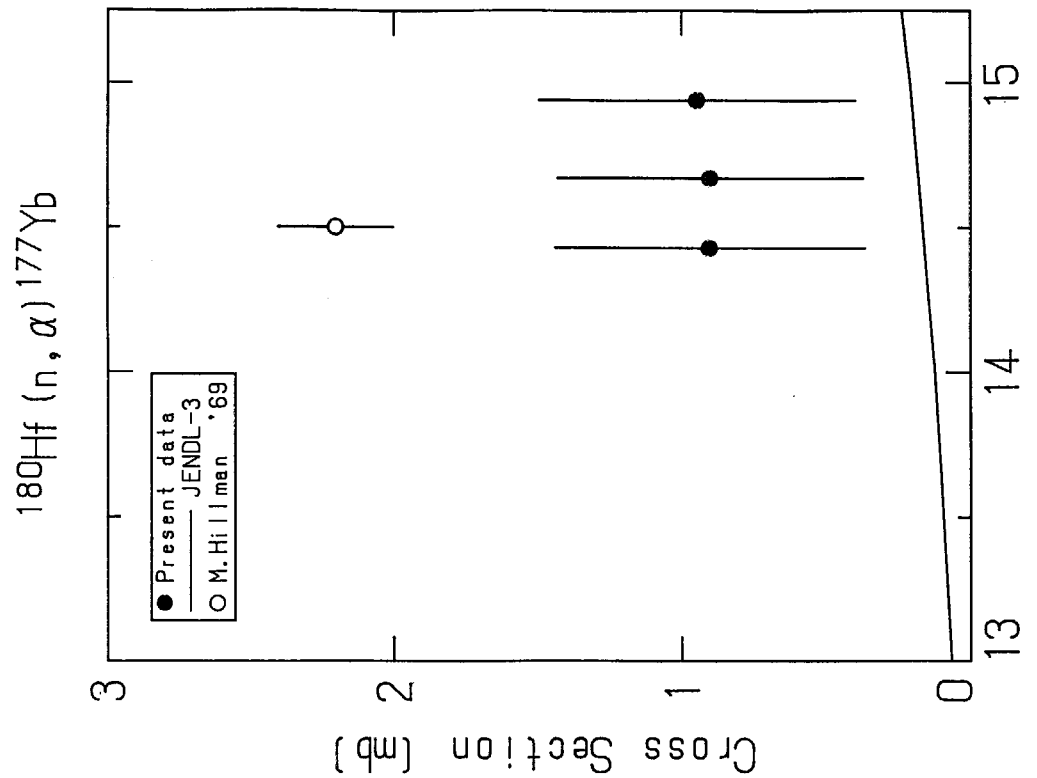

Fig. 3.78 Cross section data for ^{180}Hf (n, α) ^{177}Yb.

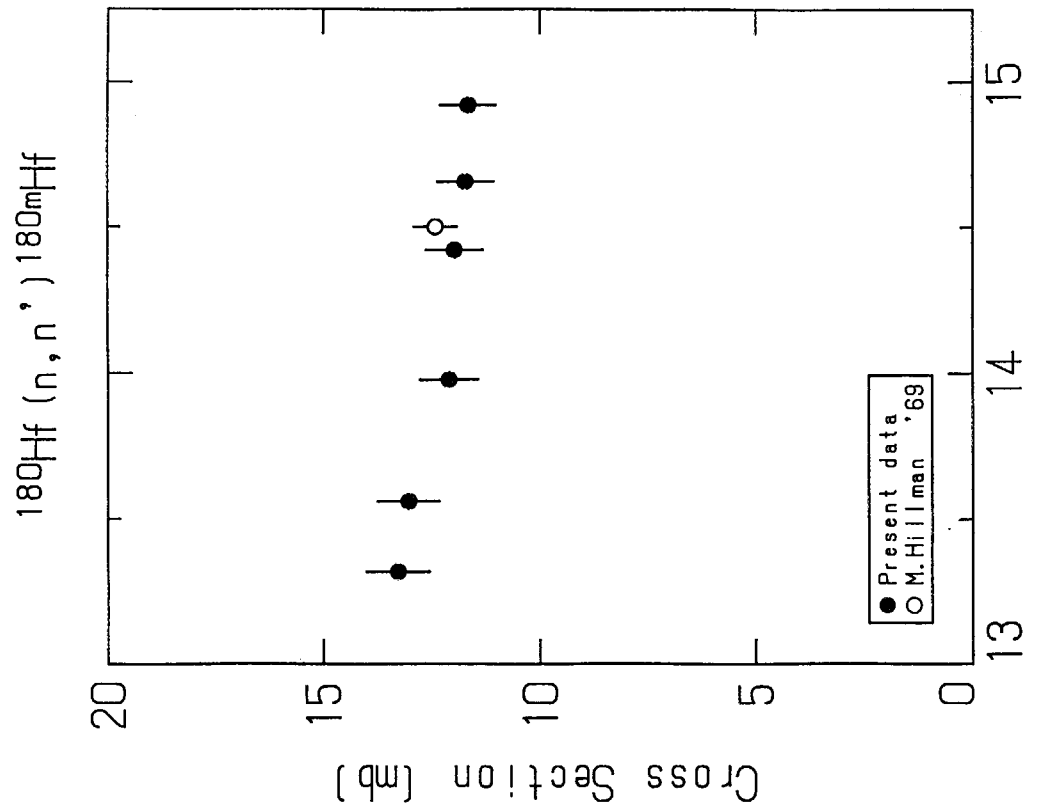

Fig. 3.77 Cross section data for ^{180}Hf (n, n') ^{180m}Hf.

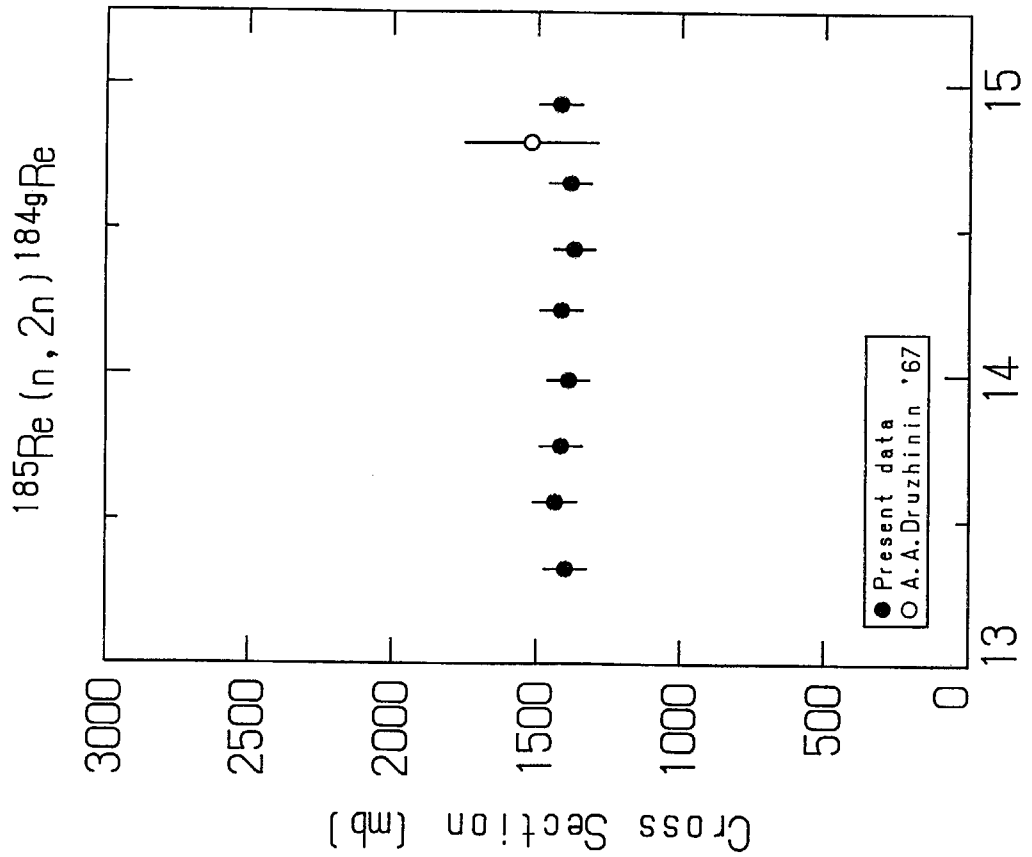

Fig. 3.80 Cross section data for ^{185}Re (n, 2n) ^{184g}Re.

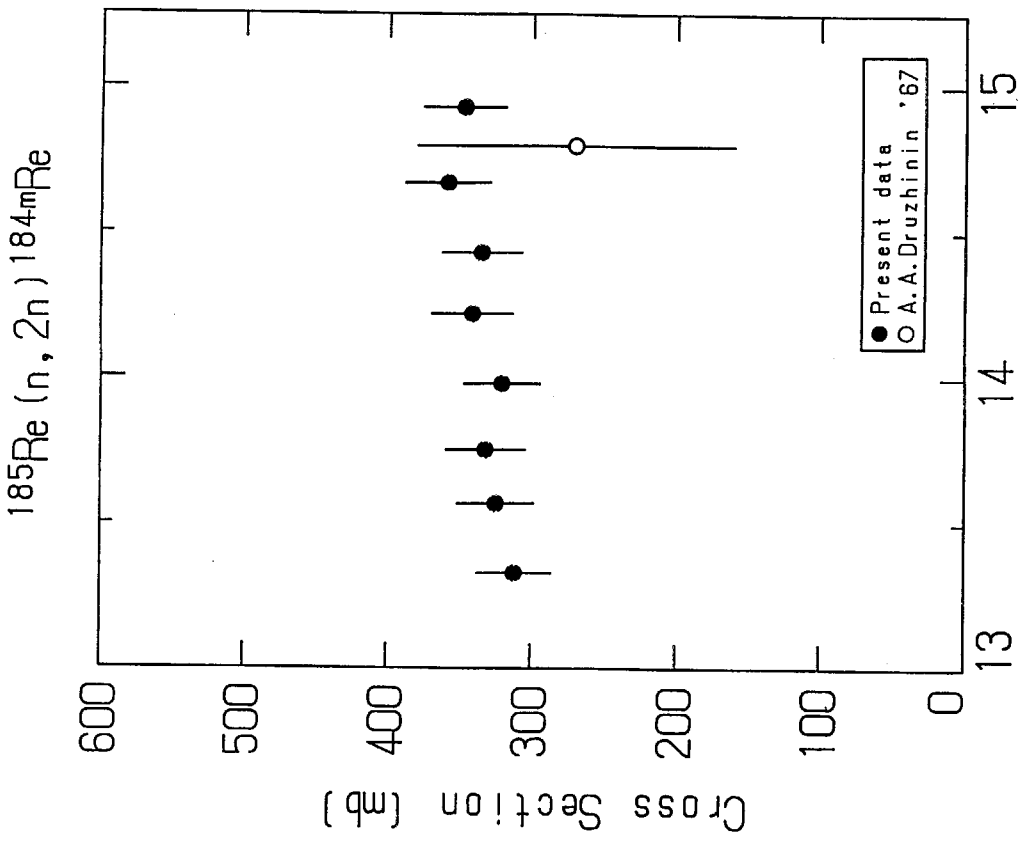

Fig. 3.79 Cross section data for ^{185}Re (n, 2n) ^{184m}Re.

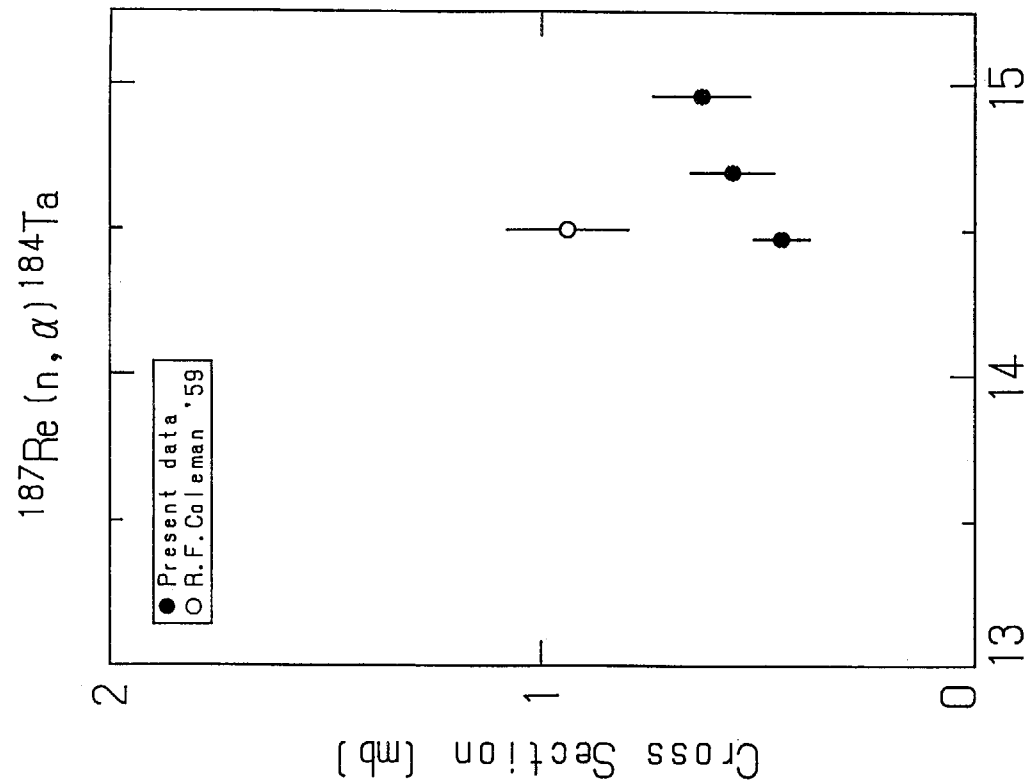

Fig. 3.82 Cross section data for ^{187}Re (n, α) ^{184}Ta.

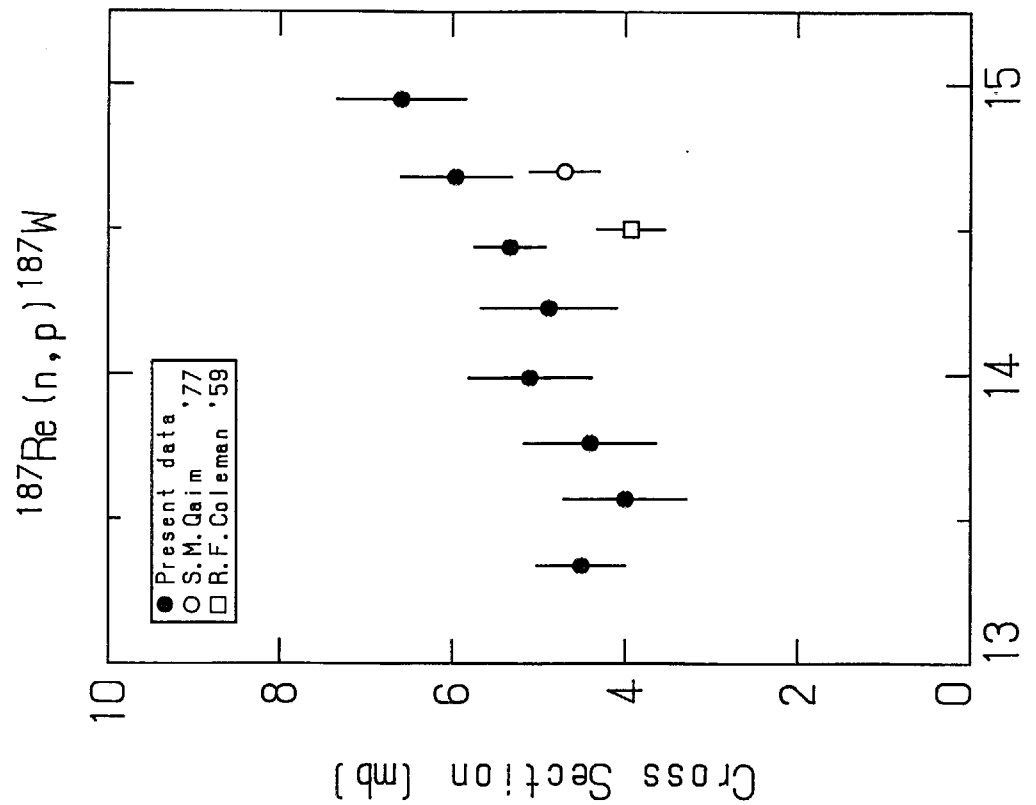

Fig. 3.81 Cross section data for ^{187}Re (n, p) ^{187}W.

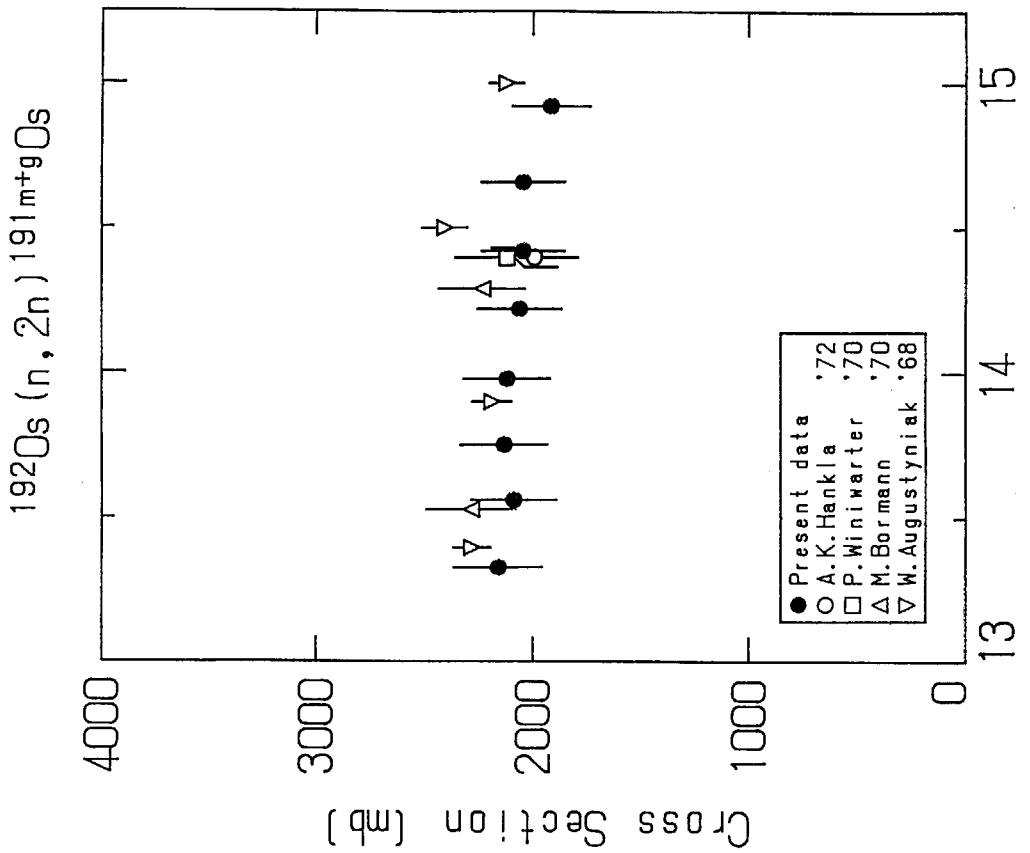

Fig. 3.84 Cross section data for ^{192}Os (n, 2n) $^{191m+g}$Os.

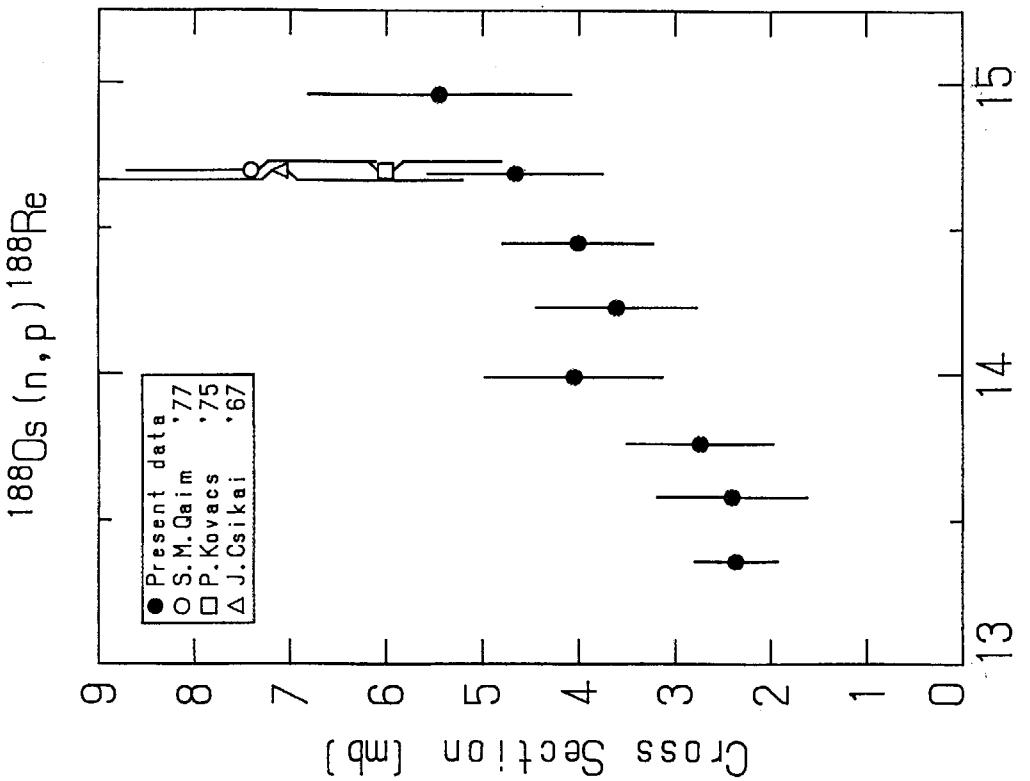

Fig. 3.83 Cross section data for ^{188}Os (n, p) ^{188}Re.

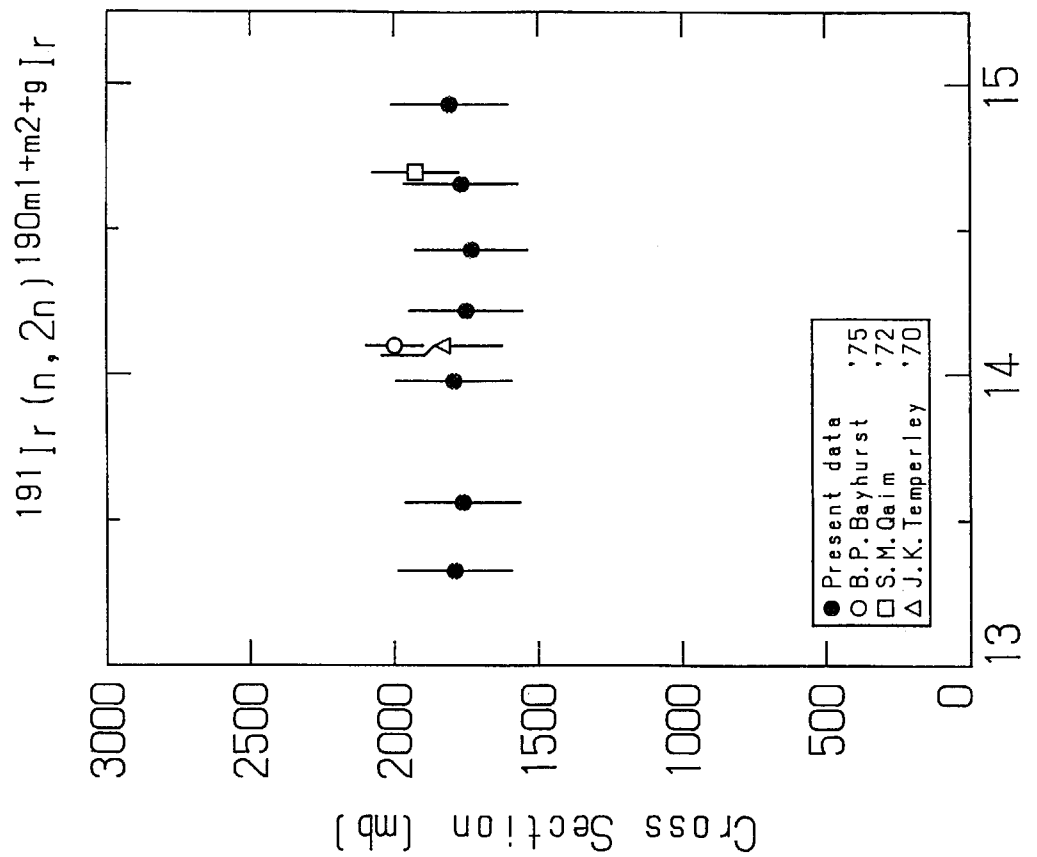

Fig. 3.86 Cross section data for ^{191}Ir (n, 2n) $^{190m1+m2+g}$Ir.

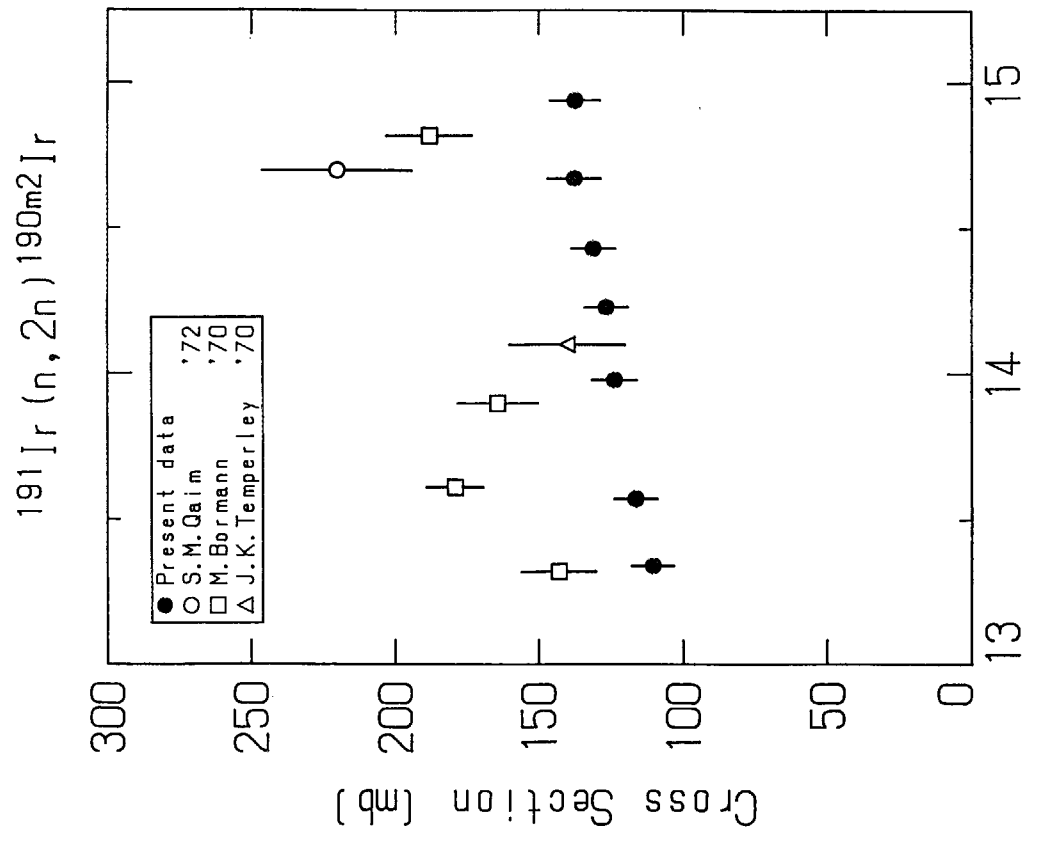

Fig. 3.85 Cross section data for ^{191}Ir (n, 2n) ^{190m2}Ir.

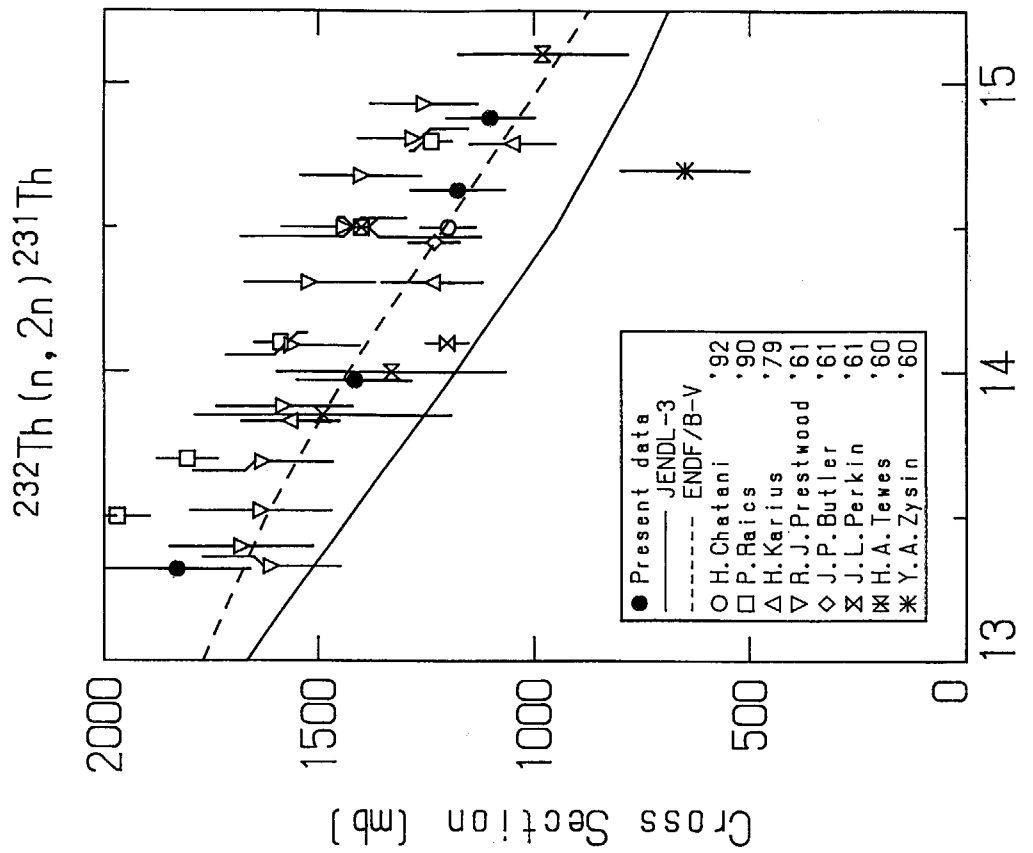

Fig. 3.88 Cross section data for ^{232}Th (n, 2n) ^{231}Th.

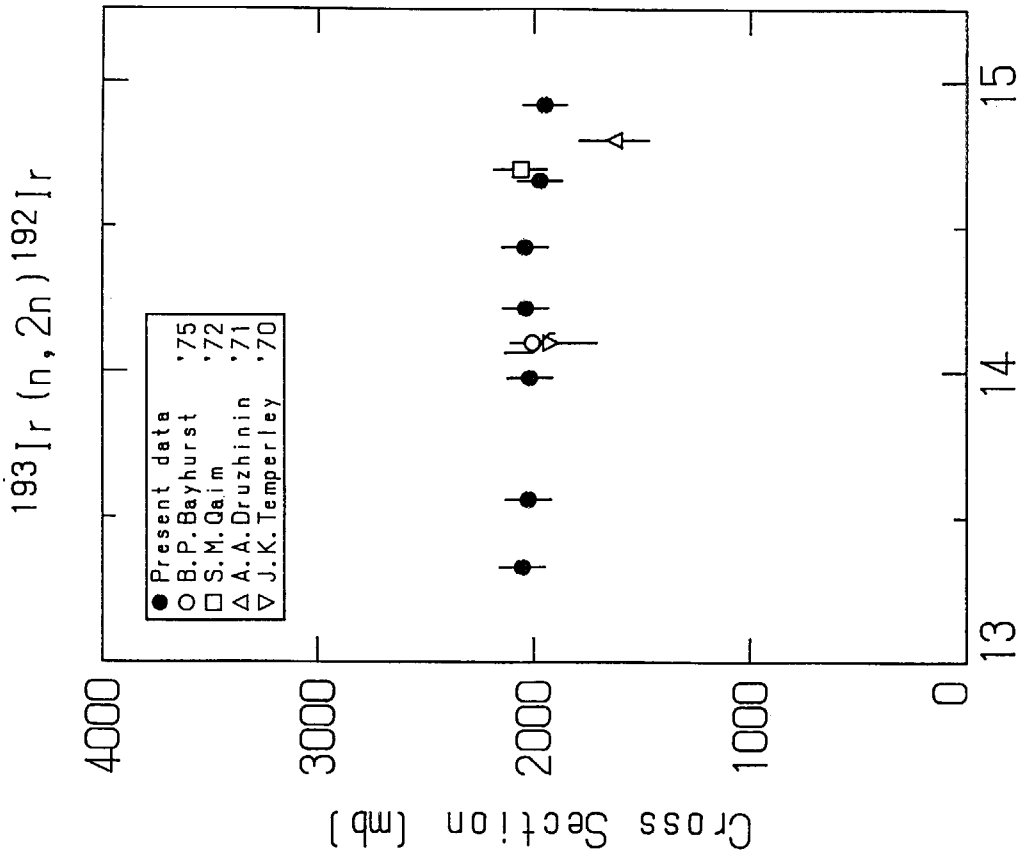

Fig. 3.87 Cross section data for ^{193}Ir (n, 2n) ^{192}Ir.

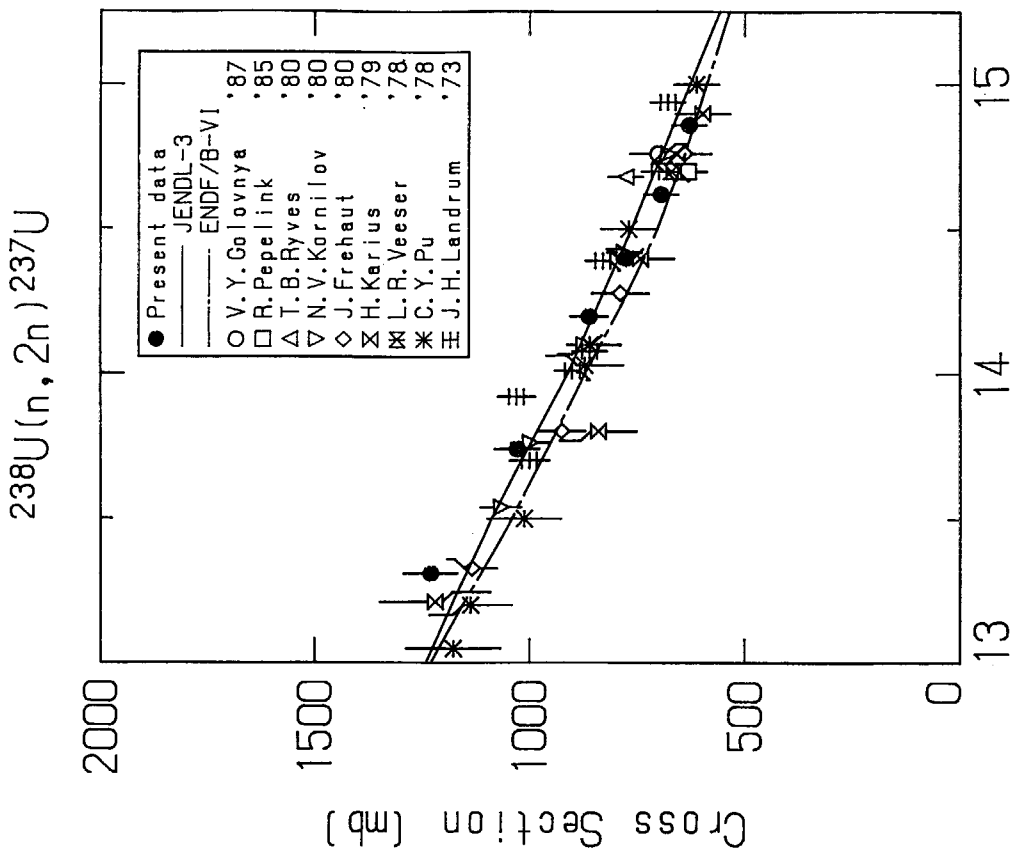

Fig. 3.89 Cross section data for ^{238}U (n, 2n) ^{237}U.

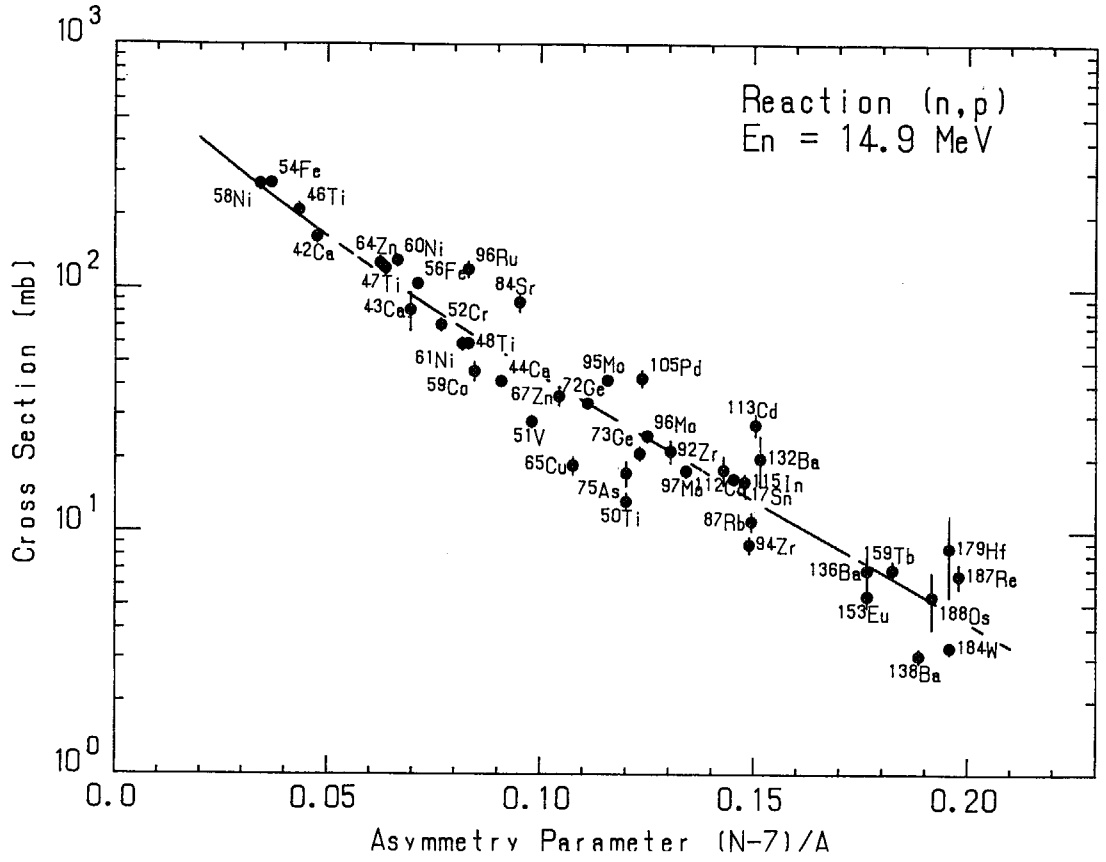

Fig. 4.1 Systematics of (n, p) reaction cross sections at 14.9 MeV.

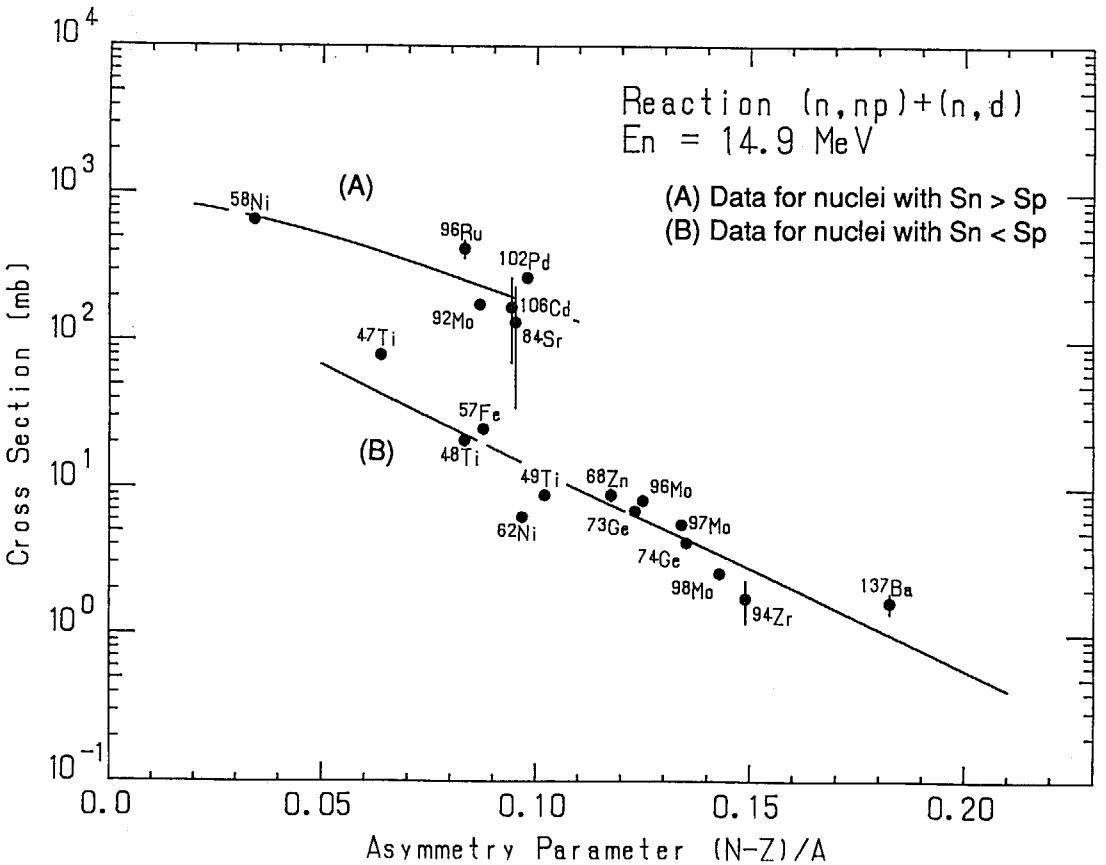

Fig. 4.2 Systematics of (n, np) reaction cross sections at 14.9 MeV.

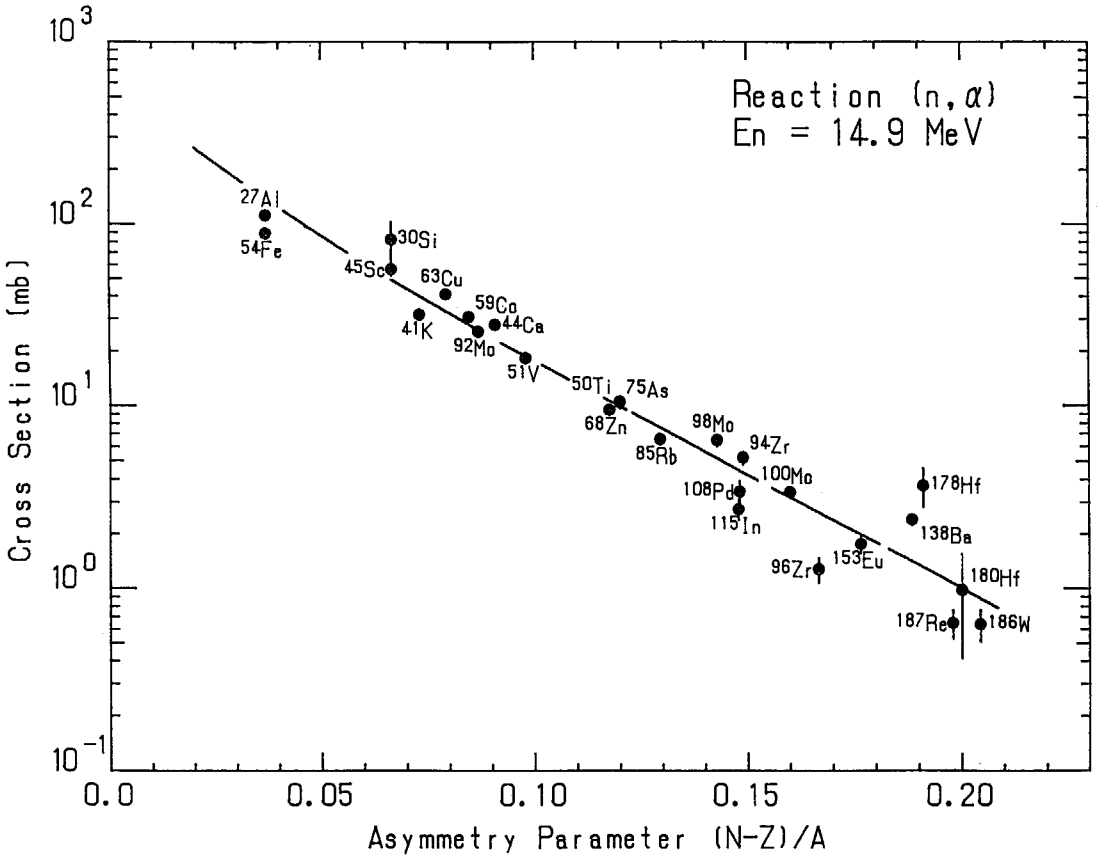

Fig. 4.3 Systematics of (n, α) reaction cross sections at 14.9 MeV.

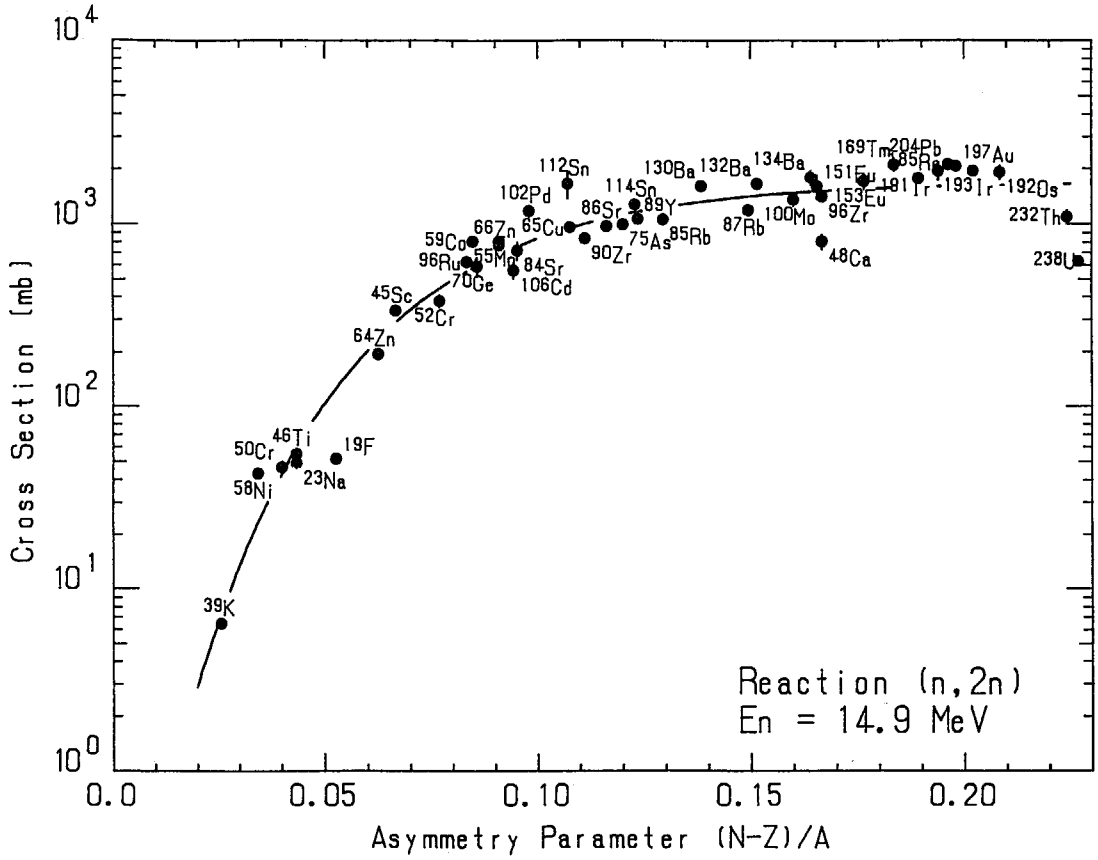

Fig. 4.4 Systematics of (n, 2n) reaction cross sections at 14.9 MeV.